9-12-2016

Biochemical Analysis of Protein-Protein and Protein-Polymer Interactions

Priya Katyal
University of Connecticut, priyak86@gmail.com

Biochemical Analysis of Protein-Protein and Protein-Polymer Interactions

Priya Katyal

University of Connecticut
2016

Proteins constitute an important part of cell machinery that performs a plethora of functions. Here, we studied three different protein systems, the practical result of which is to indicate that proteins can be studied from different perspectives. We used multiple biophysical and biochemical approaches to probe protein-protein and protein-polymer interactions. Chapters 3 and 4 focus on structural and thermodynamics aspects of protein-protein interactions, while chapter 5 has a more biochemical appeal in characterizing protein-polymer conjugates.

Through NMR studies, we identified the binding interface of integrin β3 onto the Src SH3 domain. We further tested the influence of tyrosine phosphorylation, a characteristic feature of activated β_3 receptor. Additionally, we provide key insights into the role of phosphorylated β_3 and its interaction with Src kinase. Overall, the results from these studies contribute to our current understanding of Src mediated integrin signaling.

Next, we performed a detailed study on calmodulin (CaM), which forms a globular compact structure upon binding with smooth muscle myosin light chain kinase (smMLCK). We modified CaM at its N- and C-termini and used the formation of disulfide bond to create an artificial circular protein. We studied the effect of this topological constraint on internal dynamics and molecular recognition. Using NMR relaxation techniques, we observed a slight reduction in the backbone mobility of the central loop and the C-lobe residues. ITC studies of

CaM with smMLCK revealed that in contrast to its linear counterpart, binding of cyclic CaM has a favorable change in entropy of binding *(ΔS*). Intriguingly, the overall Gibbs free energy of binding remained nearly constant between the two constructs.

Lastly, we site-specifically linked enzymes to bi-functionalized polymeric scaffolds via bioorthogonal chemistry. We present a method to prepare functionally active Cel48F-cutinase engineered protein that can be site specifically linked with phosphonate-functionalized polymers. In addition, we also present the preliminary results of Cel48F-SNAP that can covalently bind to benzylguanine derivatives. Our long-term goal is to prepare supramolecular protein-polymeric assembly that can mimic the natural cellulosome in catalyzing the conversion of cellulose to glucose, an important biochemical reaction in biofuel industry.

Collectively, these studies used multifarious approaches to explore diverse protein-protein and protein-polymer interactions.

Biochemical Analysis of Protein-Protein and Protein-Polymer Interactions

Priya Katyal

B.Pharm, University of Delhi, India, 2009

A Dissertation

Submitted in Partial Fulfillment of the

Requirements for the Degree of

Doctor of Philosophy

at the

University of Connecticut

2016

APPROVAL PAGE

Doctor of Philosophy Dissertation

Biochemical Analysis of Protein-Protein and Protein-Polymer Interactions

Presented by

Priya Katyal, B.Pharm.

Major Advisor

_____

Dr. Olga Vinogradova

Associate Advisor

_____

Dr. Yao Lin

Associate Advisor

_____

Dr. Andrew Wiemer

University of Connecticut
2016

DEDICATION

Dedicated to my dad

Acknowledgements

I would like to express my sincere gratitude to my advisor, Dr. Olga Vinogradova for allowing me to pursue Ph.D. in her lab. Throughout my Ph.D., she has given me immense freedom to develop and work on different ideas and projects. I would also like to thank Dr. Yao Lin for his constant support and encouragement. I appreciate his contributions of the projects in this thesis. I am indebted to Dr. Amy Anderson for her help. Her presence will always be missed. I am grateful to Dr. Andrew Weimer for his time and being so very helpful.

I would like to thank members of School of Pharmacy and Department of PNB - special thanks to Leslie, Mark, Kathy, Penny and Radmila. I am grateful to Vitaliy for his valuable help in NMR and for our lively conversations. I am thankful to the members of Vinogradova's lab: Lalit, Xiaochen, Khiem and special thanks to Robbins for keeping me entertained all through these years and for all the scientific inputs. I also acknowledge members of Dr. Yao Lin's group, Hongwei, Hailin, Murali and Stephen for their immense help. A huge thanks to Ranjan for introducing me to Dr. Lin. I would also like to thank Yongkun for performing the initial studies on calmodulin and cellulase.

On a personal note, I would like to thank all my friends who helped me in this journey and gave me memories to cherish for the rest of my life. I am grateful to my uncle (mamaji) and my cousin Poonam. Words are not enough to justify the unconditional support and love of my Mom, my dear sister Supreya and brother in law, Steven. I am indebted to Mohit, for his encouragement and patience, and for being there through ups and down. It wouldn't have been possible without them.

TABLE OF CONTENTS

LIST OF ABBREVIATIONS

2D	Two-dimensional
3D	Three-dimensional
AA	amino acids
ATP	Adenosine Tri-Phoshpate
β_3BP	Bi-phosphorylated (pY^{747},pY^{759}) β_3CT
β_3CT	Integrin β_3 cytoplasmic tail
β_3MP	Mono-phosphorylated (pY^{747}) β_3CT
β_3NP	Non-phosphorylated β_3CT
BMRB	Biological Magnetic Resonance Bank
CaM	Calmodulin
CD	Circular Dichroism
Cel48F	Cellulase 48 (family 48)
CT	Cytoplasmic tail
CSP	Chemical shift perturbations
DSS	4,4-dimethyl-4-silapentane-1-sulfonic acid
DTT	Dithiothreitol
ECM	Extracellular matrix
E.Coli	Escherichia coli
EDTA	Ethylene diamine tetra acetic acid
EG10	Ethylene glycol polymer (10 repeating units)
Eq.	Equation

FAK	Focal Adhesion Kinase
FPLC	Fast protein liquid chromatography
GST	Glutathione S-transferase
HPLC	High pressure liquid chromatography
HSQC	Heteronuclear single quantum correlation spectroscopy
hAGT	Human O-6-alkylguanine-DNA alkyl transferase
IPTG	Isopropyl-β-D-1-thiogalactopyranoside
kDa	Kilodalton(10^3g/mol)
MS	Mass Spectrometry
MW	Molecular weight
NMR	Nuclear Magnetic Resonance
NOESY	Nuclear Overhauser Effect Spectroscopy
PBS	Phosphated buffer saline
PDB	Protein data bank
ppm	parts per million
PRE	Paramagnetic relaxation enhancement
SDS	Sodium dodecyl sulfate
SH2	Src Homology 2
SH3	Src Homology 3
smMLCK	smooth muscle Myosin Light Chain Kinase
TCEP	Tris(2-carboxyethyl)phosphine
TOCSY	Total Correlation Spectroscopy
TrNOESY	Transfer NOESY

LIST OF FIGURES

LIST OF TABLES

Chapter 1. Introduction

The central dogma of molecular biology explains the flow of genetic information from DNA to RNA, which is further translated to make functional molecules, called proteins. Proteins constitute an important part of cell machinery that performs a magnificently diverse set of functions. They serve as structural components, are involved in cell signaling, catalyze reactions, acts as storage and transport molecules, and are therefore extensively studied. The interest in studying a specific protein arises from its participation in biologically relevant process. The biological properties a protein exhibits are conferred by its physical interaction with other molecules. These molecules, referred to as ligands can vary from being an ion, a small molecule or a macromolecule.

In this thesis, each chapter details about a specific protein, the practical result of these diverse choices of proteins is to indicate that the proteins can be studied from one or more different perspectives.

1.1 Synopsis

The following subsections describe the broad focus of each chapter.

1.1.1 Protein-protein interactions

Proteins are inherently meant to work cohesively with other proteins or act in conjunction with other scaffolds to achieve their functionalities. A detailed understanding of protein-protein interactions is fundamental for a thorough evaluation of biological processes such as blood coagulation, inflammatory response, and also for certain diseased states like cancer. By

integrating structural characterization with emphasis on molecular details, we can precisely delineate the mechanisms and the forces governing protein-protein interactions.

1.1.2 Effect of structural modifications on protein interactions

Proteins are dynamic molecules, and because of observed flexibility they can adopt different conformations in apo and bound forms. The conformational change can influence the pathway in which the protein would be involved and can further regulate its function. Of the many methods, introduction of disulfide linkage has been proven successful to emulate the well-defined conformation of proteins or to lock them in their active conformations. Though considerable research has been done in studying disulfide engineered proteins, yet its important to characterize the modified protein and its impact on protein's physical, chemical and biological properties.

1.1.3 Engineered proteins and their interaction with polymers

Subtle changes in proteins can result in customizable proteins with designed properties. New methodologies are being used to make analogues of naturally occurring proteins that show better stabilities, higher activities, and resistance to degradation with other desired properties. Given the importance of proteins in biotech industry and pharmaceutical applications, the redesigned proteins would likely be of great value with promising results. The field of chemical biology has recently been surged with designer catalytic machines, comprising of functionally active enzymes combined with synthetic polymeric scaffolds. The combination, typically called bioconjugates, has been increasingly used in biotechnology and biomedical research for widespread applications.

Here, we first investigated the structural details of protein-protein interactions in signal transduction. Secondly, we attempted to understand how a small structural change in a protein's conformation affects its dynamics and interaction. Lastly, we studied the interaction of

engineered proteins with synthetic polymers and compared the activity of the free protein with its polymeric conjugates.

1.2 Aims of the thesis

Following are the aims of the thesis:

1. *To study how tyrosine phosphorylation of β_3 integrin modulates its binding with c-Src.*

2. To investigate binding and backbone dynamics of protein under topological constrain using calmodulin as a model system.

3. To develop conjugates of Cel48F engineered protein with end-functionalized polymers.

1.3 Overview of the thesis

Following is an overview of the chapters in this thesis:

Chapter 3 (section 3.5) of the thesis provides insights into the binding of integrin with Src SH3 domain. We identified that the RGT motif of integrin sits between the RT and n-Src loop with tyrosine serving as a bridge. We also showed that the C-terminal residues of integrin adopt a polyproline type-II helix, which assists in binding of a non-PXXP motif to the Src SH3 domain. Additionally, we proposed a docking model of integrin binding to SH3 domain, and explained the importance of salt bridge formation of R^{760} of integrin CT with D^{117} of SH3.

Chapter 3 (section 3.6) expands on the results presented in chapter 3 (section 3.5). Here, we identified and characterized the role of Src SH2 domain in binding to phosphorylated integrin. The interaction of integrin β_3 with Src SH3 is abrogated upon phosphorylation of two tyrosines of β_3CT, however recent studies have shown that phosphorylated integrin can remain bound to Src. We hypothesize that $\alpha_{IIb}\beta_3$, phosphorylated at its β_3 tail, interacts with c-Src SH2 domain, a phosphotyrosine-recognizing domain. Our hypothesis is consistent with our preliminary NMR

titration data. We identified the key residues of integrin involved in mediating the interaction with Src SH2, that includes the phosphorylated tyrosine of β3 CT.

In Chapter 4, we constrained the topology of calmodulin (CaM) and studied its effect on internal dynamics and molecular recognition by its binding partner, in particular smMLCK. For this study, we first synthesized the constrained version of CaM (referred as cyclized CaM) by introducing short cystine containing peptide sequences at its N- and C-termini. The formation of disulfide bond between the two cysteines (Cys) facilitates the cyclization of the protein. Intriguingly, we observed that the thermodynamic parameters of cyclized and linear (construct having no additional constrain) version contribute differently to free energy of binding, keeping ΔG constant. We also observed subtle differences in the order parameters of linear and cyclic CaM, indicating increased backbone rigidity in the loop regions of cyclized version.

In Chapter 5, we reported development of polymer-protein conjugates of two fusion proteins with end-functionalized polymers. We constructed two different fusion proteins comprising of cutinase tag and SNAP tag respectively, with our target protein, Cel48F (family 48), an important enzymatic member of *Clostridium cellulolyticum* cellulosome. We further compared the cellulase activity of these enzymes in free and conjugated states.

Overall, these studies aimed to understand different protein-protein interactions and protein-polymer interactions using diverse biophysical and biochemical techniques.

Chapter 2. Characterization techniques

Different biophysical and biochemical approaches were pursued to conduct the studies presented in this thesis. We primarily used Nuclear Magnetic Resonance (NMR) (except for chapter 4) for structural analysis. Other biophysical techniques, including circular dichroism (CD), isothermal titration calorimetry (ITC), differential scanning calorimetry (DSC), and mass spectroscopy (MS) were used to further characterize the different protein systems. A brief description of each technique is as follow:

2.1 NMR spectroscopy of proteins

NMR is a powerful tool to determine the structures and dynamics of the proteins in solution. There has been an increasing interest in studying protein-protein interactions under physiological conditions by using NMR spectroscopy. It is widely used to delineate the location of binding interface in protein-protein interactions, and is useful in providing site-specific information on backbone and side chain dynamics. Below are the brief discussions of the different NMR techniques used in the thesis.

2.1.1 ^{15}N-HSQC (Heteronuclear Single Quantum Correlation) titration

^{15}N-HSQC based chemical shift mapping is uniquely suited to identify protein-ligand binding interfaces. Owing to its high sensitivity, it is widely used in NMR. Titrating the unlabeled compound into a solution of the labeled protein identifies the binding surface on ^{15}N-labeled target. The associated spectral changes in the ^{1}H-^{15}N HSQC spectra are monitored and mapped onto the surface of protein (with known domain fold) to identify the binding site. The chemical shifts are measured at each titration point. The chemical shift changes are converted to chemical

shifts perturbations, which are further plotted with respect to residue numbers [1]. Delta (ppm) refers to the combined HN and N chemical shift changes according to the equation:

$$\textit{Eq. 1.} \qquad \Delta\delta(HN,N) = ((\Delta\delta_{HN})^2 + 0.2(\Delta\delta_N)^2)^{1/2},$$

$$\text{where } \Delta\delta = \delta\text{bound} - \delta\text{free}$$

During titration, apart from chemical shifts perturbations, its common to observe signal broadening or complete disappearance of the peak. Such results point towards the complex exchange regime of the proteins involved. The simple case of observing smooth chemical shift perturbations in NMR spectra, suggest the system is under fast exchange (having a faster K_{off} rate) and thus, we observe a weighted average of free and bound states. Other exchange processes affect NMR, including slow and intermediate exchange and its possible to observe different exchange regimes within the same biomolecule. If the K_{off} rate is slower than the chemical shift difference between the free and bound states, then two different resonances are observed, one from free and the other representing bound signal in the spectra. As the ligand is titrated in, the free peak disappears with an increase in intensity of bound peak. The intermediate exchange is defined when the exchange rate is similar to the shift difference, and the resultant free and bound signals coalesce into one broad peak. Broadened peak, however, doesn't always indicate slow/intermediate exchange, and it is worthwhile to use other characterization techniques to get more information[2].

2.1.2 Transferred NOESY

TrNOESY experiments are suitable for weakly associating systems, where the molecular weight of the macromolecule is large compared to the ligand. It helps in identifying the bound conformation of ligand, which are under fast exchange. Since the off rate is fast, the rate of NOE build-up differs between the free and bound states. When the ligand is bound, it tends to tumble

with the macromolecule, thus having a faster rate of NOE formation. This phenomenon is observed by the presence of additional peaks in the NOESY spectra, when ligand is used in excess concentration.

2.1.3 Paramagnetic Relaxation Enhancement (PRE) experiments

PRE experiments provide unique long-range distance (10-25 Å) information that can complement NOEs, which are limited to distances of up to 5 Å. A paramagnetic label is covalently attached to one of the binding partner to produce distance-dependent line broadening in the NMR spectra. PRE profile (ratio of NMR signal intensities in the paramagnetic and diamagnetic state) of tagged mutants is determined, and the line broadening of the residues are used to map the orientation of the bound peptide. The line broadening is a result of increased R2 relaxation rates, described by Solomon-Bloembergen equation.

Eq. 2.

$$r = \left[\frac{K}{R2^{sp}} \left(4\tau_c + \frac{3\tau_c}{1 + \omega_h^2 \tau_c^2} \right) \right]$$

Where r is the distance between the electron and nuclear spins, τ_c is correlation time for this electron-nuclear interaction, ω_h is the Larmor frequency of this nuclear spin (proton) and K is a constant.

2.1.4 Triple resonance Experiments

An important step in assigning the HSQC spectra is to perform the backbone/sequential assignments using multidimensional NMR experiments. These set of experiments involve transfer of magnetization between ^{1}H, ^{15}N and ^{13}C atoms. The standard suite for backbone assignment contains of experiments HNCA, HN(CO)CA, HNCACB, HN(CO)CACB, HNCO

and HN(CA)CO. We can detect Cα, Cβ and CO groups of the given residue (i) and also for (i-1) in certain spectra. The correlation and the information given by each spectra are as listed (the signals from the nuclei in parentheses are not detected):

S.No.	**Experiment**	Information about i and i-1 residues			
1.	HNCA	$C\alpha_i$	$C\alpha_{i-1}$		
2.	HN(CO)CA	$C\alpha_{i-1}$			
3.	HNCACB	$C\alpha_i$	$C\alpha_{i-1}$	$C\beta_i$	$C\beta_{i-1}$
4.	HN(CO)CACB	$C\alpha_{i-1}$	$C\beta_{i-1}$		
5.	HN(CA)CO	CO_i	CO_{i-1}		
6.	HNCO	CO_{i-1}			

Table 2.1. Standard suite for backbone assignments. The above experiments are performed in pairs to assign the Cα, Cβ and CO groups of the i and i-1 residues.

Experiments 1&2, 3&4, 5&6 are compared in pairs to give information about the residue (i) and the preceding residue (i-1). For example, HNCA spectrum gives information about residue (i) and (i-1). The (i-1) residue is sequence confirmed by comparing the chemical shifts of the peaks in HNCA and HN(CO)CA spectra.

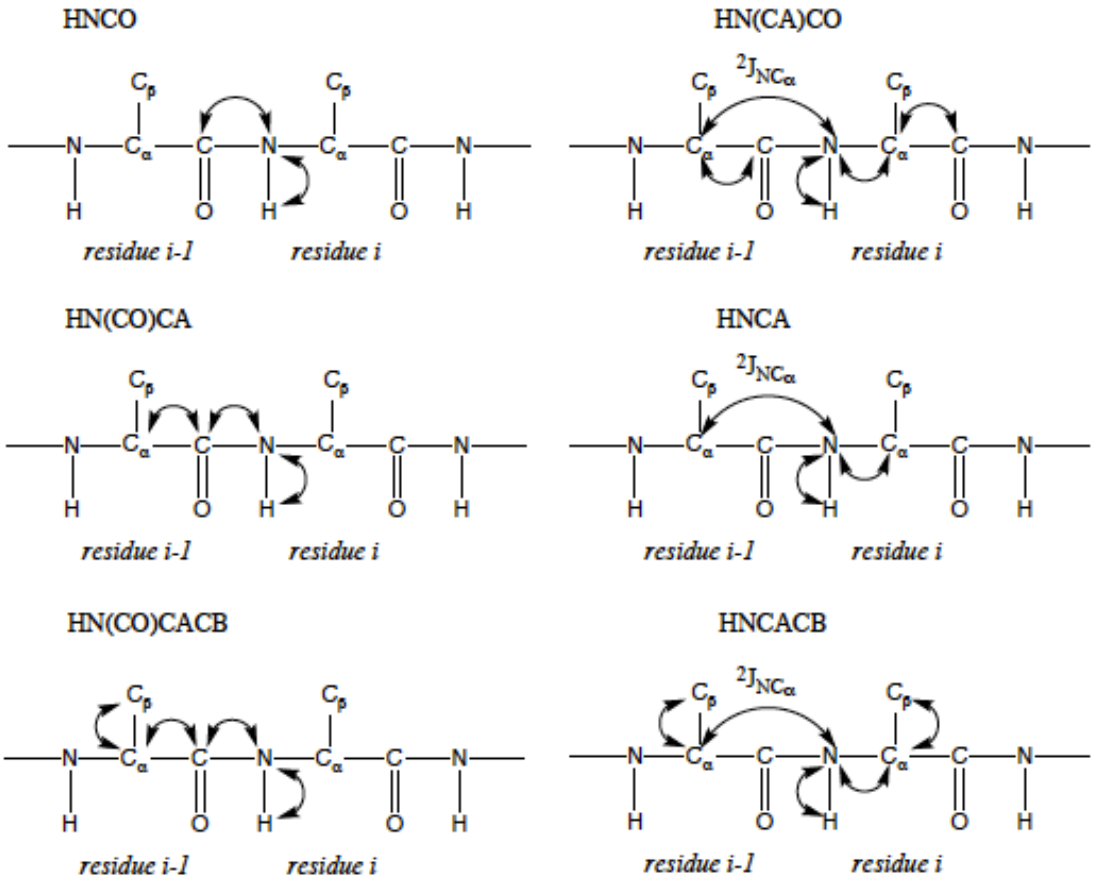

Figure 2.1 Triple resonance experiments for backbone assignments. The arrows indicate transfer of magnetization between the atoms involved. The figure was modified from [3].

2.1.5 NMR Relaxation experiments

Relaxation can be defined as the return of magnetization to its equilibrium state. Predominantly, we observe T1 and T2 relaxation:

- T1 relaxation (also known as longitudinal or spin-lattice relaxation time) is the rate at which z component of magnetization returns to equilibrium after perturbation.
- T2 relaxation (also known as transverse or spin-spin relaxation time) is the rate at which xy component of magnetization returns to equilibrium after perturbation.

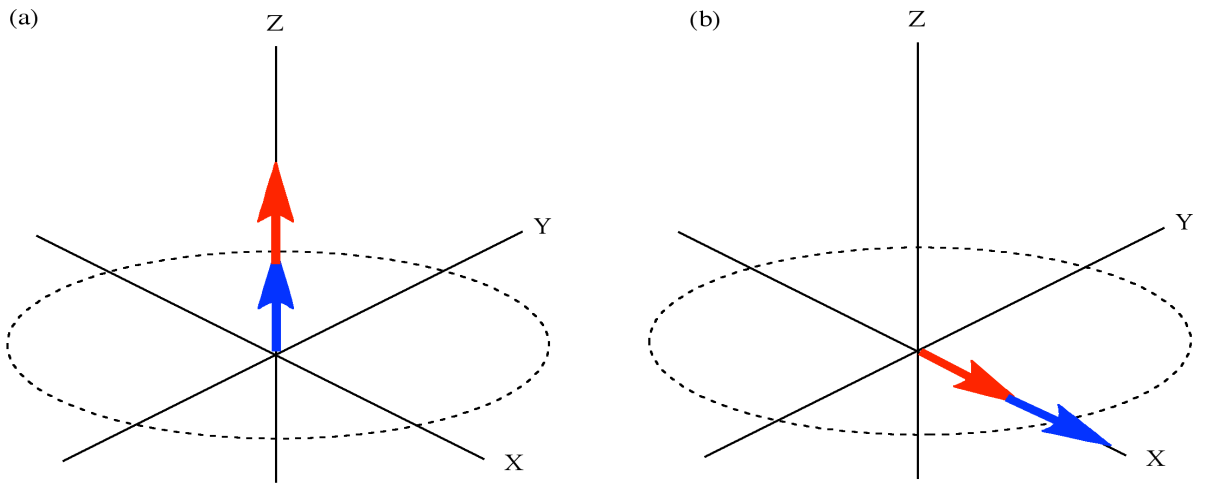

Figure 2.2 The net nuclear magnetization M_0 is aligned along the z axis. When irradiation begins, all of the individual nuclear magnetic moments become phase coherent, and this phase coherence forces the net magnetization vector M to process around the z axis. (a) Longitudinal relaxation causes recovery of the longitudinal (z) component of magnetization (from black to grey) toward M_0, at an exponential rate with time-constant T1. (b) Transverse relaxation causes shortening of the transverse component of magnetization (from blue to red), at an exponential rate with time-constant T2. The figure was taken from [4]**.**

Another relaxation parameter commonly studied is the heteronuclear nuclear Overhauser effect (NOE) where we saturate the ^{1}H signals and observe the associated changes in ^{15}N signal. These three relaxation parameters serve to determine the dynamics of the proteins in solution.

In order to relate T1, T2 and NOE with dynamics, its worth to mention the spectral density function (J(ω)). J(ω) describes the effect of motion on relaxation rate and is further related to S^2, the order parameter. S^2 is the generalized order parameter, which describes the amplitude of fast motions experienced by the individual NH bond vectors. High S^2 values, approaching 1, indicate limited motions and greater rigidity, whereas lower values indicate increasingly larger amplitude motions and greater flexibility.

2.2 Circular Dichroism (CD)

Circular dichroism is an excellent tool to determine the secondary structure of proteins. It estimates the likelihood of a protein being in a helix, beta sheet or in random coil. Each

secondary element gives a characteristic CD spectrum in the far UV spectral region (190-240nm). α-helical proteins have negative bands at 222 nm and 208 nm and a positive band at 193 nm. Proteins with β-pleated sheets have negative bands at 218 nm and positive bands at 195 nm, while disordered proteins have a negative band near 195 nm. Additionally, extended 3_{10} helix or poly-proline type II helix gives a negative band around 200nm and weaker positive band near 217nm [5].

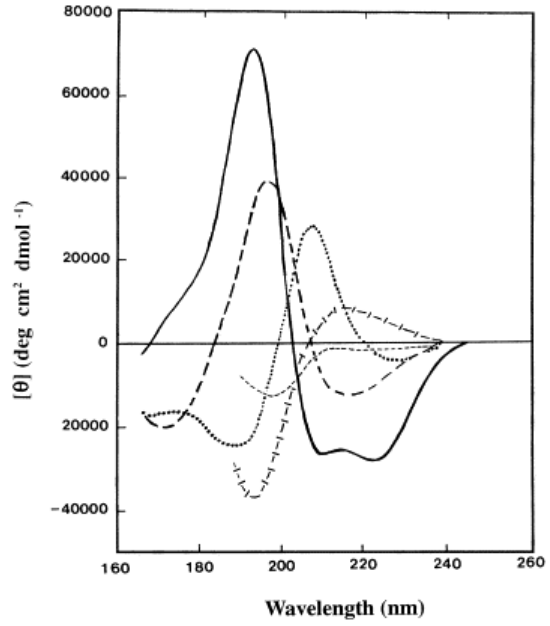

Figure 2.3 Representative CD spectra of different secondary structures. Solid line, α-helix; long dashed line, anti-parallel β-sheet; cross dashed line, extended 3_{10}-helix or poly (Pro) II helix; short dashed line, irregular structure. The figure was taken Kelly S.M. et al., *Biochimica et Biophysica Acta - Proteins and Proteomics*, 2005 [5].

2.3 Calorimetric techniques

2.3.1 Isothermal Titration Calorimetry (ITC)

ITC is a quantitative technique that can determine the complete thermodynamic profile (n, K, ΔH and ΔS) of the interaction in a single experiment. It measures the heat change on formation of a complex, when a ligand (L) is injected into the macromolecule (M) [6]. The heat released or

absorbed upon each injection of a ligand is measured with respect to the reference cell containing only the buffer. The raw data includes the plot of heat change required to maintain isothermal conditions between the sample and the reference cell. The individual peaks are further integrated and plotted with respect to total ligand-protein ratio to give the sigmoidal binding curve. The binding enthalpy (ΔH) is calculated by measuring the total heat change, while the slope of the curve gives the association constant (K_a) [7]. These parameters are further used to calculate Gibbs free energy (ΔG) and entropy of binding (ΔS) using the following equation:

Eq. 3.

$$\Delta G = - RT \, lnK_a$$

$$\Delta G_{binding} = \Delta H_{binding} - T\Delta S_{binding}$$

2.3.2 Differential scanning calorimetry (DSC)

DSC is a thermal technique, used to characterize the stability of the proteins. It measures the heat change required to denature the protein and is useful in calculating the Tm, the thermal transition midpoint of proteins. The Tm is the temperature at which the proteins have equal concentrations of native and unfolded conformations (at equilibrium). The reference and the sample cells are maintained at the same temperature as they are heated. The difference in the amount of heat required to maintain the temperature of sample cell equivalent to that of reference cell is plotted with respect to temperature.

2.4 Mass spectrometry

Mass spectrometry (MS) involves separation of molecules according to mass/size ratio. While intact protein MS is routinely used to verify the identity of proteins, the approach of MS/MS (alongwith with the use of trypsin digestion) allows identification of protein sequences and localization of sites of modifications.

2.5 References

1. http://www.bioc.aecom.yu.edu/labs/girvlab/nmr/course/.

2. Williamson, M.P., *Using chemical shift perturbation to characterise ligand binding.* Progress in Nuclear Magnetic Resonance Spectroscopy, 2013. **73**: p. 1-16.

3. http://chem.rutgers.edu/~skim/nmr_exp_TRE_backbone.html.

4. http://www-mrsrl.stanford.edu/~brian/bloch/.

5. Kelly, S.M., T.J. Jess, and N.C. Price, *How to study proteins by circular dichroism.* Biochimica et Biophysica Acta (BBA) - Proteins and Proteomics, 2005. **1751**(2): p. 119-139.

6. Jelesarov, I. and H.R. Bosshard, *Isothermal titration calorimetry and differential scanning calorimetry as complementary tools to investigate the energetics of biomolecular recognition.* Journal of Molecular Recognition, 1999. **12**(1): p. 3-18.

7. Ladbury, J.E., *Application of isothermal titration calorimetry in the biological sciences: things are heating up!* Biotechniques, 2004. **37**(6): p. 885-7.

Chapter 3. Integrins and its interaction with c-Src kinase

3.1 Integrins

3.1.1 Architecture of integrins

Integrins are a family of αβ heterodimeric receptors that act as cell adhesion molecules connecting the extracellular matrix (ECM) to the actin cytoskeleton[1]. Each integrin subunit, α and β, contains a large extracellular domain, a transmembrane (TM) domain, and a short cytoplasmic tail. The extracellular head of integrins is composed of several domains- the α subunit is composed of a propeller, a thigh, and two calf domains while the β subunit consists of a PSI domain, a hybrid domain (with an inserted I/A domain), four I-EGF domains, and a tail domain[2]. On the contrary, the cytoplasmic tails of α and β subunits are small (Figure 3.1), which are connected to the extracellular head via single spanning trans-membrane helix[3].

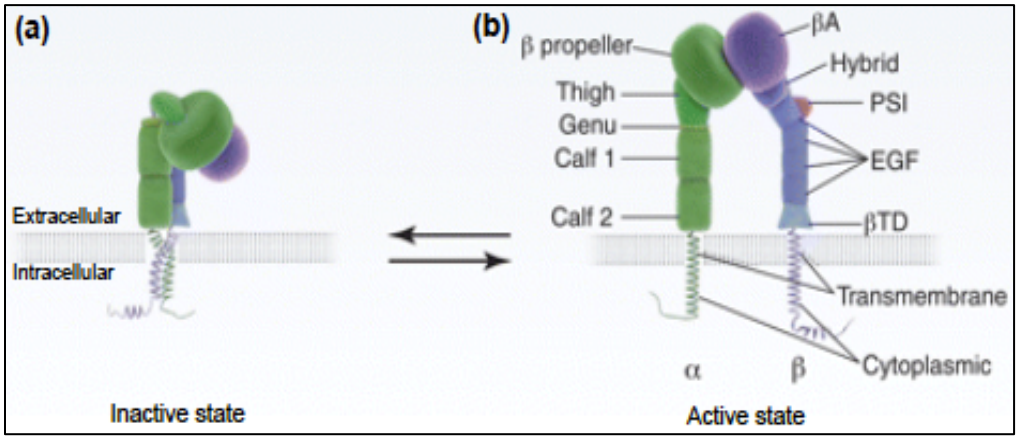

Figure 3.1 Architecture of integrin $\alpha_{IIb}\beta_3$ and schematic representation of integrin activation. In inactive state, the α and β subunits are in close association with headpiece in a bent conformation. Subsequent to integrin activation, the two subunits are separated and the headpiece straightens up, resulting in an extended integrin conformation. The α subunit is shown in green and the β subunit in violet. The figure was modified from Moser, M. et al., *Science*, 2009 [4].

3.1.2 Integrin signaling

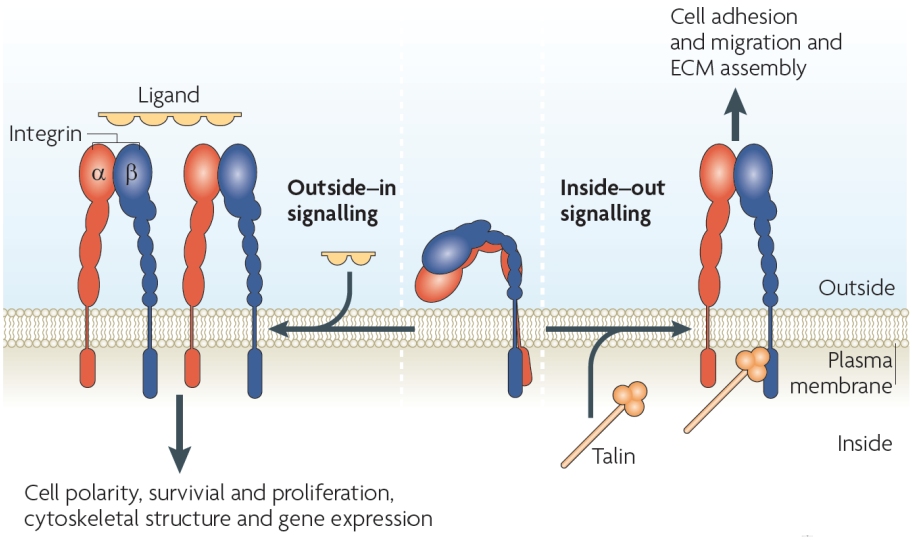

Figure 3.2 Bidirectional Integrin signaling. The right panel shows the inside-out signaling while the left panel represents the steps involved in mediating outside-in signaling. The figure was taken from Shattil, S.J. et al., *Nat Rev Mol Cell Biol*, 2010 [5]**.**

Integrins have unique characteristic of signaling bidirectionally, termed as inside-out and outside-in signaling (Figure 3.2). Of the 24 different integrin receptors, assembled form 18 α and 8 β subunits, $\alpha_{IIb}\beta_3$, an archetypical representative of the class, regulates platelet aggregation and serves as a molecular scaffold interacting with various extracellular and intracellular binding partners [1]. Unstimulated platelets express $\alpha_{IIb}\beta_3$ in a conformation inaccessible to ligands, preventing platelet-platelet interaction [3, 6]. In inactive state, the α and β subunits are in close association with the headpiece in a bent conformation. Inside-out signaling, initiated by separation of heterodimeric cytoplasmic tails cause an overall conformational change that propagates across the membrane to the extra-cellular domain of the receptor [3]. The extracellular domain of $\alpha_{IIb}\beta_3$ binds to its ligands with a high affinity and couples the platelets

together to form an aggregate [3, 6]. An increase in ligand binding induces a cascade of signaling events into the cell, collectively referred to as outside-in signaling[1]. The integrin β_3 cytoplasmic tail (CT) is involved in propagation of outside-in signaling by binding to protein tyrosine kinases (PTKs) and other signaling proteins [1, 7, 8].

3.1.3 Role of β3 Cytoplasmic tail in signaling

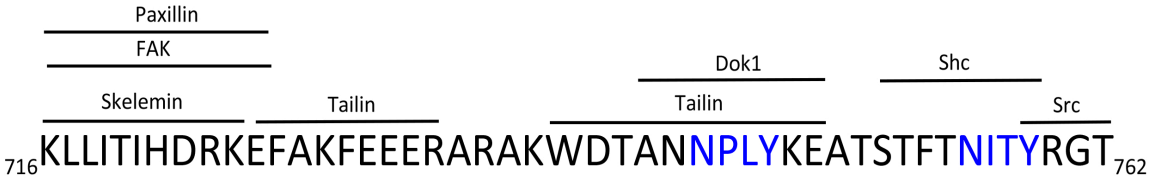

Figure 3.3 Binding of different adaptor proteins along the sequence of β_3 cytoplasmic tail. The lines indicate the motifs involved in binding to β_3 tail. Tyrosine-bearing motifs are colored in blue. The figure was modified from Legate, K.R. et al., *J Cell Sci*, 2009 [9]**.**

β_3 cytoplasmic tail is devoid of any catalytic activity but is composed of 47 residues comprising of various motifs to which many of the proteins and kinases have been shown to bind (Figure 3.3)[9]. The different motifs include the membrane proximal HDRK motif, known to bind skelemin, FAK and paxillin [10, 11]; the adaptor binding tyrosine-bearing motifs, namely, NPXY and NXXY. Upon integrin activation, these tyrosines get phosphorylated and act as a hub for proteins containing PTB domains, like Shc, DokI, and many others [12, 13]. More recently, the C-terminal RGT motif has been shown to bind Src kinase. This interaction between integrin and Src kinase is identified to have important role in outside-in signaling and has been a subject of intensive research [7, 14, 15].

3.2 Src kinase

3.2.1 Structural organization of Src

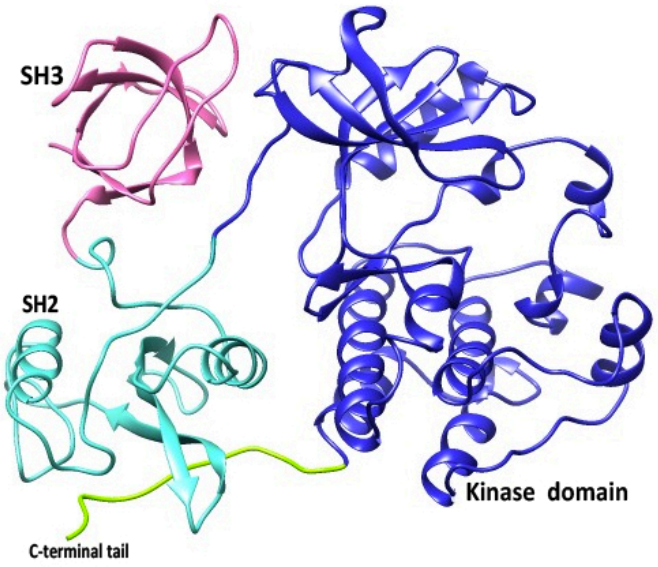

Figure 3.4 Structural representation of full length Src (PDB: 2SRC)[16]. The different domains are color coded as pink: SH3 domain, cyan: SH2 domain, blue: catalytic domain, green: pY_{527} bearing C-terminal tail.

c-Src belongs to the family of Src family protein tyrosine kinases (SFKs), other members include Fyn, Yes, Blk, Fgr, Hck, Lck, Lyn, and Yrk. c–Src, Fyn and Yes are ubiquitously expressed while other members are expressed in specific tissues. All the members are structurally similar and consist of SH3, SH2 and kinase domain [17].

The c-Src kinase is a multi-domain protein tethered to the plasma membrane by a N-terminal myristoylation sequence [16]. It consists of a (i) unique domain (ii) SH3 domain, (iii) SH2 scaffold domain, and (iv) catalytic kinase domain, followed by a tyrosine (Y^{527}) containing C-terminal regulatory sequence. The intramolecular interactions between the domains including (i) the interaction between the SH3 domain and the linker connecting the SH2 and kinase domains,

and (ii) the binding of SH2 domain to the phosphorylated Y^{527} at the C-terminal tail of the kinase domain, maintain Src in a resting state with a closed conformation [18]. v-Src, the first oncogene isolated from Rous Sarcoma Virus, was found to lack the C-terminal region that contains Tyr^{527}, making it continually active [19].

Typically, Src is maintained in an inactive state, but gets activated transiently during cellular events such as mitosis, or upon adhesion of platelets to fibrinogen [20].Abnormal activation of Src, either by mutation (as in v-src) or loss of regulatory control, can lead to drastic results with repercussions in several cancers, including colon and breast cancer [21].

3.2.2 Regulation of Src

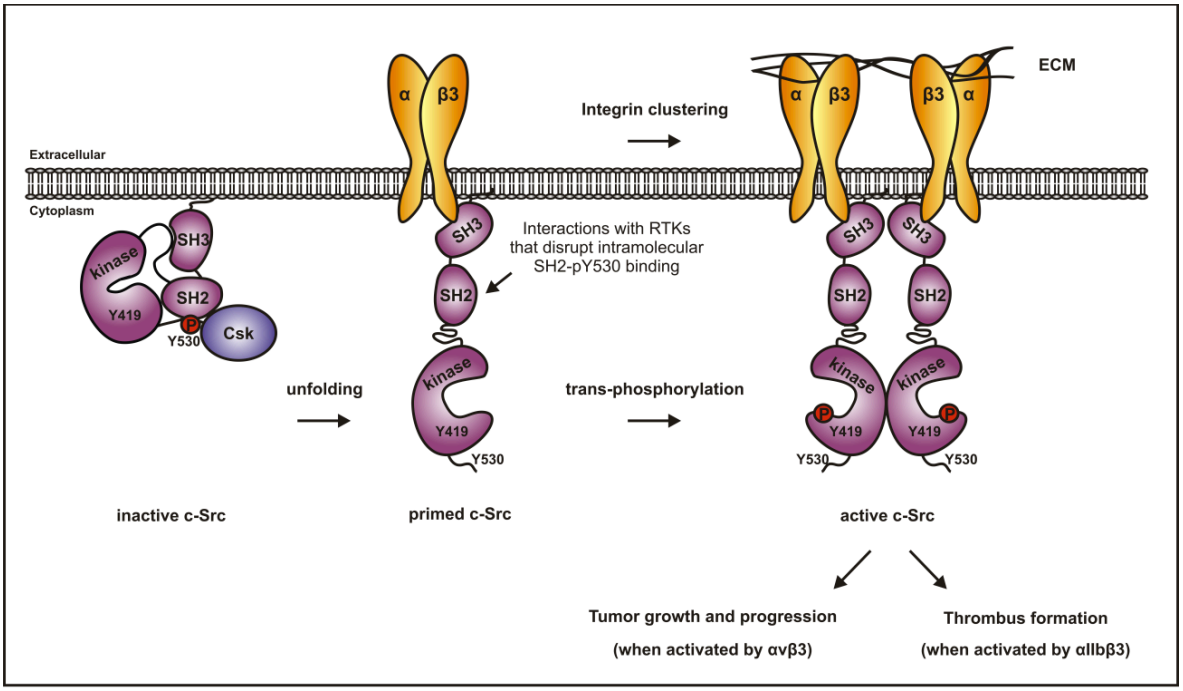

Figure 3.5 Model of c-Src activation by β_3. The figure was taken from Huveneers S., et al., *Scientific World Journal*, 2010 [21].

The tyrosine phosphorylation status of Src regulates its activity, the key residues being Y^{416} and Y^{527}. Phosphorylation of Y^{416} activates the kinase whereas when Y^{527} is phosphorylated, it serves

as a negative regulator of Src activity. Csk, a C-terminal Src kinase associates with Y^{527} of c-Src; the phosphorylated Y^{527} further interacts with SH2 domain of Src, suppressing Src activity [16, 22]. On the contrary, PTP-1B, a phosphatase dephosphorylates Y^{527}, relieving this inhibitory interaction [8, 18]. Various factors, including association of Src with its binding partners, trigger trans-autophosphorylation of Y^{416} (present within the activation loop of Src), resulting in an increased catalytic activity of Src kinase (Figure 3.5).

3.3 Role of integrins in Src activation

Several studies have shed light on the importance of interaction of integrins with Src. The interaction has been implicated in platelet adhesion, cytoskeletal reorganization and bone remodeling. Integrins (upon its interaction with the extracellular matrix) cluster and congregate several signaling and adaptor proteins [1, 23]. These sites of integrin clusters are involved in formation of focal adhesions that regulate diverse arrays of cellular functions such as cell motility, migration, differentiation and proliferation [1]. One of the initial events that occur upon integrin activation is the increase in catalytic activity of SFKs [24]. Src kinase plays an important role in mediating integrin dependent adhesion signaling by phosphorylating other downstream kinases and adaptor proteins. De Virgilio (2004) showed the close proximity of $\alpha_{IIb}\beta_3$ and Src in living cells, using Bioluminescence resonance energy transfer (BRET) and bimolecular fluorescence complementation (BiFC) [25]. Biochemical studies have emphasized that integrin not only acts as a substrate for Src kinase [26] but is also believed to bind Src SH3 domain through its terminal residues, in particular the RGT motif. However, until the beginning of the current studies, it wasn't clear as where the RGT motif binds the SH3 domain. The present study was carried out to address this issue. A better understanding is warranted, as myriad of details remains elusive about the integrin mediated Src activation.

3.4 Clinical significance

Extensive studies of both, integrin and Src kinase, have established a critical role of this interaction in thrombosis and hemostasis as well as in regulation of platelet adhesion [27]. Current pharmacological approaches to prevent platelet-dependent thrombotic complications of cardiovascular disorders include $\alpha_{IIb}\beta_3$ antagonism with inhibitors of ligand binding at the extracellular matrix [28]. A novel antithrombotic approach targeting of $\alpha_{IIb}\beta_3$ signaling at the level of β_3 extreme C-terminus using β_3-derived membrane permeable myristoylated peptides has been proven successful [29]. However, there is still an unmet need for more effective and safe antiplatelet drugs for chronic indications. Our studies reveal not only the structural details of new therapeutic targets for the treatment of thrombosis and neoplastic diseases, but also provide new insights into understanding the molecular details of the fundamental process of platelet adhesion and c-Src activation.

Outline

In this project, we focused our efforts in studying the association of β_3 cytoplasmic tail with c-Src. Section 3.5 provides insights into the binding of integrin with Src SH3 domain. We identified that the RGT motif of integrin sits between the RT and n-Src loop with tyrosine serving as a bridge. We also showed that the C-terminal residues of integrin adopt a polyproline type-II helix, which assists in binding of a non-PXXP motif to the Src SH3 domain. Additionally, we proposed a docking model of integrin binding to SH3 domain, and explained the importance of salt bridge formation of R^{760} of integrin CT with D^{117} of SH3.

Section 3.6 expands on the results presented in section 3.5. Here, we identified and characterized the role of Src SH2 domain in binding to phosphorylated integrin. The interaction of integrin β_3 with Src SH3 is abrogated upon phosphorylation of two tyrosines of β_3CT, however recent

studies have shown that phosphorylated integrin can remain bound to Src. We hypothesize that $\alpha_{IIb}\beta_3$, phosphorylated at its β_3 tail, interacts with c-Src SH2 domain, a phosphotyrosine-recognizing domain. Our hypothesis is consistent with our preliminary NMR titration data. We identified the key residues of integrin involved in mediating the interaction with Src SH2, and identified the integrin-binding interface on Src SH2. Further experiments are necessary to fully characterize the interaction, and to expound its functional relevance in integrin-Src signaling pathway.

3.5 Structural insights into the recognition of β_3 integrin cytoplasmic tail by the SH3 domain of Src kinase

3.5.1 Overview

Shattil and co-workers [7, 8] have shown that outside-in signaling in platelets is mediated by a direct interaction of carboxyl terminus β_3 integrin with SH3 domain of Src kinase. Src SH3 domain, has been extensively studied and structurally characterized in both free and ligand bound states (PDB: 1RLQ, 1QWF, 1NLP). It consists of two antiparallel β sheets positioned at right angles to one another. The β strands are linked via RT loop, n-Src loop, distal loop, and a short 3_{10}-helix [30, 31]. In general, SH3 domains are known to favor peptides bearing a PxxP motif [32]. The PxxP motif adopts a polyproline type II (PPII) helix and binds between the RT loop and n-Src loop. The selectivity of these peptides is further enhanced by basic residues, arginines or lysines, which flank the core motif. In addition, other mechanisms may contribute towards the specificity of this interaction with the SH3 domain [33]. Although two classes of peptides, class I—(R/K)xxPxxP and class II—PxxPx(R/K), [32-34] are considered as canonical SH3 binding targets, accumulating evidence suggests that SH3 can also recognize non-PxxP motifs [32, 35, 36]. The exact molecular details of such recognition still remain unclear.

However, some non-PxxP peptides have been shown to occupy the same interface as PxxP motifs [37].

In this project, we present the NMR data and a docked model of SH3 with cytoplasmic integrin β_3. We also show that the C-terminal RGT motif of β_3 adopts a partial PPII type helix facilitating its interaction with the RT and n-Src loops of SH3 in an orientation opposite to that obtained from X-ray studies [14]. Finally, NMR titration studies demonstrate no interaction with the phosphorylated β_3, supporting the idea of a constitutive interaction between non-stimulated/resting (non-phosphorylated) β_3 integrin and the SH3 domain of Src kinase.

3.5.2 Materials and methods

Peptides

β_3 heptapeptide (NITYRGT^{762}), mono (ATSTFTNITpYRGT^{762}), and bi-phosphorylated (RAKWDTANNPLpYKEATSTFTNITpYRGT^{762}) C-termini of β_3 (MP-Cβ_3 and BP-β_3 respectively) were synthesized chemically (Genemed Synthesis; NEO-peptides).

Expression and purification

Cloning, expression, and purification of cytosolic β_3 was done as described elsewhere [3]. The human Src SH3 (residue 80–144) in pGEX-4T1 vector was expressed in BL21(DE3) after induction with 1mM IPTG. To produce ^{15}N-isotopically labeled Src SH3, cells were grown in M9 minimal media containing $^{15}NH_4Cl$. GST-tagged SH3 was purified in PBS buffer (140mM NaCl, 27mM KCl, 10mM Na_2HPO_4, 1.8mM KH_2PO_4, pH 7.2) using Pierce Glutathione Agarose resin (Thermo Scientific). SH3 was eluted by either cleavage with thrombin or by using 10mM glutathione in PBS buffer. The eluate was further purified through HiLoad 16/60 Superdex 75 column (GE Healthcare) equilibrated with PBS buffer.

NMR spectroscopy

All experiments were performed at 25°C using 0.1mM protein samples (unless otherwise mentioned), on 600 MHz magnet (Agilent) equipped with inverse-triple resonance cold probe.

^{15}N-HSQC titration

Concentrated stock solutions of β_3 peptides were prepared in the same buffer as Src and added to the ^{15}N-labeled SH3 domain at different peptide to protein molar ratios. Each data point was also reverse titrated beginning from the saturated conditions for the peptides. Experiments were performed at pH 5.8. The SH3 spectra at different pH were collected as a negative control. All the spectra were collected with 2048 complex data points in t2 and 128 increments in t1 dimensions and zero filled to 2048 x 1024 data points. The spectra were processed with NMRPipe and analyzed by CCPN software suite [38]. Chemical shift assignments for SH3 domain were obtained from BMRB database entry 3433 [31]. The shifts were adjusted to match our experimental conditions.

Transferred NOE

β_3 heptapeptide was mixed with GST-fused SH3 at pH 6.5. Different peptide to SH3 ratios were investigated to find the optimal one for NOE transfer in two-dimensional proton NOESY experiments with the mixing time of 400 ms. A negative control with just the GST tag was performed under the same conditions at an optimized heptapeptide to GST ratio of 200 to 1. Partial ^{1}H resonance assignments for the heptapeptide were obtained by collecting TOCSY (mixing time of 70 ms) and NOESY (mixing time of 400 ms) spectra.

Paramagnetic Relaxation Enhancement (PRE) experiment

In order to introduce a spin label, β_3 mutant was constructed with an additional cysteine residue after the terminal YRGT sequence using QuikChange site-directed mutagenesis kit (Agilent). Prior to the reaction, the mutant was reduced by 1mM TCEP, which was subsequently removed

by washing on a PD-10 column (GE Healthcare). The reduced β_3 mutant was allowed to react overnight with either an excess of cysteine specific spin label, 3-maleimido-PROXYL, hereafter referred to as mProxyl (Sigma-Aldrich), or 1-oxyl-2,2,5,5-tetramethylpyrroline-3-methyl) methanethiosulfonate, hereafter referred to as MTSL (Alexis Biochemicals). The reactions were performed at room temperature at a pH of 7.0. The unreacted spin label was separated from the tagged mutant by reverse phase HPLC on PROTO C4 column (The Nest Group). Attachment of the tag was confirmed through mass spectrometry. ^{15}N -HSQC spectrum of SH3 in the presence of tagged β_3 mutant (as well as a control with untagged mutant) was collected under the same conditions as used for wild type β_3 titrations.

Circular dichroism

CD experiments were done on PiStar 180 Spectrometer (Applied Photophysics, UK). The sample was prepared by dissolving β_3 heptapeptide in 20 mM phosphate buffer at pH 6.5. Spectrum was collected in the far UV range at 25°C with a step resolution of 0.5 nm, bandwidth of 3.0 nm and data averaging of 30 s/point.

Electrostatic potentials mapping

The potential files used for mapping were prepared from the respective PDB files by Adaptive Poisson–Boltzmann Solver (APBS) [39], a program that maps the electrostatic potential energy based on Poisson–Boltzmann equation. The resultant (.pqr and.in) files from pdb2pqr webserver served as input for APBS calculations. APBS webserver as well as Chimera's APBS built-in tool were used to prepare the electrostatic potential maps, which further rendered the electrostatic surface using Chimera's Electrostatic Surface Coloring tool. Alternatively the surface potential was also directly mapped using Coulombic surface mapping.

3.5.3 Results

Previous studies have identified the C-terminal RGT^{762} motif of β_3 integrin [7, 27] as the binding site for Src kinase through its SH3 domain. Hence we decided to map the binding site of this interaction onto the surface of SH3 using solution NMR. First, the full length unlabeled β_3 cytoplasmic tail (hereafter referred to as β_3CT) was titrated against ^{15}N -labeled SH3. The ^{15}N -HSQC spectra of SH3, shown in Figure 3.6, clearly indicate significant chemical shift differences when compared to the spectrum from free protein (shown in black). This titration was performed at an SH3 to β_3 molar ratios of 1:1, 1:3, and 1:5 while maintaining a constant pH throughout the experiment. The observed chemical shift differences, shown in Figure 3.7 (a), were concentration dependent, reproducible, and specific to the interaction. Additionally, control experiments with the SH3 domain at different pH showed no similar effect, validating the perturbations being a consequence of binding. Amino acids affected the most, belong to the RT loop (residues R^{95} to L^{100}) and the n-Src loop (E^{115} to W^{118}), with Y^{131} perturbed in isolation. The RT loop amide peaks (R^{95}, T^{96}) were broadened upon titration, a manifestation of conformational exchange [4] (Fig. 3.7(c) and also shown in Fig. 3.8); while the peak intensities corresponding to the residues from the n-Src loop remained unaffected, suggesting a single conformation within this loop. Next, we tested β_3 heptapeptide, composed of the last seven β_3 residues containing the RGT motif. Chemical shift perturbation pattern obtained with β_3 heptapeptide (Fig. 3.7 (b)) closely resembled the one obtained with the full-length β_3CT. The insets in Figure 3.7 represent the mapping of the chemical shifts onto the surface of SH3 domain (PDB: 1SRL) in the presence of full-length β_3CT (Fig. 3.7 (a)) and β_3 heptapeptide Fig. 3.7(b). The similar binding interfaces between the two confirms that the C-terminal motif of β_3 is sufficient to define its binding to Src SH3 domain.

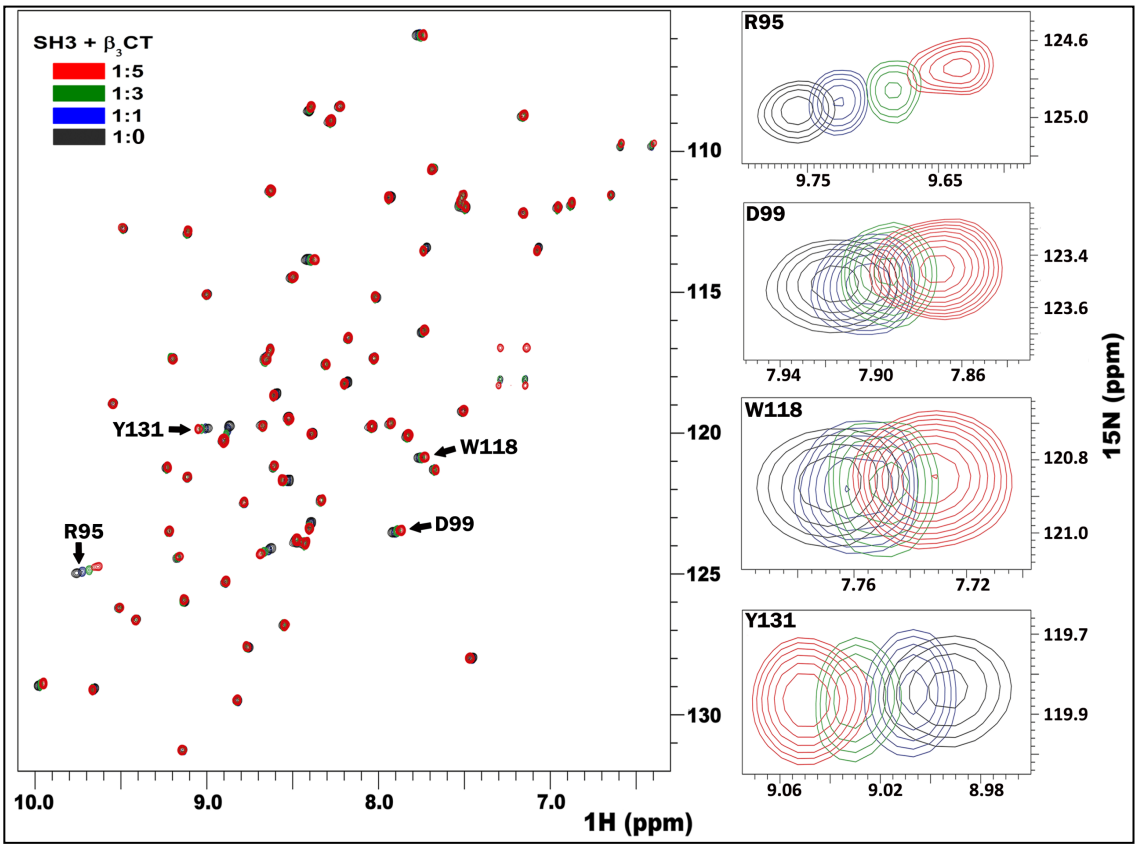

Figure 3.6 The superimposition of ^{15}N -HSQC spectra of Src SH3 (shown in black) in the presence of varying molar excess of β_3CT as shown in blue (1:1), green (1:3) and red (1:5). Also shown to the right are several individual residues displaying significant shifts.

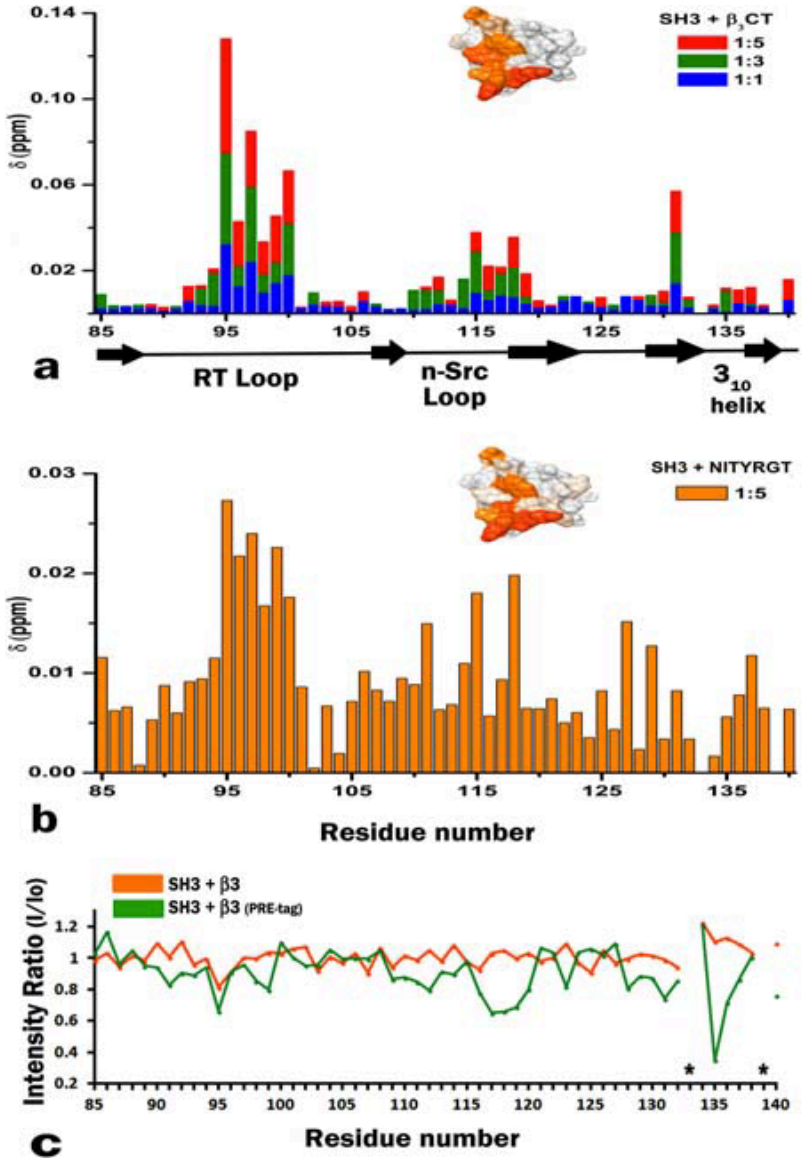

Figure 3.7 (**a**) Chemical shift differences in SH3 HSQC spectra upon β_3CT binding at different molar ratios. Bars are colored according to the different ratios as presented in Figure 3.6; Delta (ppm) refers to the combined HN and N chemical shift changes according to the equation: $\Delta\delta(HN,N) = ((\Delta\delta_{HN}^2 + 0.2(\Delta\delta_N)^2)^{1/2}$, where $\Delta\delta = \delta_{bound} - \delta_{free}$; The inset shows the chemical shift differences (obtained from 1:5 ratio) mapped onto the surface of SH3 domain (PDB: 1SRL), where the darker color represents the residues maximally affected. (**b**) Chemical shift differences obtained from the ^{15}N HSQC spectrum of SH3 upon binding to β_3 heptapeptide also at 1:5 ratio, further mapped onto the surface of SH3 domain (inset). (**c**) Paramagnetic relaxation enhancement data of the backbone amide groups of SH3 in the presence of PRE tagged β_3CT (green) in comparison to the untagged β_3CT (orange). The asterisk mark represents proline residues.

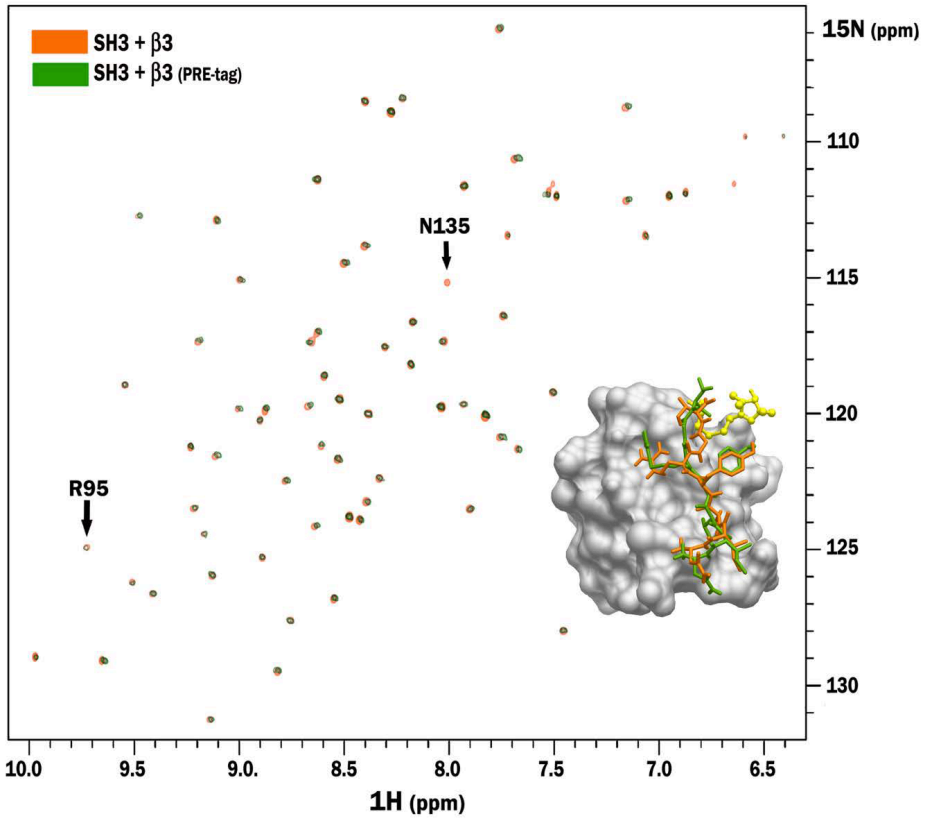

Figure 3.8 Superimposition of the ^{15}N -HSQC spectra of SH3 in the presence of wild type β3CT (orange) and mutant with paramagnetic tag attached to its C-terminus end (green). The inset shows surface representation of the docked SH3 model with the heptapeptide (orange) and heptapeptide with PRE tag (green, attached tag is shown in yellow).

We further used the chemical shifts mapping approach to test the influence of tyrosine phosphorylation, a characteristic feature of activated β_3 receptor, [40], on its binding to Src kinase. These titrations were performed against ^{15}N-labeled SH3 with mono-(pY^{747}) or bi-(pY^{747}&pY^{759})-phosphorylated β_3-derived peptides ($MPC\beta_3$ and $BP\beta_3$ respectively, refer to the Material and Methods section). Since no chemical shift differences were found in either case, even at a high molar ratio of 1 to 5 (Fig. 3.9), we concluded that tyrosine phosphorylation prevents SH3 from binding to β_3. This finding is consistent with the previously suggested mechanism of constitutive interaction of Src with unactivated/resting, non-phosphorylated integrin β_3 [7].

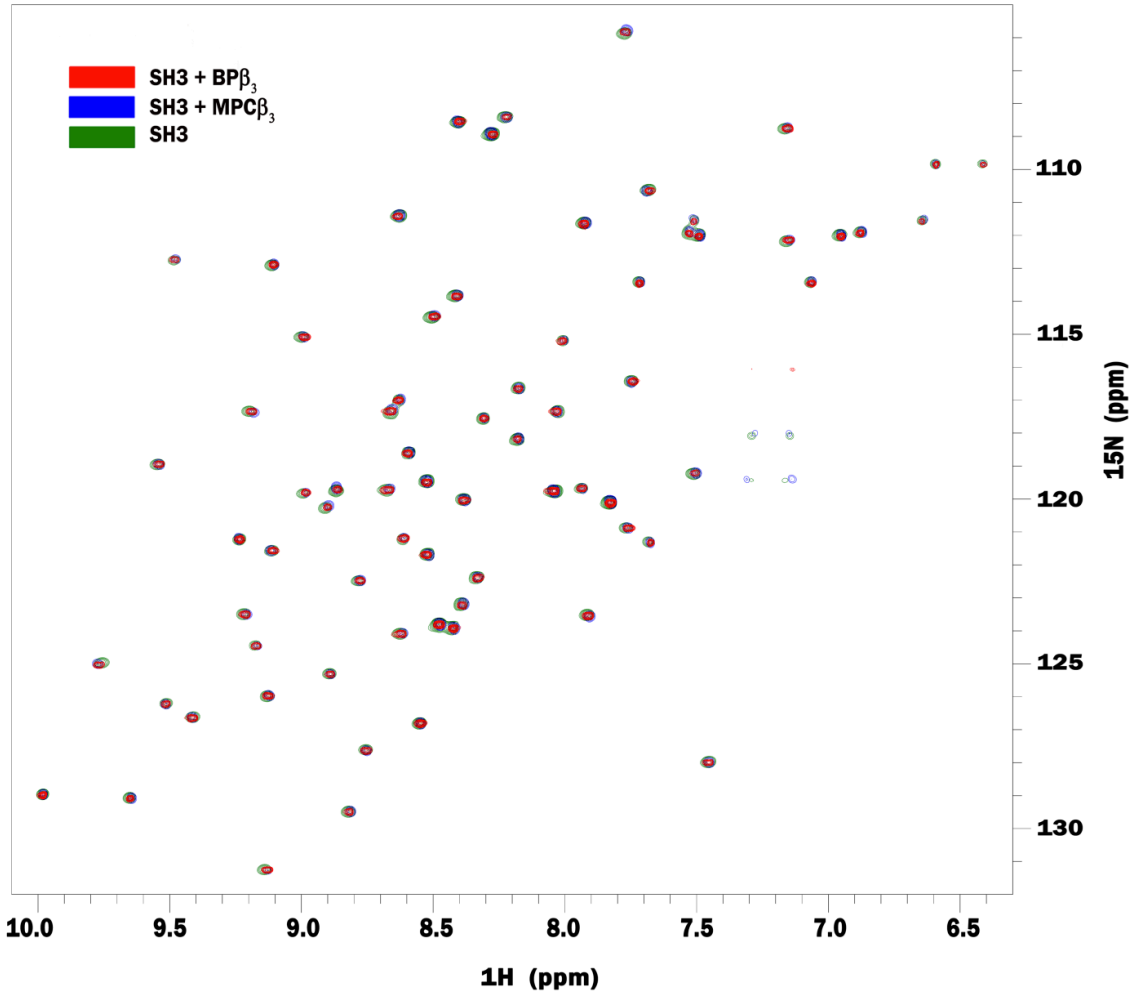

Figure 3.9 Superimposition of the ^{15}N -HSQC spectra of SH3 obtained alone (green) and in the presence of peptides: C-terminus monophosphorylated β3 (MPCβ3) (blue), and biphosphorylated β3 (BPβ3) (red).

We additionally carried out Paramagnetic Relaxation Enhancement (PRE) experiments to ascertain the orientation of bound integrin. A paramagnetic spin label was attached to the β_3 mutant containing a cysteine residue added to its C-terminal end (Figure 3.10). The nitroxide radical from the spin label attenuates peak intensities of nearby residues allowing direct mapping of its location onto the binding surface. Since the label is attached next to the RGT motif,

maximum attenuation is expected for SH3 residues adjacent to the ones involved in binding of this motif. To test whether the addition of a paramagnetic tag affected the interaction, we compared the spectra of SH3 in the presence of wild type β_3CT and its tagged mutant (Fig. 3.8). Since no significant differences were observed we proceeded with the PRE analysis to study this interaction.^{15}N -HSQC spectra were collected at an SH3 to β_3 mutant ratios of 1:2 and 1:4. Peak intensities for SH3 in complex with the tagged β_3 mutant were normalized to the intensities of SH3 in complex with the untagged mutant. Maximum attenuation was observed for the residue N^{135} (with its side chain signals broadened beyond detection; Fig. 3.8) and a moderate decrease for Y^{136} suggesting their close proximity to the tag. A moderate decrease in the intensities of the n-Src loop also confirmed its positioning near-to the β_3 RGT motif, while the RT loop was less affected, showing similar intensities to the bound untagged β_3 (Fig. 3.7 (c), shown in orange). Attaching the tag to a cysteine residue present at the end of the C-terminus makes it quite flexible, hence preventing the quantitative analysis of the PRE data for structure calculations. However, having the N^{135} residue from the SH3 domain in close proximity to the nitric oxide from the tag, allowed us to reliably predict the orientation of the RGT motif within the SH3 binding interface.

(a)

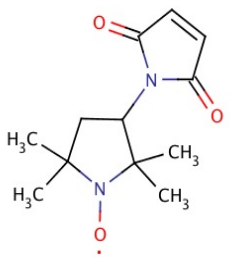

m-proxyl

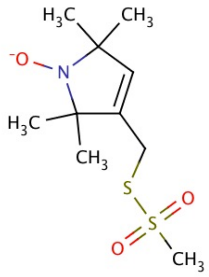

MTSL

(b)

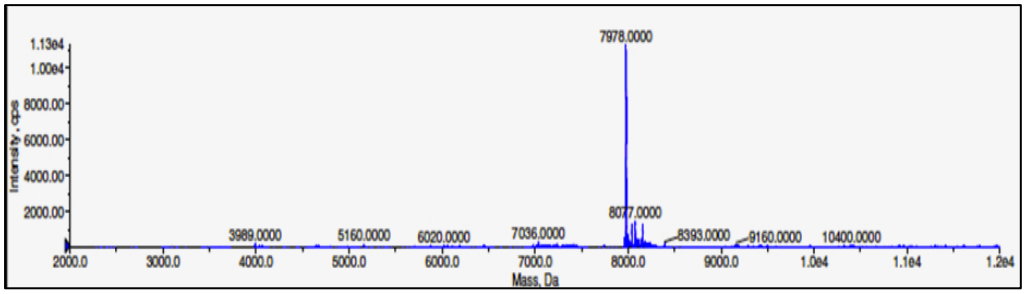

Figure 3.10 (a) Chemical structure of PRE tags: 3-maleimido proxyl and MTSL. (b) MS spectrum of m-proxyl tagged β3

To further define the molecular details of the complex, in particular, the conformation of integrin C-terminus bound to the SH3 domain, we employed transferred NOE (trNOE). This method is best suited to study weakly associating systems comprising of small ligands bound to large molecules. NOESY spectrum of β_3 heptapeptide, collected in the presence of GST-fused SH3 at an optimized peptide to protein molar ratio of 200 to 1, demonstrates the additional peaks manifesting the binding (Fig. 3.11 (a)). These peaks were absent in the control experiment with GST alone. Although partial assignments for the bound heptapeptide were made, insufficient amount of distance restraints deterred us from obtaining the complete structure of the complex. As no medium-range NOEs characteristic for α-helical secondary structure were observed, we speculate that upon binding the peptide exists as an ensemble of random coil and extended conformers. The secondary structure of the heptapeptide was further probed by circular

dichroism (CD). The spectra showed a negative band at 197 nm and a positive band at 229 nm Fig. 3.11 (b), reflecting the presence of a left handed PPII helix. Molar ellipticities per residue for these two bands are somewhat weaker for β_3 heptapeptide when compared to the values reported in literature for peptides adopting a polyproline type II helix conformation [41, 42]. This suggests that β_3 heptapeptide might adopt a partial PPII type helical conformation.

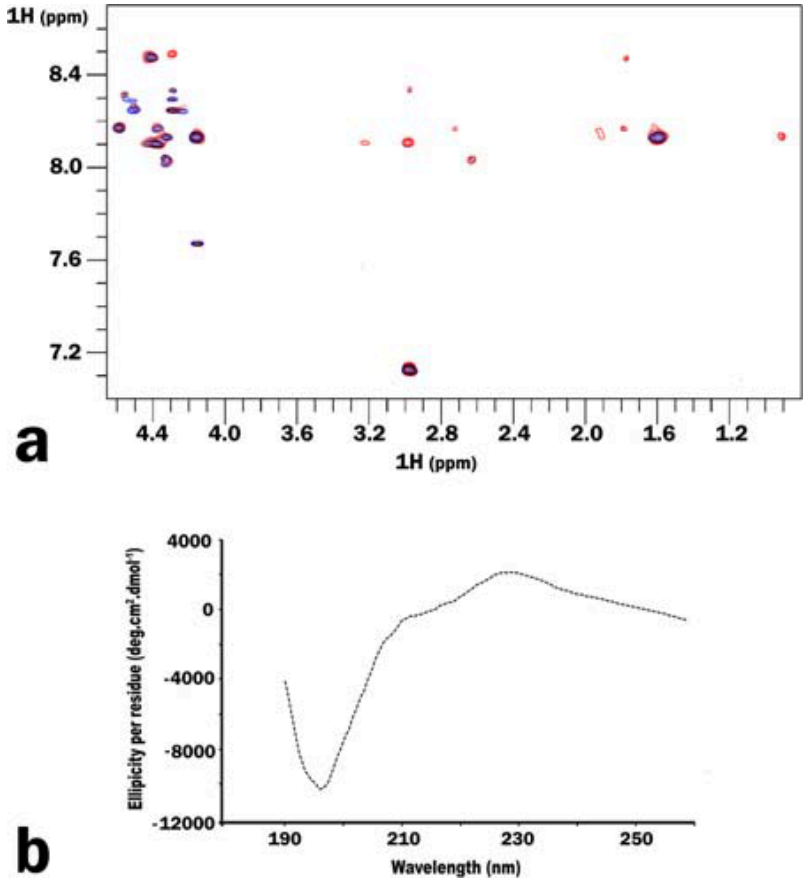

Figure 3.11 (**a**) Superimposition of the NOESY spectra obtained for β_3 hepta-peptide alone (blue) and in the presence of GST-SH3 (red). (**b**) Circular dichorism spectrum obtained for β_3 hepta-peptide shows a negative band at 197 nm and a positive band at 229 nm, typical for a partial polyproline type II-like helix.

Various models of β_3 heptapeptide were generated (with or without C-terminal paramagnetic label attached) using the Haddock (High Ambiguity data driven protein–protein DOCKing) web server [43, 44] to investigate the binding of β_3 heptapeptide to SH3 domain (PDB: 1SRL). The ambiguous interaction restraints (AIRs) were defined by NMR titration and PRE experiments with the starting conformation of the heptapeptide consistent with our trNOE and CD data. Cluster analysis of the resulting 200 water-refined models reveals 72% (with the paramagnetic tag) and 69% (without tag) of these models belong to a single cluster. Both clusters accommodate very similar binding interfaces as shown in the inset of Supporting Information Figure 3.8. The backbone root mean square deviation (RMSD) from the lowest energy model for the conformers from the cluster with tag is 1.1 Å, while for the conformers from the cluster without tag is 1.3 Å.

3.5.4 Discussion

The initial events in β_3 integrin outside-in signaling rely on its association with the SH3 domain of Src kinase. We have deduced the molecular details of this interaction using NMR. Chemical shifts mapping experiments depict the C-terminus of β_3 located between the RT and n-Src loops of SH3 domain, with Y^{131} from the β4 strand serving as a bridge between the two. As per our PRE results, the RGT motif binds to the pocket formed by the n-Src loop. The preceding NITY motif makes occasional intermediate contacts with the RT loop rendering its conformational heterogeneity.

The experimental data allowed us to obtain a reliable docked model of the complex using the HADDOCK web server. We are certain that our docking model provides a more accurate representation of the binding interface Fig. 3.12 (c) than the recent X-ray model (PDB: 4HXJ) containing the RGT tri-peptide [14] (Fig. 3.12(d)) for the following reasons: (i) We have used

the longer construct, full length β_3 cytoplasmic tail, in addition to the heptapeptide. According to our model, the RGT motif binds to n-Src loop while the remainder of the β_3 tail extends into the RT loop. The "fishing hook" arrangement presented in the X-ray structure, which places integrin on top of SH3, would not explain the conformational exchange in the RT loop observed in our titration experiments. Moreover, our CD data shows that the heptapeptide has a partial PPII helix, a characteristic feature of SH3 binding ligands, which tend to interact between the RT and the n-Src loops. (ii) We have attached the paramagnetic tag to the C-terminal end of RGT sequence, which allowed us to orient the RGT motif unambiguously with respect to its SH3 binding pocket. If the orientation were to be as per the X-ray structure, we would have seen the PRE effect opposite to the current site on SH3's surface. Moreover, the weak electron density map, used to fit the small RGT tri-peptide, could easily lead to an ambiguous orientation. This ambiguity is further accentuated by the following two observations form the X-ray structure: the average B-factor for RGT is 67 $Å^2$, much higher than that of the SH3 domain itself (13.5 $Å^2$), and the asymmetric unit of the crystal structure containing two SH3 molecules binds to a single RGT peptide (Figure 3.13). (iii) Our model also supports the biochemical studies that have clearly shown the importance of R^{760} from integrin β_3 YRGT motif and D^{117}, W^{118}, and Y^{131} residues from the SH3 domain. According to our model, the partial PPII characteristic of the peptide allows arginine side chain from the RGT motif to be positioned between the aromatic residues W^{118} and Y^{131} within the specificity pocket. This allows R^{760} to easily interact with either of the residues, while no such interactions occur in the X-ray model. Additionally, the guanidinium group of R^{760} forms a salt bridge with the side chains of either D^{99} or D^{117} or with both, as shown by some conformers of the ensemble, while in the X-ray model this crucial arginine exhibits predominantly hydrophobic contacts with a single backbone amide hydrogen

bonded to D^{117}. (iv) Furthermore, the electrostatic surface potential of SH3, presented for the apo-domain in Figure 3.14(a) and for our model in Figure 3.14(c) provides a more plausible binding opportunity that is driven by polar interactions between the negatively charged groove on the SH3 surface and positively charged side-chain of R^{760}, proving critical for the complex formation [14] and shown to enhance selectivity (as an R/Kxx or xR/K addition) when linked to PxxP, the canonical SH3 binding motif [33]. The surface potential for SH3 domain calculated based upon the coordinates from the X-ray complex (PDB: 4HXJ), presented in Figure 3.14(b), makes it electrostatically unfavorable to place the negatively charged carboxyl end of the peptide into the negatively charged groove on SH3.

The X-ray structure of the inactive Src kinase (PDB: 2SRC) shows the linker connecting the SH2 and the kinase domains in close proximity to the RT and n-Src loops of SH3 domain [16]. The question remains whether β_3 binds to Src kinase in its inactive closed form in the presence of the linker, and, if so, how does the linker affects its affinity for Src kinase. Or, alternatively, β_3 might bind to the open form, replacing the linker, thus preventing Src kinase from becoming inactive and maintaining a small population of active kinase partially poised to start the activation process induced by integrin microclustering.

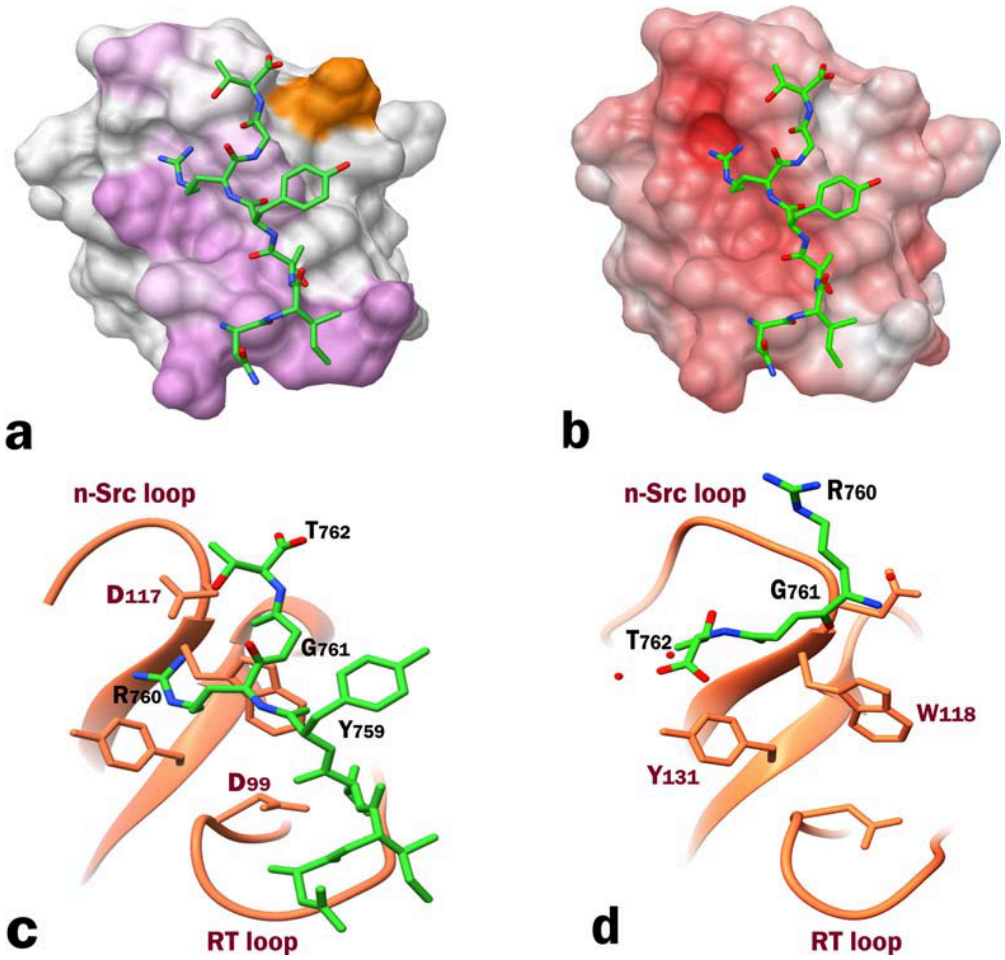

Figure 3.12 (a) β_3 heptapeptide docked onto Src SH3 domain using HADDOCK program. Chemical shift perturbations are mapped in purple. Additionally, the residue most affected by the spin label is shown in orange. (b) Electrostatic surface potential of SH3 domain bound to β_3 heptapeptide (colored with +6kT/e). (c) A ribbon representation of the binding interface obtained from the docked model highlighting R^{760} which could make potential contacts with either D^{99} or D^{117} in the specificity zone. (d) X-ray structure of the RGT peptide in complex with SH3 domain (PDB: 4HXJ) comparatively showing the reverse orientation of the peptide.

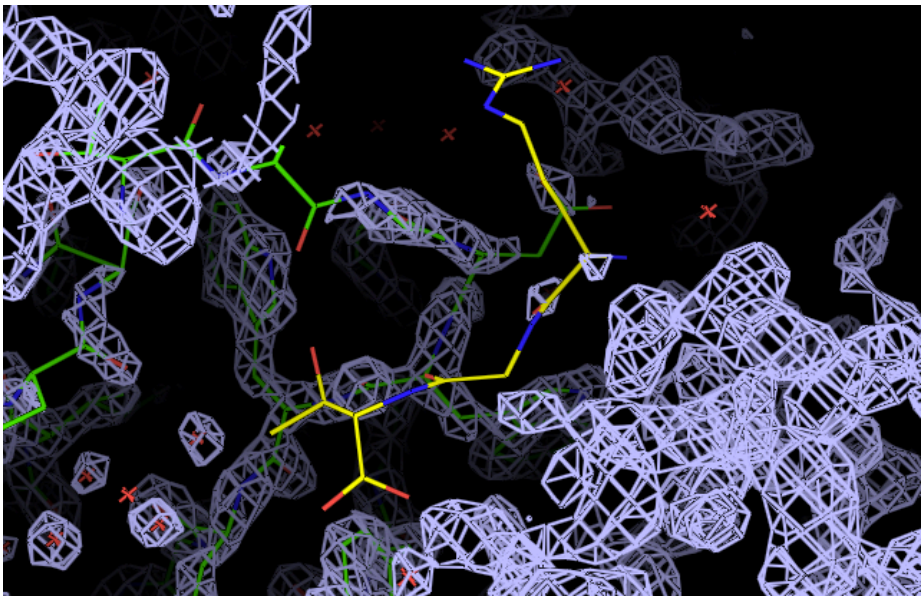

Figure 3.13 Electron Density for the RGT Peptide. The wire representation of protein is shown in green while peptide atoms are shown in yellow. (PDB: 4HXJ)

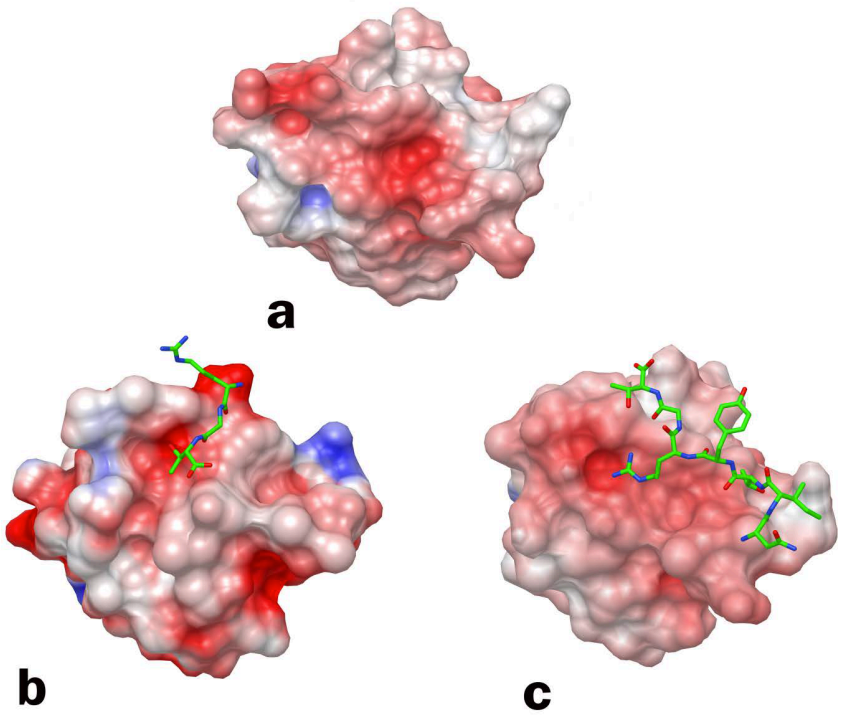

Figure 3.14 The electrostatic surface (colored with +6 kT/e) of SH3 domain alone (pdb code: 1SRL, panel a) and our docked model with integrin β_3 heptapeptide (panel c) are mapped using the more rigorous Adaptive Poisson-Boltzmann Solver (APBS) with the electrostatic potential

energy calculated based on Poisson-Boltzmann equation. The X-ray model (pdb code: 4HXJ, panel b) is mapped using Coulombic Surface in an attempt to match its representation from the article. [14]

In light of the proposed mechanism of outside-in signaling [18], where some integrin β_3 molecules are primed for activation of Src kinase, the weak binding as observed from our trNOE experiments seem pertinent. In addition, we have further investigated whether SH3 domain binds to the phosphorylated β_3 and found no interaction, suggesting that Src can be associated with integrin through its SH3 domain only in the resting non-phosphorylated state of the receptor. We believe that this weak but constitutive interaction would keep Src tethered to the integrin and consequently bring two or more Src kinases to close proximity upon integrin activation via clustering [7]. This, in turn, would aid in trans-activation of the kinase through auto-phosphorylation of Y^{418} in the Src activation loop.

3.5.5 Conclusions

In conclusion, our chemical shifts mapping data in concert with PRE, trNOE and CD studies have confirmed the RGT^{762} motif of β_3 integrin as the binding site for Src kinase. We have used these data to generate a reliable model of the complex through docking. Furthermore, we have shown that tyrosine phosphorylation of β_3 cytoplasmic tail prevents it from binding to SH3, corroborating the reports of a constitutive interaction between resting integrin β_3 and Src kinase [7].

3.6 Identification and structural characterization of β3 integrin cytoplasmic tail as a binding partner of c-Src SH2

3.6.1 Overview

In resting platelets, Src forms a complex with $\alpha_{IIb}\beta_3$ integrin through the interaction involving c-Src SH3 domain and the carboxyl-terminal region of the β_3 cytoplasmic tail [7, 8, 14, 45]. When the platelets gets stimulated, as exemplified by phosphorylation of Y^{747} and Y^{759} (present within the β_3CT), the activated β_3 prevents its binding to the SH3 domain [45]. Interestingly, it was found that the activated β_3 could still be bound to Src, making it catalytically active [15]. Based on the recent findings and our preliminary data, we hypothesized that phosphorylated β_3 recruits SH2, the phosphotyrosine-recognizing domain of Src, which we believe regulates Src activation. Overall, our proposed work should serve as a foundation for structural understanding of integrin mediated Src activation with focus on Src SH2 domain as a central key regulatory element.

The Src homology 2 (SH2) spans the region between the amino acids sequence 140- 250 in c-Src. It consists of a central β-sheet flanked by two α-helices. It is known to bind to pYEEI motif with a strong affinity and can also bind peptides with two phosphorylated tyrosines [46, 47]. The phosphorylation of second tyrosine, although not essential, increases the affinity of the binding peptides. The phosphotyrosine binds into a deep pocket formed near the central sheet of SH2 domain, while the residues, C-terminal to the phosphotyrosine, bind to the region composed of C-terminal residues of SH2. This region comprises of a hydrophobic pocket that binds to the hydrophobic residues in Y+3 position, conferring specificity to the peptides that bind Src SH2 domain [48].

3.6.2 Methods

Expression and purification

β_3 was expressed and purified as previously [3]. Two mutants of β_3 ($Y^{747}F$ and $Y^{759}F$) were prepared using Quikchange site directed mutagenesis kit. Tyrosine phosphorylation of β3CT and its mutants was achieved in vitro by using Src kinase, as described by Anthis et al [49], and is briefly described in next section. The Src SH2 domain (residues 143-245) containing pET28 SacB AP vector, generously provided by Pawson lab, was expressed in BL21 (DE3) cell line. Purification of Src SH2 domain is performed according to the protocol from QIAGEN under nondenaturing conditions followed by gel-filtration on HiLoad 16/60 Superdex 75 column in 20mM MES, 50mM NaCl, 1mM DTT buffer at pH 6.0. Cultures are grown in minimal media with $^{15}NH4Cl$ as the sole nitrogen source.

Phosphorylation of integrin tails by Src kinase

We used a similar protocol as described by Anthis et al [49]. Briefly, Src and β_3 were added at a ratio of 1:75 and the phosphorylation was performed overnight (~16hours) at RT in 50 mM Tris pH 7.3, 20 mM MgCl2, 10 mM MnCl2, 2 mM ATP. Phosphorylated tails were separated from unphosphorylated tails by HPLC and were identified by mass spectrometry (Figure 3.15) and NMR.

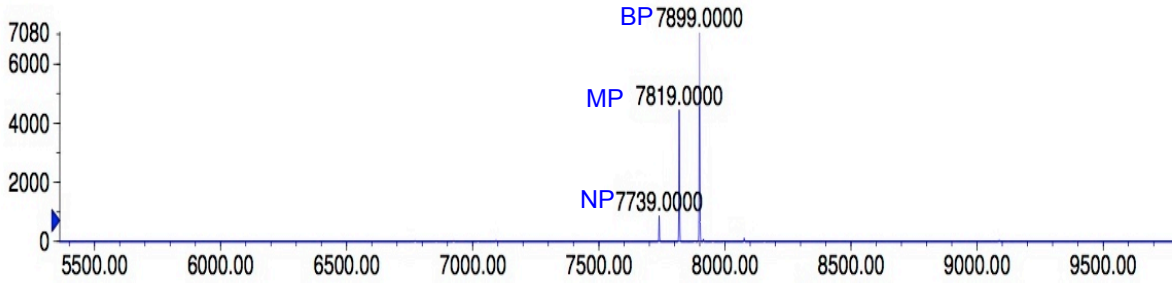

Figure 3.15 MS spectrum of β_3 integrin tails by Src. The largest peak represents the bis-phosphorylated β_3; NP (Non phosphorylated, MW of 7739); MP (mono-phosphorylated, MW of 7819 including the additional 79 Da due to single phosphate moiety); and BP (bis-phosphorylated, MW of 7899 with additional 158 Da due to double phosphate groups).

NMR sample preparation

The heteronuclear NMR experiments were performed on uniformly ^{15}N-labeled 0.1mM Src SH2 samples (unless mentioned otherwise), with or without binding partners (β_3CT BP full length / β_3CT $Y^{747}F$ and $Y^{759}F$ and their phosphorylated versions/β_3 derived phosphorylated peptide) at different concentrations on Varian Inova 600 MHz equipped with inverse-triple resonance cold probe at 30°C. The samples were prepared in pH 6 (unless mentioned otherwise) in the SEC buffer as above, with 10% D2O and 1mM DSS acting as an internal standard. Similar experiments were carried with non-phosphorylated β_3CT as a control. ^{15}N-HSQC titrations were also performed by titrating non-labeled Src SH2 into ^{15}N-labeled phosphorylated β_3 CT, to confirm binding from both sides. All the NMR data was processed by nmrPipe and analyzed by CCPN software suite. The structure of apo v-Src SH2 has been solved with NMR (BMRB accession: 6503) [50]. Using similar buffer conditions we were able to transfer about ~70% of assignments. Chemical shift assignments for β3BP were obtained from the previous studies performed by our lab [51].

3.6.3 Results

Through NMR binding studies, we demonstrate that SH2 domain of Src can interact with bis-phosphorylated β_3CT. Phosphorylation of β_3CT was achieved using a previously reported in vitro assay and confirmed using MS. Bi-phosphorylated tail was further separated using reverse phase HPLC. ^{15}N-labeled β3BP was titrated with NL Src SH2 at 1:1, 1:3 and 1:5 ratio of β_3BP to Src SH2 (Figure 3.16). The signals from residues ^{747}pYKEATST^{753} and R^{760} were broadened while G^{761} showed chemical shift perturbations (Figure 3.17). On the contrary, pY^{759} showed minimal perturbation. Additionally, control experiments with ^{15}N-β_3NP showed no such effect.

Further insights about the binding of β_3BP to the Src SH2 domain were obtained by recording ^{15}N-HSQC spectra of Src SH2 in the presence β_3BP and its (YtoF) mutants. Increasing concentration of β_3BP when titrated into ^{15}N-labeled Src SH2 domain showed reproducible and consistent chemical shift perturbations pattern at 1:1, 1:3 and 1:5 ratio, as shown in Figure 3.18. Additionally, we observed peak broadening effect in HSQC spectra, and few peaks disappeared completely. The associated chemical shift perturbations and broadened peaks were monitored and when mapped on the surface of the known structure (pdb: 1HCS) formed a continuous binding region onto the surface of SH2 (Figure 3.19).

Furthermore, we phosphorylated two different mutants, β_3 $Y^{747}F$ and $\beta_3Y^{759}F$, and studied the effect of mono-phosphorylated β_3 on the binding pattern. Despite some subtle differences in the chemical shift perturbation pattern, the spectral analysis of Src SH2 in the presence of β_3 $Y^{759}F$ (MP) showed a similar peak broadening effect as wild type (Figure 3.20 a). On the other hand, addition of β_3 $Y^{747}F$ (MP) resulted in spectral changes, whereby the peaks, which were broadened in wild type, now either reappeared or exhibited perturbations when compared with the spectra of apo Src SH2 (Figure 3.21 b). These results indicate that the presence of second phosphorylated tyrosine is not entirely essential, however, it may improve the overall binding of integrins to SH2 domain.

Additionally, we also performed ITC experiments using a peptide corresponding to bi-phosphorylated integrin (*RAKWDTANNPLpYKEATSTFTNITpYRGT*^{762}) as the titrant. We reached saturation within a few initial injections, thus further optimization is required to obtain a correct estimation of dissociation constant and other thermodynamic parameters.

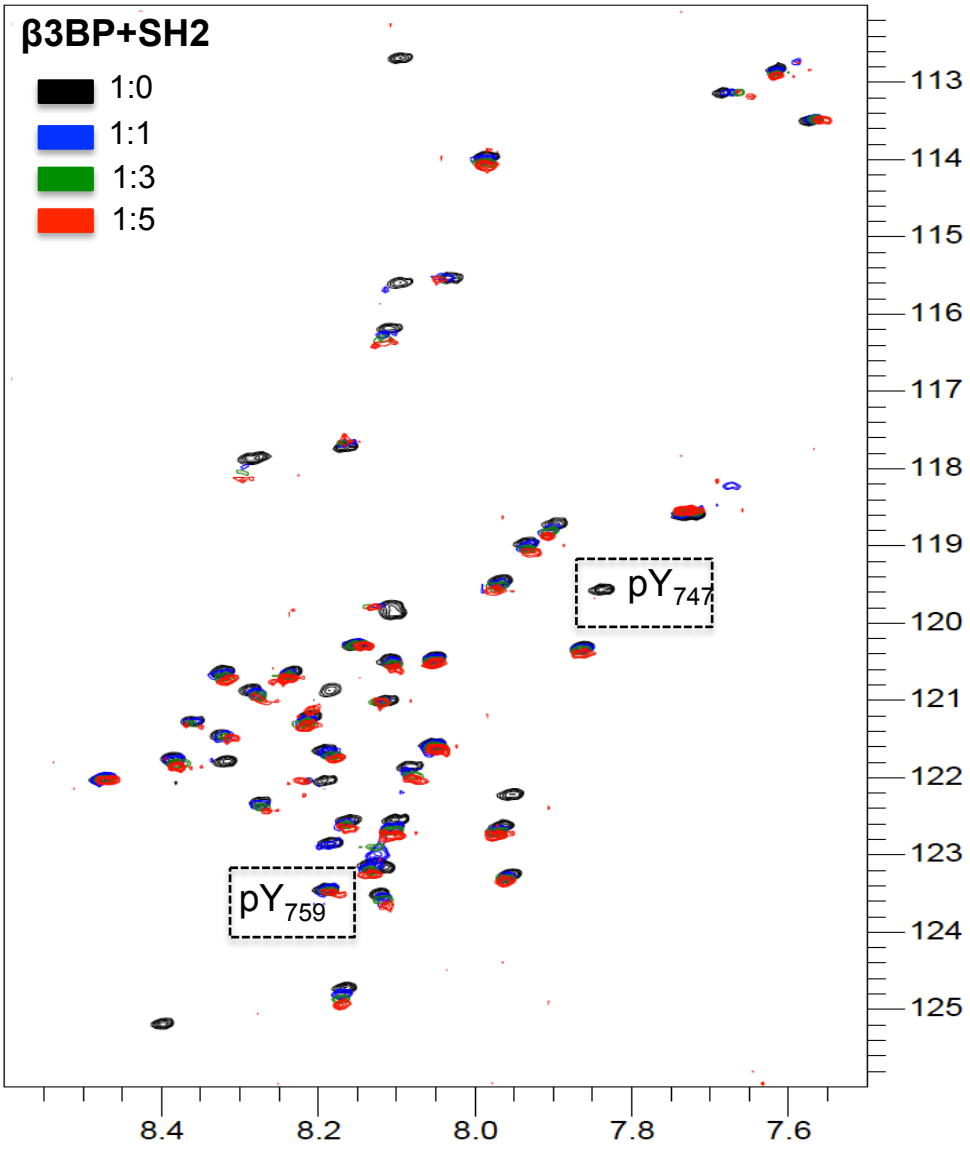

Figure 3.16 The superimposition of ^{15}N-HSQC spectra of β3BP (shown in black) in the presence of varying molar excess of Src SH2 as shown in blue (1:1), green (1:3) and red (1:5).

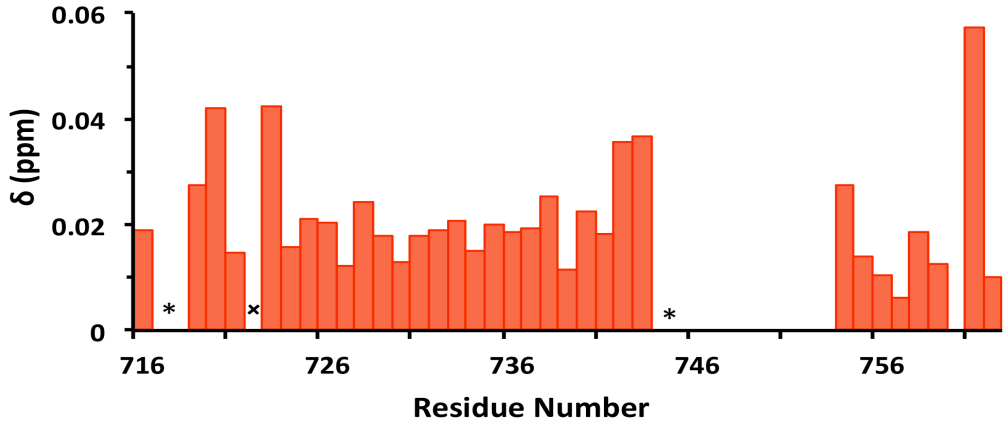

Figure 3.17 Chemical shift differences in β_3CT HSQC spectra upon SH2 binding at 1:5 molar ratio. The asterisk mark represents proline and overlapping residues. The x represents weak intensity signal in apo form, thus not included in analysis.

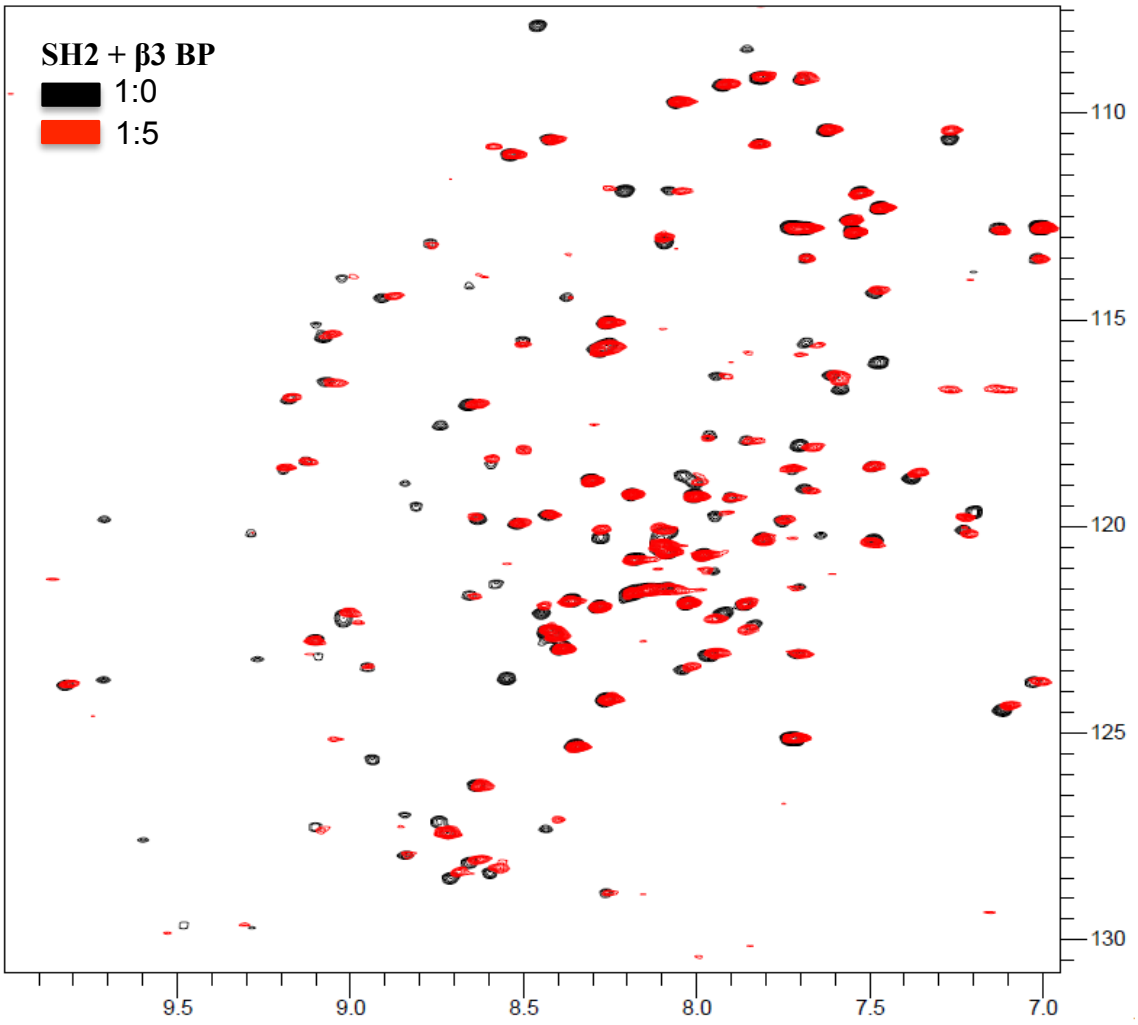

Figure 3.18 The superimposition of ^{15}N-HSQC spectra of Src SH2 (shown in black) in the presence of β_3 BP at 1:5 ratio (red).

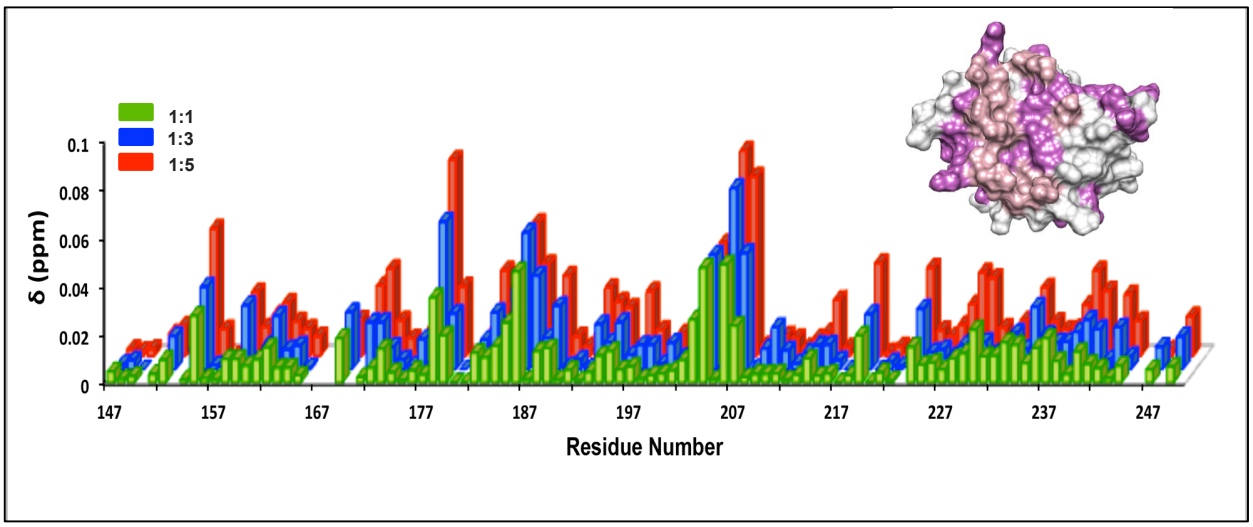

Figure 3.19 Chemical shift differences in ^{15}N Src SH2 spectra upon β_3 BP binding at varying ratios (Green 1:1, blue 1:3 and red 1:5 molar ratio. Delta (ppm) refers to the combined HN and N chemical shift changes according to the equation: $\Delta\delta(HN,N) = ((\Delta\delta HN2 + 0.2(\Delta\delta N)2)1/2$, where $\Delta\delta = \delta bound - \delta free$. The inset shows the chemical shift differences and broadened peaks (obtained from 1:5 ratio) mapped onto the surface of SH2 domain (PDB: 1HCS).

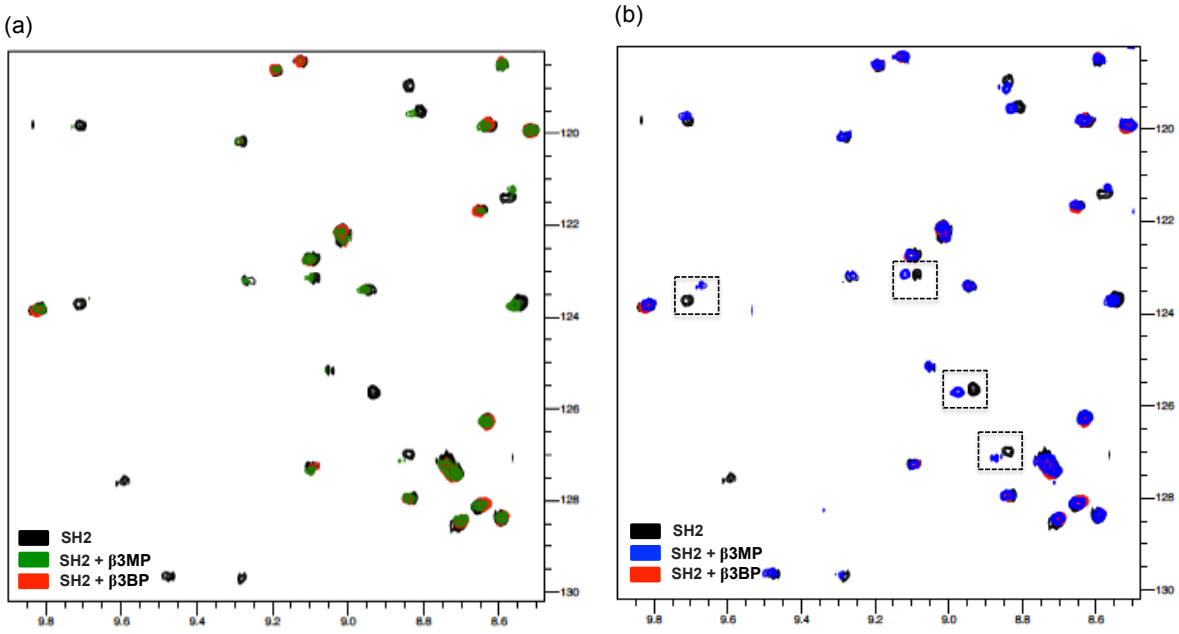

Figure 3.20 (a) The superimposition of ^{15}N-HSQC spectra of Src SH2 (shown in black) in the presence of β_3 $Y^{759}F$ (MP) (green) (b) The superimposition of ^{15}N-HSQC spectra of Src SH2 (shown in black) in the presence of β_3 $Y^{747}F$ (MP) (blue). The ^{15}N-HSQC spectra of Src SH2 in the presence of β_3 BP (red) is shown for comparison.

3.6.4 Discussion

The amino acids sequence following the phosphotyrosine residue play a vital role in defining the specificity of the peptides binding SH2 domain [52]. The pYEEI, a high affinity peptide has an optimal sequence for SH2 binding whereby residue Ile at +3 position sits into the hydrophobic pocket [48]. Integrin β_3 has two tyrosines present within its cytoplasmic tail, having pYKEATS and pYRGT motifs. Owing to the presence of a glutamate at +2 position (similar to YEEI) and alanine, a hydophobic residue at +3 position of the pY^{747}, we believe SH2 preferentially binds to it and allows it to sit into the phosphotyrosine-binding pocket of SH2.

Recently, Wu et al reported that activated β3 remain bound to c-Src, subsequent to which there is an increase in Src activity [15]. We, for the first time, identified the role of SH2 domain in binding to activated β3, characterized by phosphorylation of Y^{747} and Y^{759}. It is imperative to further study the molecular and structural details of this interaction in signaling pathway, and within the more complex cellular context.

In resting state, the intramolecular interaction between SH2 domain and pY^{527} bearing C-terminal tail of the kinase domain, maintain Src in a closed conformation [18]. Although, the sequence of events involved in β_3 mediated Src activation remains unclear, Src kinase activation has been achieved by disrupting this relatively weak interaction by using high affinity phosphopeptides [53]. On similar lines, we believe that phosphorylated β_3 can displace pY^{527} from SH2, thereby activating Src. It is logical to reason that binding of β_3 can directly displace pY^{527} or it may affect the dynamics/conformation of SH2, and ultimately increasing the kinase activity. Further experiments are needed to investigate the role of β_3 in displacing pY^{527}.

3.7 Conclusions and Future directions

Because the SH2 domain is a known phosphotyrosine-recognizing domain, we tested the ability of the phosphorylated β_3 to interact with the SH2 domain of c-Src. These results demonstrate that the phosphotyrosines and its adjacent residues are critical in mediating interaction between the SH2 domain and integrins. However, further experiments are necessary to confirm and characterize the interaction. In addition, we are proposing to utilize Nanodiscs, a discoidal nanolipoprotein with a phospholipid bilayer covered by an amphipathic protein coat. Nanodiscs, incorporated with and without phosphorylated β_3 will be titrated into ^{15}N-Src SH2 to study the interaction under membrane mimetic conditions.

3.8 References

1. Hynes, R.O., *Integrins: bidirectional, allosteric signaling machines.* Cell, 2002. **110**(6): p. 673-87.

2. Campbell, I.D. and M.J. Humphries, *Integrin Structure, Activation, and Interactions.* Cold Spring Harbor Perspectives in Biology, 2011. **3**(3): p. a004994.

3. Vinogradova, O., et al., *A structural mechanism of integrin alpha(IIb)beta(3) "inside-out" activation as regulated by its cytoplasmic face.* Cell, 2002. **110**(5): p. 587-97.

4. Moser, M., et al., *The Tail of Integrins, Talin, and Kindlins.* Science, 2009. **324**(5929): p. 895.

5. Shattil, S.J., C. Kim, and M.H. Ginsberg, *The final steps of integrin activation: the end game.* Nat Rev Mol Cell Biol, 2010. **11**(4): p. 288-300.

6. Vinogradova, O., et al., *A structural basis for integrin activation by the cytoplasmic tail of the α(IIb)-subunit.* Proceedings of the National Academy of Sciences of the United States of America, 2000. **97**(4): p. 1450-1455.

7. Arias-Salgado, E.G., et al., *Src kinase activation by direct interaction with the integrin beta cytoplasmic domain.* Proc Natl Acad Sci U S A, 2003. **100**(23): p. 13298-302.

8. Arias-Salgado, E.G., et al., *Specification of the direction of adhesive signaling by the integrin beta cytoplasmic domain.* J Biol Chem, 2005. **280**(33): p. 29699-707.

9. Legate, K.R. and R. Fassler, *Mechanisms that regulate adaptor binding to beta-integrin cytoplasmic tails.* J Cell Sci, 2009. **122**(Pt 2): p. 187-98.

10. Chen, L.M., D. Bailey, and C. Fernandez-Valle, *Association of beta 1 integrin with focal adhesion kinase and paxillin in differentiating Schwann cells.* J Neurosci, 2000. **20**(10): p. 3776-84.

11. Gorbatyuk, V., et al., *Skelemin Association with $\alpha_{IIb}\beta_3$ Integrin: A Structural Model.* Biochemistry, 2014. **53**(43): p. 6766-6775.

12. Calderwood, D.A., et al., *Integrin β cytoplasmic domain interactions with phosphotyrosine-binding domains: A structural prototype for diversity in integrin signaling.* Proceedings of the National Academy of Sciences, 2003. **100**(5): p. 2272-2277.

13. Songyang, Z., et al., *The Phosphotyrosine Interaction Domain of SHC Recognizes Tyrosine-phosphorylated NPXY Motif.* Journal of Biological Chemistry, 1995. **270**(25): p. 14863-14866.

14. Xiao, R., et al., *Structural framework of c-Src activation by integrin beta3.* Blood, 2013. **121**(4): p. 700-6.

15. Wu, Y., et al., *The Tyrosine Kinase c-Src Specifically Binds to the Active Integrin $\alpha_{IIb}\beta_3$ to Initiate Outside-in Signaling in Platelets.* The Journal of Biological Chemistry, 2015. **290**(25): p. 15825-15834.

16. Xu, W., et al., *Crystal structures of c-Src reveal features of its autoinhibitory mechanism.* Mol Cell, 1999. **3**(5): p. 629-38.

17. Boggon, T.J. and M.J. Eck, *Structure and regulation of Src family kinases.* Oncogene, 0000. **23**(48): p. 7918-7927.

18. Shattil, S.J., *Integrins and Src: dynamic duo of adhesion signaling.* Trends Cell Biol, 2005. **15**(8): p. 399-403.

19. Vogt, P.K., *Retroviral oncogenes: a historical primer.* Nat Rev Cancer, 2012. **12**(9): p. 639-48.

20. Bjorge, J.D., A. Jakymiw, and D.J. Fujita, *Selected glimpses into the activation and function of Src kinase.* Oncogene, 2000. **19**(49): p. 5620-5635.

21. Huveneers, S. and E.H. Danen, *The interaction of Src kinase with beta3 integrin tails: a potential therapeutic target in thrombosis and cancer.* ScientificWorld Journal, 2010. **10**: p. 1100-5.

22. Obergfell, A., et al., *Coordinate interactions of Csk, Src, and Syk kinases with [alpha]IIb[beta]3 initiate integrin signaling to the cytoskeleton.* J Cell Biol, 2002. **157**(2): p. 265-75.
23. Liu, S., D.A. Calderwood, and M.H. Ginsberg, *Integrin cytoplasmic domain-binding proteins.* J Cell Sci, 2000. **113 (Pt 20)**: p. 3563-71.

24. Legate, K.R., S.A. Wickstrom, and R. Fassler, *Genetic and cell biological analysis of integrin outside-in signaling.* Genes Dev, 2009. **23**(4): p. 397-418.

25. de Virgilio, M., W.B. Kiosses, and S.J. Shattil, *Proximal, selective, and dynamic interactions between integrin alphaIIbbeta3 and protein tyrosine kinases in living cells.* J Cell Biol, 2004. **165**(3): p. 305-11.

26. Law, D.A., L. Nannizzi-Alaimo, and D.R. Phillips, *Outside-in Integrin Signal Transduction: αβ-(GP IIb-IIIa) TYROSINE PHOSPHORYLATION INDUCED BY PLATELET AGGREGATION.* Journal of Biological Chemistry, 1996. **271**(18): p. 10811-10815.

27. Ablooglu, A.J., et al., *Antithrombotic effects of targeting alphaIIbbeta3 signaling in platelets.* Blood, 2009. **113**(15): p. 3585-92.

28. Hers, I., et al., *Inhibition of platelet integrin alpha(IIb)beta(3) by peptides that interfere with protein kinases and the beta(3) tail.* Arterioscler Thromb Vasc Biol, 2000. **20**(6): p. 1651-60.

29. Su, X., et al., *RGT, a synthetic peptide corresponding to the integrin beta 3 cytoplasmic C-terminal sequence, selectively inhibits outside-in signaling in human platelets by disrupting the interaction of integrin alpha IIb beta 3 with Src kinase.* Blood, 2008. **112**(3): p. 592-602.

30. Cordier, F., et al., *Ligand-induced strain in hydrogen bonds of the c-Src SH3 domain detected by NMR.* J Mol Biol, 2000. **304**(4): p. 497-505.

31. Yu, H., et al., *Solution structure of the SH3 domain of Src and identification of its ligand-binding site.* Science, 1992. **258**(5088): p. 1665-8.

32. Mayer, B.J., *SH3 domains: complexity in moderation.* J Cell Sci, 2001. **114**(Pt 7): p. 1253-63.

33. Zarrinpar, A., R.P. Bhattacharyya, and W.A. Lim, *The structure and function of proline recognition domains.* Sci STKE, 2003. **2003**(179): p. RE8.

34. Feng, S., et al., *Two binding orientations for peptides to the Src SH3 domain: development of a general model for SH3-ligand interactions.* Science, 1994. **266**(5188): p. 1241-7.

35. Kishan, K.V., et al., *The SH3 domain of Eps8 exists as a novel intertwined dimer.* Nat Struct Biol, 1997. **4**(9): p. 739-43.
36. Mongiovi, A.M., et al., *A novel peptide-SH3 interaction.* EMBO J, 1999. **18**(19): p. 5300-9.

37. Kami, K., et al., *Diverse recognition of non-PxxP peptide ligands by the SH3 domains from p67(phox), Grb2 and Pex13p.* EMBO J, 2002. **21**(16): p. 4268-76.

38. Vranken, W.F., et al., *The CCPN data model for NMR spectroscopy: development of a software pipeline.* Proteins, 2005. **59**(4): p. 687-96.

39. Baker, E.K., et al., *A genetic analysis of integrin function: Glanzmann thrombasthenia in vitro.* Proc Natl Acad Sci U S A, 1997. **94**(5): p. 1973-8.

40. Phillips, D.R., et al., *Effect of Ca2+ on GP IIb-IIIa interactions with integrilin: enhanced GP IIb-IIIa binding and inhibition of platelet aggregation by reductions in the concentration of ionized calcium in plasma anticoagulated with citrate.* Circulation, 1997. **96**(5): p. 1488-94.

41. Kelly, M.A., et al., *Host-guest study of left-handed polyproline II helix formation.* Biochemistry, 2001. **40**(48): p. 14376-83.

42. Rucker, A.L. and T.P. Creamer, *Polyproline II helical structure in protein unfolded states: lysine peptides revisited.* Protein Sci, 2002. **11**(4): p. 980-5.

43. de Vries, S.J., M. van Dijk, and A.M. Bonvin, *The HADDOCK web server for data-driven biomolecular docking.* Nat Protoc, 2010. **5**(5): p. 883-97.

44. Dominguez, C., R. Boelens, and A.M. Bonvin, *HADDOCK: a protein-protein docking approach based on biochemical or biophysical information.* J Am Chem Soc, 2003. **125**(7): p. 1731-7.

45. Katyal, P., R. Puthenveetil, and O. Vinogradova, *Structural insights into the recognition of beta3 integrin cytoplasmic tail by the SH3 domain of Src kinase.* Protein Sci, 2013. **22**(10): p. 1358-65.

46. Waksman, G., et al., *Binding of a high affinity phosphotyrosyl peptide to the Src SH2 domain: crystal structures of the complexed and peptide-free forms.* Cell, 1993. **72**(5): p. 779-90.

47. Songyang, Z., et al., *SH2 domains recognize specific phosphopeptide sequences.* Cell, 1993. **72**(5): p. 767-78.

48. Xu, R.X., et al., *Solution Structure of the Human pp60c-src SH2 Domain Complexed with a Phosphorylated Tyrosine Pentapeptide.* Biochemistry, 1995. **34**(7): p. 2107-2121.

49. Anthis, N.J., et al., *β Integrin Tyrosine Phosphorylation Is a Conserved Mechanism for Regulating Talin-induced Integrin Activation.* The Journal of Biological Chemistry, 2009. **284**(52): p. 36700-36710.

50. Taylor, J.D., et al., *NMR assignment of the apo and peptide-bound SH2 domain from the Rous sarcoma viral protein Src.* J Biomol NMR, 2005. **32**(4): p. 339.

51. Deshmukh, L., et al., *Tyrosine Phosphorylation as a Conformational Switch: A CASE STUDY OF INTEGRIN β3 CYTOPLASMIC TAIL.* Journal of Biological Chemistry, 2011. **286**(47): p. 40943-40953.

52. Gan, W. and B. Roux, *Binding Specificity of SH2 Domains: Insight from Free Energy Simulations.* Proteins, 2009. **74**(4): p. 996-1007.

53. Mandine, E., et al., *High-affinity Src-SH2 ligands which do not activate Tyr527-phosphorylated Src in an experimental in vivo system.* Biochemical and Biophysical Research Communications, 2002. **298**(2): p. 185-192.

Chapter 4. Binding and Backbone Dynamics of Protein under Topological Constrain: Calmodulin as a Model System

4.1 Introduction

Over the last twenty years, hundreds of cyclized proteins (i.e., N- and C- termini linked together), have been identified in nature and implicated in a wide range of biological activities [1, 2]. Owning to their unique folding topology, circular proteins show remarkable thermal, chemical, and enzymatic stability [3, 4]. A few cyclic derivatives of polypeptides and larger proteins have been developed using various methods [4-6], resulting in enhanced resistance toward denaturation and proteolysis when compared with their linear counterparts. While much progress has been made in elucidating the structure and corresponding biological activities of circular proteins [7, 8], the physical basis of how the circular topology modulate the functions of proteins (e.g., molecular recognitions) remain elusive. Particularly, how does the topological constrain affect the protein's internal dynamics and subsequently, their thermodynamic properties. It is conceivable that the circularization of a protein with flexible ends may reduce its conformational entropy. Since the changes of protein conformational entropy are potentially linked to the free energy of protein-ligand association, the circularization may change the binding affinity of the protein to its receptor. Herein, we attempt to understand the effect of circularization on protein dynamics and molecular recognition using calmodulin (CaM) as a model system.

The use of CaM as the model system is based on the fact that it is an extensively studied protein known to interact with a variety of target proteins involved in many aspects of cellular function [9]. CaM is composed of two, N- and C-, globular lobes, each containing a pair of helix-loop-helix motifs (EF-hands) that bind calcium ions. When bound to four calcium ions, CaM adopts a

dumbbell configuration comprising of two lobes tethered by a central flexible linker (Figure 4.1 (a)) [10, 11]. Upon binding to target proteins, the flexibility of the central linker (residues 78–81) allows the two lobes to adjust their relative orientation, resulting in the collapse of CaM into a more rigid globular fold (Figure 4.1 (b)) [12]. This mechanism is sometimes referred to as the wrap-around mode of binding [12, 13]. Since CaM undergoes a large conformational change upon binding, we wanted to investigate whether cyclization affect the binding and dynamic behavior of calmodulin.

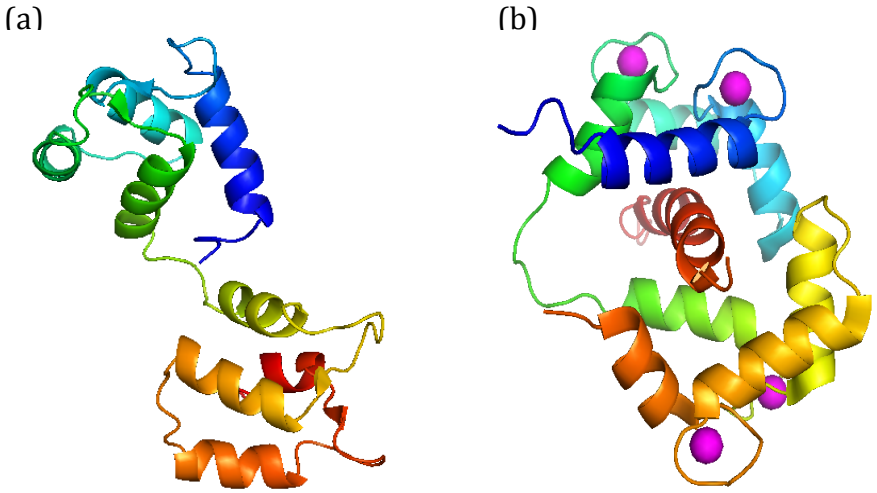

Figure 4.1 (a) NMR structure of Calmodulin. The N- and C-lobe are connected by the central linker (b) NMR structure of the complex of Ca^{2+}-CaM with the smMLCK peptide. The N- and C-lobe wraps around the smMLCK peptide (red helix) (PDB: 2K0F).

We investigated CaM interactions, in its linear and artificial cyclized forms, with its natural ligand by isothermal titration calorimetry (ITC). We found that the cyclization affects the enthalpy of calmodulin binding to its ligand, which is compensated by a favorable change in the entropy of calmodulin binding to its ligand, although the overall binding affinity of interaction remains the same. Since the conformational entropy of proteins is manifested as the motion between different structural states, characterization of protein dynamics provides a means to measure conformational entropy. Thus, we use nuclear magnetic resonance spectroscopy (NMR)

to compare the backbone dynamics of the CaM constructs in both the linear and circularized states. We observed a small reduction in the flexibility of CaM, which may contribute to the lower conformational entropy. The effect of cyclization was more pronounced in the C-lobe with a slight increase in rigidity of the central loop.

4.2. Experimental Section

Expression and purification

The gene encoding modified CaM was ordered from GenScript, in which the His_6-tag, thrombin cleavage site and a peptide sequence (LCTPSR) were placed at the N-terminus of calmodulin (residues 2-149, Uniprot P62161). Another similar peptide sequence (LCTPSR) was placed at the C-terminus just before the stop codon. The gene was inserted into the pET-28b vector (Novagen) between the NcoI and XhoI restriction sites. The resulting plasmid was -transformed in the BL21(DE3) cells (Invitrogen). The cells were incubated in LB media with kanamycin with shaking at 37°C until OD_{600} = 0.6. The temperature was lowered to 18 °C, and 100 μM IPTG was added to induce expression of the CaM. The cells were harvested by centrifugation after 12-16h. His_6-tagged CaM was purified using Ni-agarose resin (Thermo Scientific) in Tris buffer, pH 8, 300mM NaCl. Purifed CaM was then eluted using a concentration gradient of imidazole (concentration ranging from 5mM to 1M). Eluates were subjected to SDS-PAGE analysis and fractions containing CaM were pooled and extensively dialyzed using 20mM Tris, pH 8. The dialyzed sample was further purified using anion exchange chromatography (Resource Q) and the peak corresponding to CaM was further purified through HiLoad 16/60 Superdex 75 column (GE Healthcare) equilibrated with 100mM KCl, pH 6.3.

Isothermal Titration Calorimetry (ITC)

Isothermal titration calorimetry was performed on a low volume Nano ITC, manufactured by TA instruments, USA. The (smMLCKp) peptide ARRKWQKTGHAVRAIGRLSS, corresponding to the calmodulin binding region of smooth muscle myosin light chain kinase, was synthesized by Applied Biosystems, Inc., and further purified by reverse phase HPLC. All experiments were carried out in 20 mM phosphate buffer, pH 6.3, 100 mM KCl, 6.1 mM $CaCl_2$ at 35°C with a stirring speed of 200 rpm. Each titration consisted of twenty 2.5 µl injections with 300 s time intervals. As a control, the heat of dilution was also measured by injecting peptide into buffer solution containing no CaM. The heat of binding was obtained as the difference between the heat of reaction and the corresponding heat of dilution. Data analysis was done in NanoAnalyze Software suite using an "independent" model. In all cases, a stoichiometry of 1 ± 0.1 was revealed.

Differential scanning calorimetry (DSC)

The purified linear and cyclic CaM at concentrations of 0.3 mM were used for the experiments. The samples were referenced against the buffer obtained as a filtrate from the concentration step. Prior to the run, the samples were degassed using vacuum degasser. Thermograms were obtained by scanning from 10 to 130°C at 1°C/h (scanning rate) at a constant pressure of 3 atm. In total, three sets of heating, cooling cycles were done using NanoDSC (TA Instruments, USA). The data was corrected for baseline with a thermogram obtained from the buffer scans.

NMR Spectroscopy

To produce ^{13}C and ^{15}N isotopically labeled CaM, cells were grown in M9 minimal media containing ^{13}C glucose (2.5g/ltr) and $^{15}NH_4Cl$ (1.1g/ltr) as the sole source of carbon and nitrogen. NMR samples were prepared as described in Barbato et al [11]. Briefly, a 1mM CaM was prepared in 95% H_2O/5% D_2O, 6.1mM $CaCl_2$, and 100mM KCl, pH 6.3. The backbone ^{1}H, ^{13}C,

and ^{15}N resonances were assigned based on triple-resonance experiments: HNCA, HNCO, HNCACB, HN(CO)CA, HN(CA)CO and CBCA(CO)NH, collected using Varian/Agilent BioPack sequences.

Heteronuclear–^{15}N NOEs, longitudinal (R1), and transverse (R2) ^{15}N relaxation rates were measured using standard two-dimensional methods [14]. Steady-state hetero-nuclear ^{1}H-^{15}N NOE values were determined from spectra recorded with 3s relaxation delay and in the presence and absence of a proton presaturation period of 4s. ^{15}N-T1 values were measured from the spectra recorded with 7 different durations relaxation delays of T= 0.03, 0.08, 0.14, 0.3, 0.5, 0.85 and 1ms. ^{15}N-T_2 values were determined from the spectra recorded with 7 different durations of the delay: T= 0.01, 0.03, 0.05, 0.09, 0.13, 0.170 and 0.25ms. T1, T2 and NOE values were extracted by a curve-fitting subroutine included in the CCPN software suite[15]. All experiments were performed at 35°C on 600 MHz magnet (Agilent, USA) equipped with inverse-triple resonance cold probe. All spectra were processed with NMRPipe [16] and analyzed by CCPN software suite. The generalized order parameter (S^2) was obtained using the FAST-modelfree program [17].

4.3 Results

4.3.1 CaM Constructs Design and the Evidence of Cyclization

We added a sequence (LCTPSR) at both the N- and C-termini of calmodulin, which appeared to be sufficient for the formation of disulfide bond between the two cysteines (Cys) to facilitate the cyclization of the protein (Figure 4.2 a). CaM circularization, via the oxidation of the two introduced Cys occurred spontaneously during the purification process. Examining the protein by sodium dodecyl sulfate polyacrylamide gel electrophoresis (SDS-PAGE) shows that the CaM existed in a circular form in solution, with the N- and C- termini connected (Lane 5 in Figure 4.2

b). The disulfide link is stable against the temperature changes up to 95˚C (Lane 7). The reduced counterpart is only obtained by adding β-ME with simultaneous heating the protein (Lane 8). The CaM in its cyclic form (c-CaM) is well separated from the reduced form in the SDS-PAGE as the result of the changes in its electrophoretic mobility by circularization. The electrophoretic mobility of the linear CaM (l-CaM), where cysteines have been mutated to alanines, is shown in lanes 1-4 and resembles that of the reduced c-CaM (Lane 8). The molecular weights of cyclized and linear CaM were measured using MS and the presence of disulfide linkage within c-CaM was confirmed by MS/MS. The thermal stability of the calcium saturated linear and circular CaM were examined by Differential scanning calorimetry (DSC). Though we were able to estimate the transition temperatures, *Tm,* complete analysis of the calorimetric data was not performed owing to the limitations with data fitting at higher temperatures. The transition temperatures of linear and cyclic CaM were found to be similar, 113˚C and 114˚C respectively (Figure 4.3), demonstrating high thermal stability for both the constructs. Interestingly, in addition to the major peak the melting curve of c-CaM, depicts an additional shoulder peak at 95˚C. We speculate that this peak arises from the breakage of the disulfide bond present within the cyclic CaM and may reflect the separation of N and C domains. However, the overall thermal stability of CaM is not significantly affected upon cyclization, which is not extraordinary owing to the resistance of CaM to heat denaturation in calcium-loaded state [18].

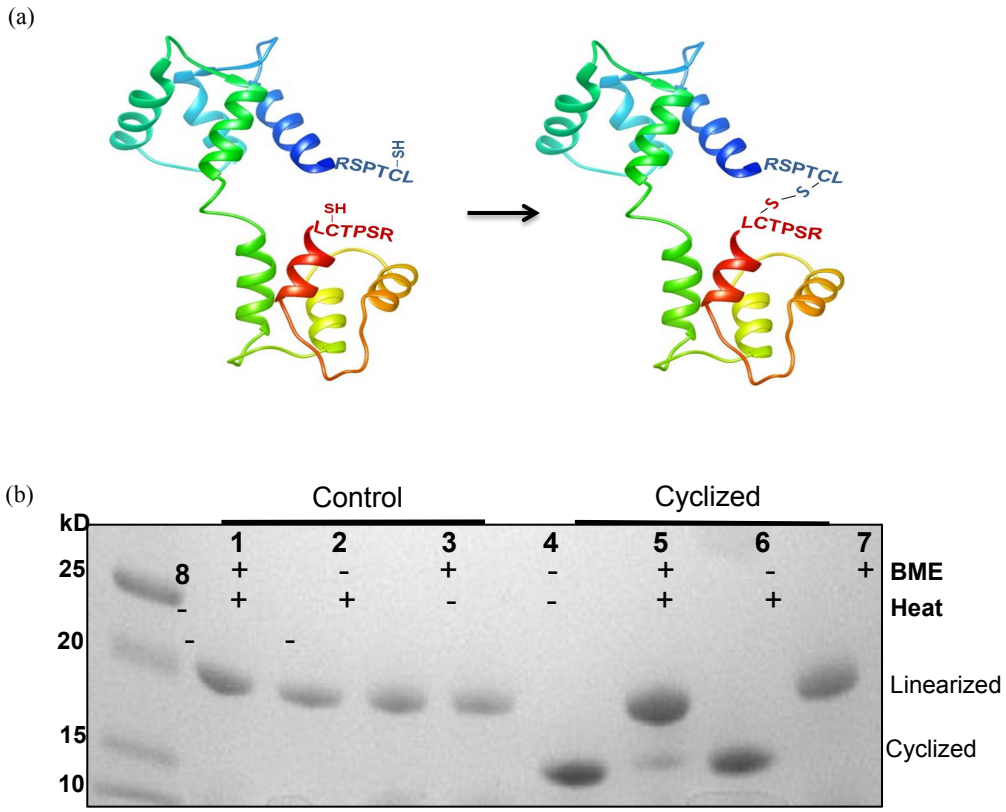

Figure 4.2 (a) Scheme for CaM cyclization showing the additional peptide sequence added to facilitate disulfide bond formation, and (**b**) CaM migration patterns on SDS-PAGE gel under different sample conditions. Control represents Linear CaM where both the Cys are mutated to alanine.

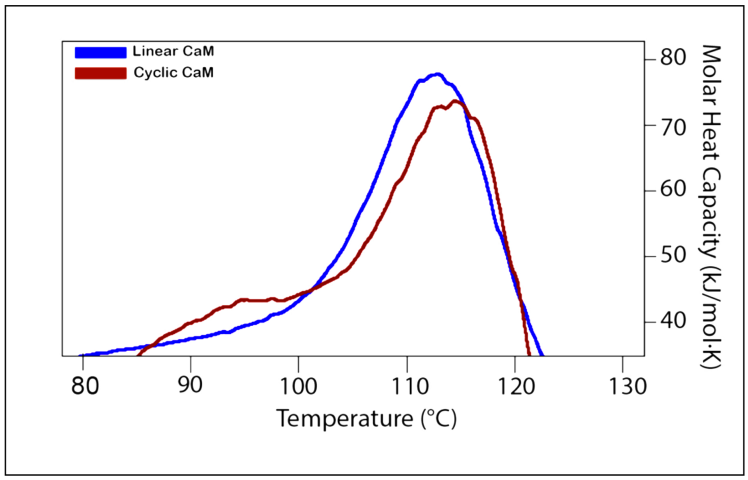

Figure 4.3 DSC thermograms of linear calmodulin (blue) and cyclic CaM (red)

4.3.2 Molecular recognition

We used ITC to study the interaction of calcium-saturated linear and cyclic CaM constructs with its well established ligand, a peptide representing the calmodulin-binding domain of the smooth muscle myosin light chain kinase (smMLCKp). Figure 4.4 presents binding isotherms at 35°C for the linear (Figure 4.4 a) and cyclic (Figure 4.4 b) forms of the protein, respectively. Changes in the Gibbs free energy (ΔG) for the formation of CaM-peptide complex, and the contributions from enthalpy (ΔH) and entropy ($-T\Delta S$) derived from the isotherms are shown in Figure 4.4 c. Binding of smMLCKp to l-CaM is dominated by a large favorable change in the binding enthalpy, which compensates the unfavorable change in the binding entropy. Upon cyclization, the enthalpy term is significantly reduced. However, the associated loss in the overall binding enthalpy is compensated by the change in the entropy term, converting it from unfavorable to a favorable factor promoting the interaction. Thus, the overall ΔG of ligand binding remains very similar between the two constructs (Table 1).

Thermodynamic Factor	Linear CaM (kJ/mol)	Cyclic Cam (kJ/mol)
ΔG	-39.24	-39.46
ΔH	-57.04	-15.06
-TΔS	17.8	-24.4

Table 4.1 Thermodynamic profiles of smMLCK peptide binding to linear and cyclic Calmodulin.

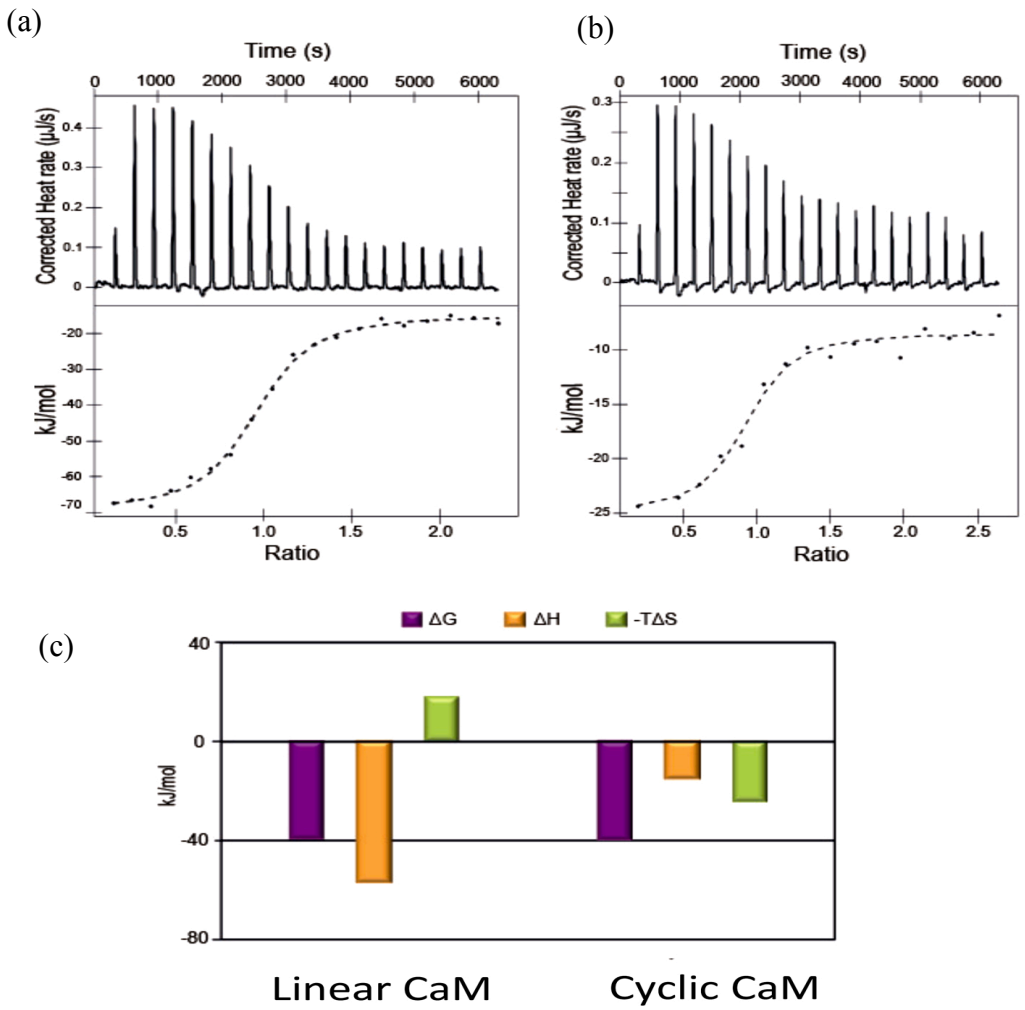

Figure 4.4 Traces of the calorimetric titration and the binding isotherms obtained for **(a)** l-CaM and **(b)** c-CaM with peptide ligand, smMLCKp, at 35 °C **(c)** Comparison of the thermodynamic origins for smMLCKp binding to the l-CaM and c-CaM.

Binding of calcium-saturated linear and cyclic CaM was also compared using chemical shifts mapping experiments, through ^{15}N-HSQC spectra, where non-labeled smMLCK peptide was titrated into ^{15}N-labeled CaM. This titration was performed at CaM to smMLCKp molar ratios of 1:2 at a pH 6.3. The chemical shift perturbations observed for our modified l-CaM construct (Figure 4.5) are consistent with CaM binding to smMLCK peptide previously observed [11]. The effect was similar for c-CaM construct (Figure 4.5), suggesting that the topological constrain did not impede the formation of a collapsed globular structure of CaM in the presence of smMLCK peptide.

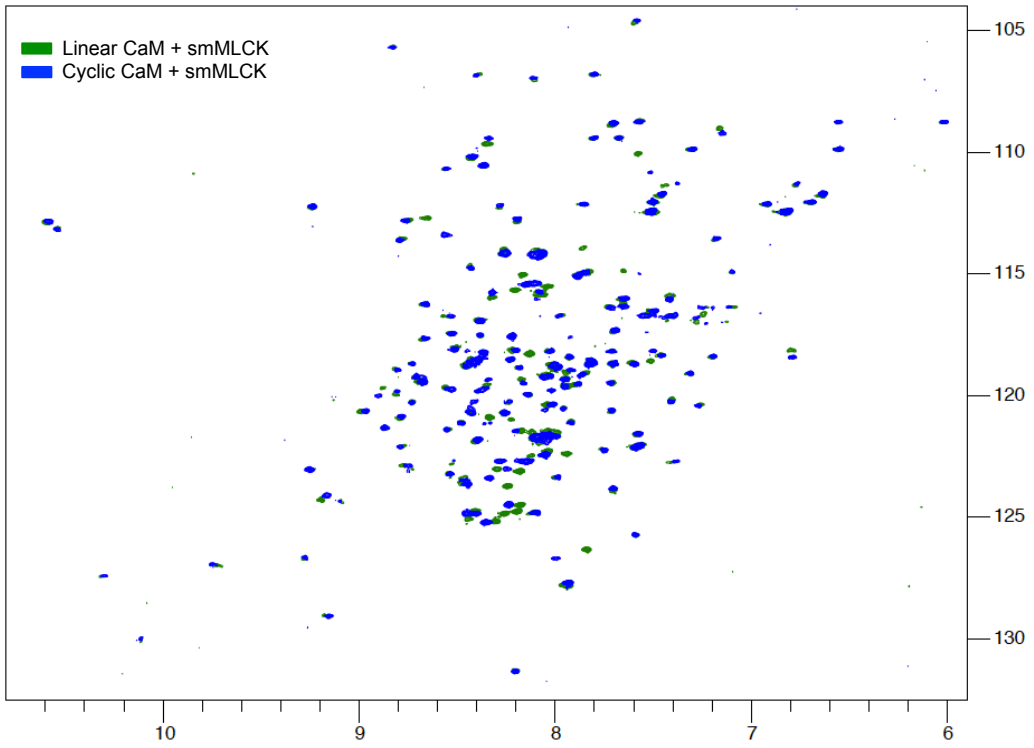

Figure 4.5 The superimposition of ^{15}N-HSQC spectra of linear CaM (shown in green) and cyclic CaM (blue) in the presence of smMLCK at a ratio of 1:2.

4.3.3 Backbone Dynamics

To assess the backbone dynamics of c-CaM and l-CaM we used ^{15}N relaxation experiments (Figure 4.6). The amide ^{15}N relaxation rates, R_1 and R_2, and the steady-state heteronuclear ^{15}N $\{^1H\}$ NOEs are influenced by the local backbone dynamics on a time scale ranging from picoseconds to nanoseconds [14]. The order parameter (S^2), which describes the amplitude of fast motions experienced by the individual NH bond vectors, was obtained using Model-free approach for l-CaM and c-CaM (Figure 4.7 (a) and 4.7(b)[17]. High S^2 values, approaching 1, indicate limited motions and greater rigidity, whereas lower values indicate larger amplitude of motions and more flexibility [11]. The residues showing spectral overlap in the ^{15}N-HSQC and those associated with erroneous values in Model-free fitting (error >10%) were omitted from the relaxation analysis. As shown in Figure 4.7, the S^2 values were very similar for the N–terminal domain and for most of the residues within the C-lobe. Although we expected a greater rigidity of the central helix, we observed only a slight reduction in the mobility of the central linker residues upon cyclization. In comparison to the linear CaM, the loops present within the C-lobe of the cyclized form experience a considerable loss in their flexibility, possibly due to their proximity to the cyclization site.

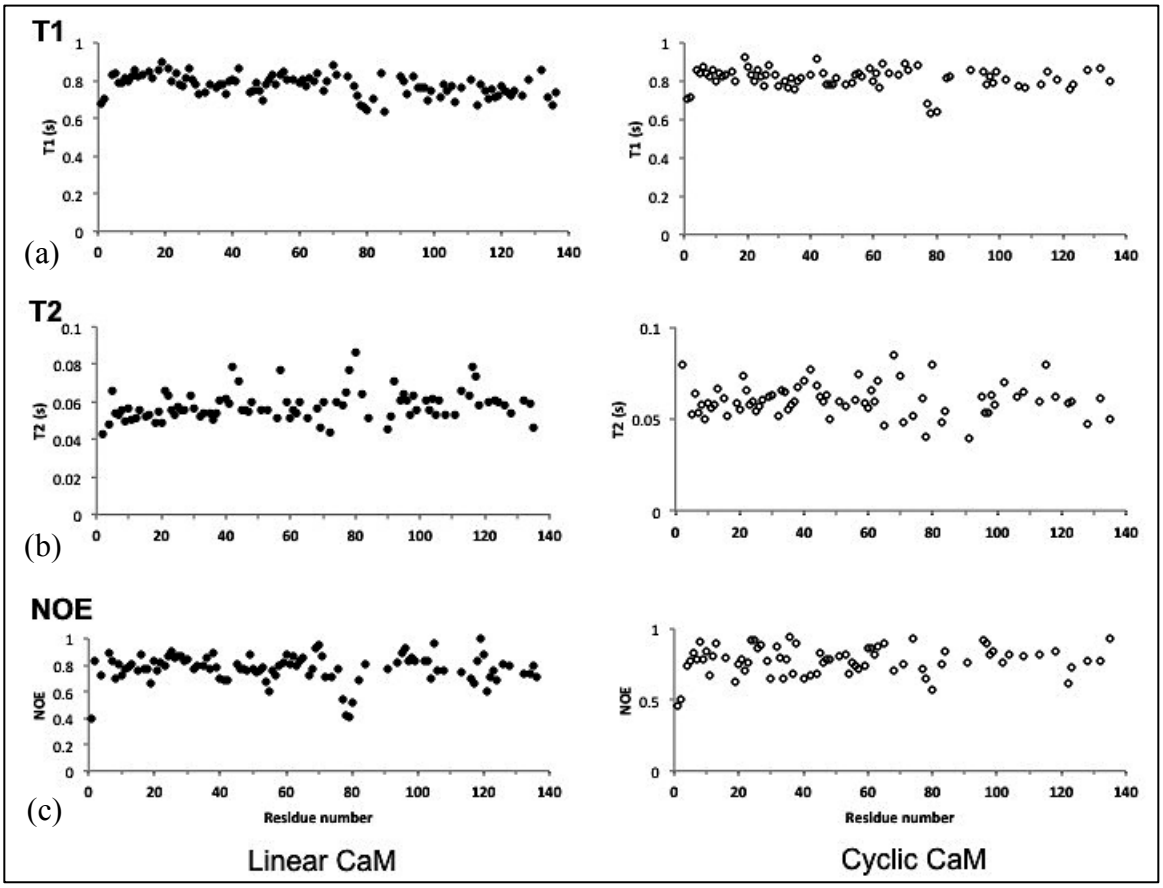

Figure 4.6 (a)-(c) Comparison of the ^{15}N relaxation time, T1, T2, and heteronuclear NOE measured at 600 MHz for the linear CaM and cyclic CaM.

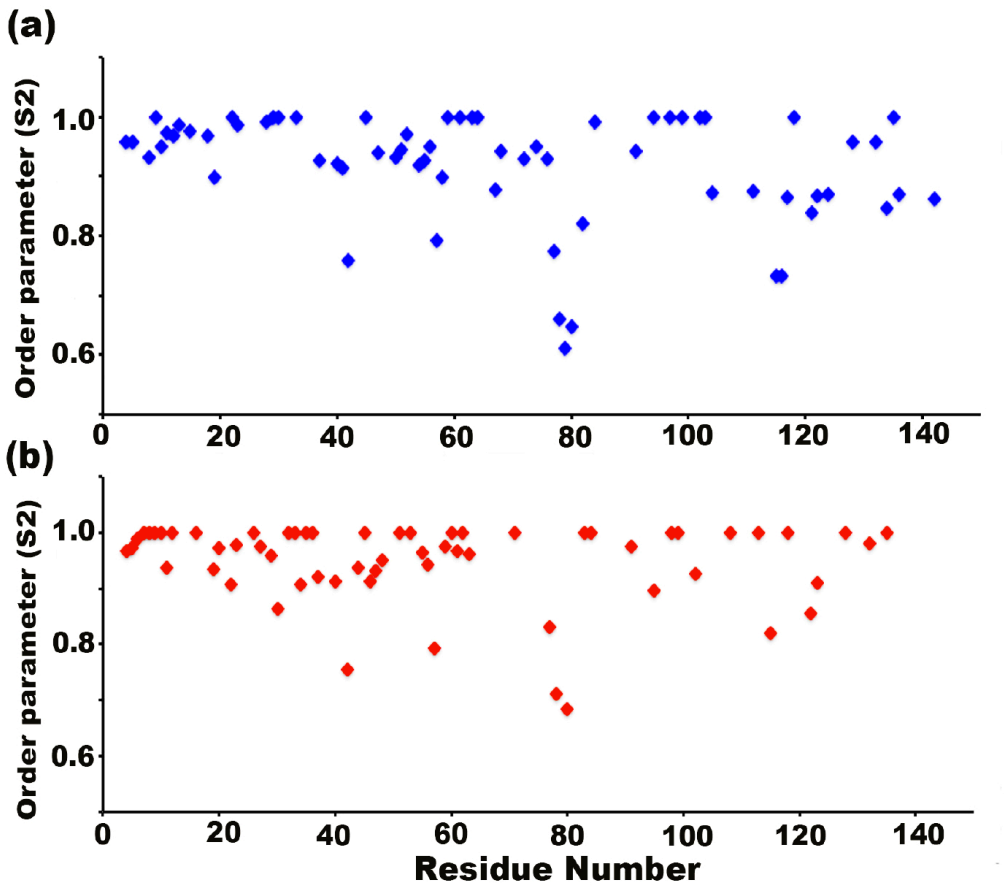

Figure 4.7 Plots of the order parameter (S^2) values with respect to residue number of (a) l-CaM and (b) c-CaM. S^2 values are calculated using FAST model free software using R1, R2 and NOE relaxation data [17].

4.4 Discussion

The concept of protein cyclization has been increasingly appreciated as cyclic variants exhibit higher thermal stability and resistance to proteases, thus resulting in an overall better stability of potential biologicals. Different strategies towards this ultimate goal have adopted from the ones employed by nature and/or designed *de novo*. In particular, adding cysteine containing short peptides to the N- and C-termini have been found successful in circularization of the protein without affecting its overall fold and biological activities [6]. Similarly, we were able to obtain a cyclic protein by introducing cysteine-containing sequence (LCTPSR) at the N- and C- termini of the protein. Since wild type calmodulin does not bear native cysteine residues [19], the formation of a disulfide bond only occurred between the two cysteines we incorporated at the extensions of the N- and C-termini. Previous studies by Tan *et al*, demonstrated the abrogation of nanomolar (nM) binding affinity of CaM to its ligand, when cysteine mutations were introduced within the structure of CaM [20]. In contrast, the modified -CaM used in the present study, maintained its binding profile with the smMLCK peptide, though the dissociation constant (K_d) is only slightly increased (from few nanomolars to hundreds of nanomolars). Thus, our modified versions of CaM constructs mimic the native system with minimal perturbations in its three-dimensional conformations.

According to the previous calorimetric studies, interactions of CaM with different peptides are usually driven by a large favorable change in enthalpy [21]. However, in some cases the enthalpic term is also accompanied by a favorable change in entropy [9]. Thus, the binding interface of calmodulin is thermodynamically fluid and has been a subject of wide interest and extensive investigations in the field [10, 21-23]. Our ITC results indicate that the backbone cyclization of CaM results in an enthalpic-entropic compensation, and, thereby, shifting the

enthalpy driven process to, largely, the entropy driven interaction. As conformational entropy of backbone residues can be assessed using the established relationship of NMR-derived order parameter and entropy [24], we used NMR spectroscopy to study the relaxation properties of the circularized CaM.

The ^{15}N relaxation data allowed us to calculate S^2, the order parameter representing the degree of flexibility. The S^2 values obtained for the residues of linear CaM follow the same trend as the ones of the wild type (wt) CaM, though the average absolute values are slightly higher due to increase in the size of our constructs. The l-CaM has S^2 value of 0.94 for the N-terminal domain and 0.89 for the C-terminal domain. However, for the cyclized CaM, the values for N- and C-terminal domains were found to be 0.95 and 0.94, respectively. This is indicative of a reduction in flexibility of C-terminal domain of calmodulin upon cyclization. Previous studies by Barbato *et al* on wt CaM have shown that the N- and the C-domain of CaM behave isotropically while the residues in the central helix exhibit a high degree of flexibility [11]. Due to the bigger size of our constructs, the S^2 values for l-CaM and C-CaM are on the upper limit, restraining our ability to calculate conformational entropy using the classical approach.

It appears that C-lobe of l-CaM possesses greater backbone mobility, which is considerably reduced upon cyclization and may get further reduced upon binding to the smMLCKp. Thus for c-CaM, the reduced backbone mobility may confer entropic advantages to the ligand binding. On the other hand, the linear counterpart experiences a strong network of hydrogen bonding (as indicated by enthalpy change) while at the same time; it has to undergo a tremendous conformational change to form a compact structure. The total change in entropy also entails the contribution from side chains as upon binding to smMLCK peptide, the side chains of wt CaM

has been shown to exhibit a range of motion[25], while the backbone dynamics of wt CaM gets minimally perturbed.

4.5 Conclusions and future directions

CaM, a calcium modulated protein was modified using a disulfide linkage. A subtle change in the structure was enough to alter the enthalpy-entropy contributions, however, it was remarkable to observe that the free energy remain constant. To further qualify these changes, we studied the backbone dynamics of CaM. Despite the conformational change of the protein, the flexibility of backbone residues weren't significantly affected. Previous studies identified that dynamics of side chains (of wt-CaM) contribute significantly to the binding of smMLCK. It would be useful to study the dynamics of side chain residues and identify the factors contributing to the enthalpy-entropy compensation. Besides, one can also perform H-D exchange experiments in apo and bound forms to study the effect of solvation that contributes significantly to the entropy term.

4.6 References

1. Mulvenna, J.P., C. Wang, and D.J. Craik, *CyBase: a database of cyclic protein sequence and structure.* Nucleic acids research, 2006. **34**(Database issue): p. D192-4.

2. Wang, C.K.L., et al., *CyBase: a database of cyclic protein sequences and structures, with applications in protein discovery and engineering.* Nucleic acids research, 2008. **36**(Database issue): p. D206-10.

3. Trabi, M. and D.J. Craik, *Circular proteins--no end in sight.* Trends in biochemical sciences, 2002. **27**(3): p. 132-8.

4. Iwai, H. and A. Pluckthun, *Circular beta-lactamase: stability enhancement by cyclizing the backbone.* FEBS letters, 1999. **459**(2): p. 166-72.

5. Iwai, H., A. Lingel, and A. Pluckthun, *Cyclic green fluorescent protein produced in vivo using an artificially split PI-PfuI intein from Pyrococcus furiosus.* The Journal of biological chemistry, 2001. **276**(19): p. 16548-54.

6. Iwakura, M. and S. Honda, *Stability and reversibility of thermal denaturation are greatly improved by limiting terminal flexibility of Escherichia coli dihydrofolate reductase.* Journal of biochemistry, 1996. **119**(3): p. 414-20.

7. Camarero, J.A., et al., *Rescuing a destabilized protein fold through backbone cyclization.* J Mol Biol, 2001. **308**(5): p. 1045-62.

8. Grantcharova, V.P. and D. Baker, *Circularization changes the folding transition state of the src SH3 domain.* Journal of molecular biology, 2001. **306**(3): p. 555-63.

9. Marlow, M.S., et al., *The role of conformational entropy in molecular recognition by calmodulin.* Nature chemical biology, 2010. **6**(5): p. 352-8.

10. Andre, I., et al., *Salt enhances calmodulin-target interaction.* Biophys J, 2006. **90**(8): p. 2903-10.

11. Barbato, G., et al., *Backbone dynamics of calmodulin studied by* ^{15}N *relaxation using inverse detected two-dimensional NMR spectroscopy: the central helix is flexible.* Biochemistry, 1992. **31**(23): p. 5269-78.

12. Roth, S.M., et al., *Structure of the smooth muscle myosin light-chain kinase calmodulin-binding domain peptide bound to calmodulin.* Biochemistry, 1991. **30**(42): p. 10078-84.

13. Papish, A.L., L.W. Tari, and H.J. Vogel, *Dynamic light scattering study of calmodulin-target peptide complexes.* Biophys J, 2002. **83**(3): p. 1455-64.

14. Kay, L.E., D.A. Torchia, and A. Bax, *Backbone dynamics of proteins as studied by* ^{15}N *inverse detected heteronuclear NMR spectroscopy: application to staphylococcal nuclease.* Biochemistry, 1989. **28**(23): p. 8972-9.

15. Vranken, W.F., et al., *The CCPN data model for NMR spectroscopy: development of a software pipeline.* Proteins, 2005. **59**(4): p. 687-96.

16. Delaglio, F., et al., *NMRPipe: a multidimensional spectral processing system based on UNIX pipes.* J Biomol NMR, 1995. **6**(3): p. 277-93.

17. Cole, R. and J.P. Loria, *FAST-Modelfree: a program for rapid automated analysis of solution NMR spin-relaxation data.* J Biomol NMR, 2003. **26**(3): p. 203-13.

18. Masino, L., S.R. Martin, and P.M. Bayley, *Ligand binding and thermodynamic stability of a multidomain protein, calmodulin.* Protein Sci, 2000. **9**(8): p. 1519-29.

19. Chattopadhyaya, R., et al., *Calmodulin structure refined at 1.7 A resolution.* J Mol Biol, 1992. **228**(4): p. 1177-92.

20. Tan, R.Y., Y. Mabuchi, and Z. Grabarek, *Blocking the Ca2+-induced conformational transitions in calmodulin with disulfide bonds.* J Biol Chem, 1996. **271**(13): p. 7479-83.

21. Frederick, K.K., et al., *Conformational entropy in molecular recognition by proteins.* Nature, 2007. **448**(7151): p. 325-9.

22. Brokx, R.D., et al., *Energetics of target peptide binding by calmodulin reveals different modes of binding.* The Journal of biological chemistry, 2001. **276**(17): p. 14083-91.

23. Ehrhardt, M.R., J.L. Urbauer, and A.J. Wand, *The energetics and dynamics of molecular recognition by calmodulin.* Biochemistry, 1995. **34**(9): p. 2731-8.

24. Yang, D. and L.E. Kay, *Contributions to Conformational Entropy Arising from Bond Vector Fluctuations Measured from NMR-Derived Order Parameters: Application to Protein Folding.* Journal of Molecular Biology, 1996. **263**(2): p. 369-382.

25. Lee, A.L., et al., *Temperature dependence of the internal dynamics of a calmodulin-peptide complex.* Biochemistry, 2002. **41**(46): p. 13814-25.

Chapter 5. Conjugation study of engineered cellulase with end functionalized polymers

The chapter is written in the '*Methods*' style. A version of Chapter 5 is under preparation for publication.

5.1 Introduction

The field of chemical biology has recently been surged with designer catalytic machines, comprising of functionally active enzymes combined with synthetic polymeric scaffolds [1, 2]. The combination, typically called bioconjugates, has been increasingly used in biotechnology and biomedical research for widespread applications [1, 3-5]. Several methods have been employed to prepare protein-polymer conjugates, which include direct labeling of free reactive thiol or amine groups, incorporation of unnatural amino acids, or use of enzyme-based modifications [6, 7]. Amongst an array of enzyme based protein-polymer conjugation techniques, a highly selective approach is to fuse the protein of interest to enzymatic domains/tags that can covalently conjugate with different chemical reporters [1, 5].

The strategy of using enzyme based covalent functionalization of proteins confers many advantages [7]. It is particularly attractive because the labeling can be controlled at the site of enzymatic catalysis, resulting in formation of highly specific, efficient and stable covalent adducts. Being selective and irreversible in nature, the complexes formed, evades the need for additional purification and do not require subsequent separation steps [8]. Other advantages include the use of a range of end-functionalized polymers having different scaffolds, and the use of milder conditions as compared to other chemical reactions. Since direct labeling of target protein may lead to functional loss, labeling through additional enzymatic tags provides successful alternate route. The challenge associated with the use of such fusion proteins is to express the protein of interest without interfering its native activity. Recombinant DNA

technology, which involves manipulation of DNA at molecular level, alongwith rational design of the fusion construct have provided effective solutions in expressing engineered proteins that maintain their functionality [9].

In our current study, we have used two most prevalent enzymes, namely Cutinase, and human O6-alkylguanine-DNA alkyl transferase (hAGT), referred as SNAP-tag, that can be self-modified to achieve labeling with differently functionalized polymers [10, 11]. The cutinase-tag is a 22kDa serine esterase, consisting of Ser-His-Asp catalytic triad [12]. The catalytic serine residue forms a covalent complex with the phosphonate-functionalized molecules/polymers [13]. On similar lines, SNAP tag, a 21kDa alkyl transferase, can irreversibly react with benzyl-guanine derivatives. The enzyme transfers the benzyl group from O6-benzylguanine derivatives to its active cysteine residue to form highly specific covalent adducts [11, 14].

We constructed two different fusion proteins comprising of cutinase tag and SNAP tag respectively, with our target protein, Cel48F (family 48), an important enzymatic member of *Clostridium cellulolyticum* cellulosome [15]. A cellulosome (shown in Figure 5.1) is a multi enzyme unit comprising of a non-catalytic protein scaffold to which many cellulolytic enzymes (cellulase) bind to organize into a supramolecular array of protein-enzyme complex [15, 16]. The cellulolytic enzymes act in concert to catalyze the conversion of cellulose to glucose. This catalytic conversion is of considerate importance in biofuel industry, as the resultant sugars can be further fermented into fuel alcohol [17].

Considering the biotechnological significance of the cellulolytic enzymes and inspired by the hydrolytic efficiency of natural cellulosomes, we are interested in creating artificial cellulosomes by replacing the protein scaffold with the polymeric scaffold, to which various cellulases can be conjugated.

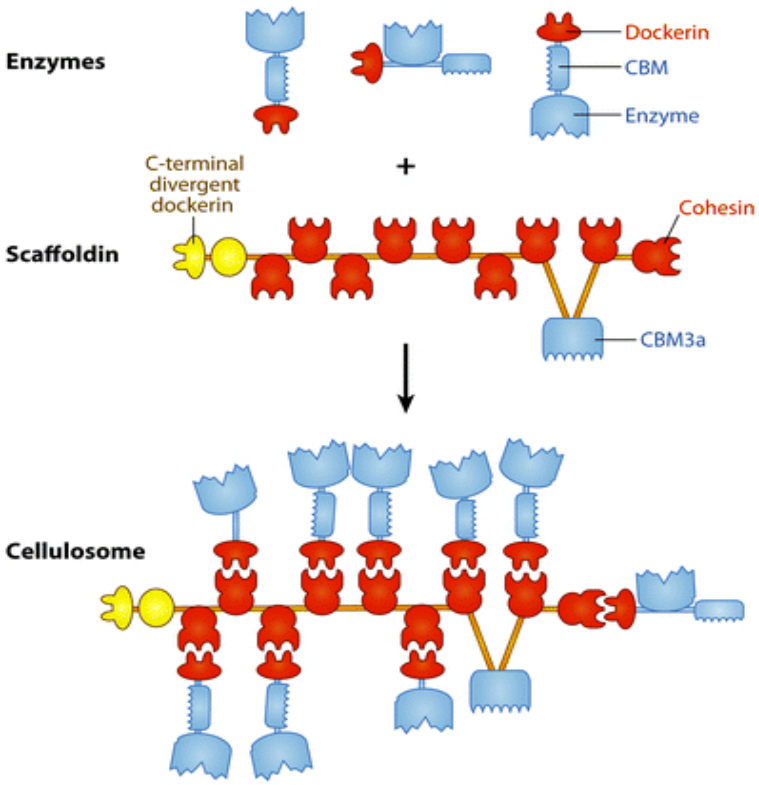

Figure 5.1 A cellulosome assembly. The enzymatic unit consists of a catalytic domain of cellulase enzyme, a non-catalytic carbohydrate binding module (CBM) and a dockerin unit. The scaffoldin is a non-catalytic unit comprising of cohesins that bind to Dockerin to form a cellulosome assembly. Cel48F enzyme used in our studies lacks the CBM. The figure is taken from Fontes, C.M. et al., *Annu Rev Biochem*, 2010 [15].

Taken together, we present a method to prepare functionally active Cel48F-cutinase engineered protein that can be site specifically linked with phosphonate-functionalized polymers (Figure 5.2). In addition, we also present the preliminary results of a differently tagged cellulase, namely, Cel48F-SNAP that can covalently bind to benzylguanine derivatives (Figure 5.2). By precisely controlling the number of functional groups on the polymeric scaffold, we can fine-tune the number of cellulase enzymes being conjugated on to the polymer. The advantages associated with this approach are its modular nature and the flexibility of decorating the polymeric scaffold with different functional groups. Here, we have developed a general route to site-specifically link

enzymes to bi-functionalized polymer scaffolds via bioorthogonal chemistry. Our long-term goal is to employ a similar strategy to other members of cellulases and prepare supramolecular assembly that mimics the natural cellulosome.

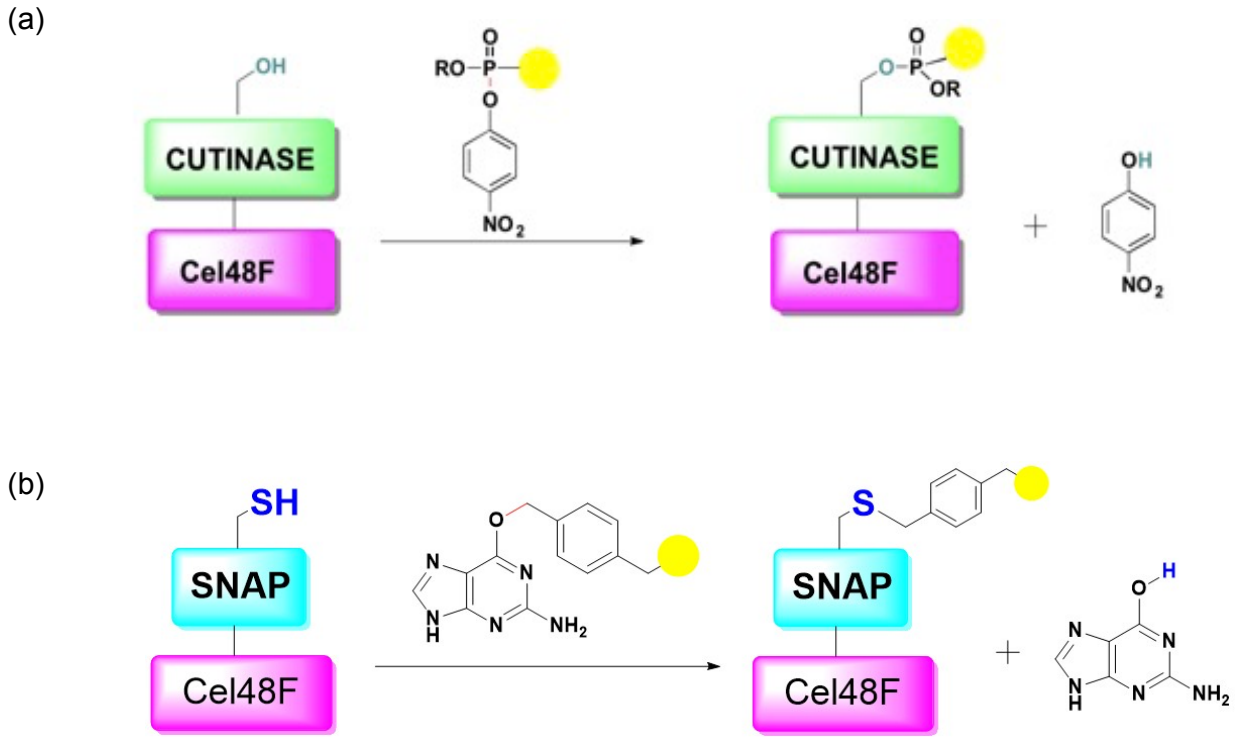

Figure 5.2 (a) Labeling of Cutinase tagged fusion protein with phosphonate derivatives. (b) Labeling of SNAP tagged fusion protein with benzylguanine derivatives.

5.2 Materials

Equipment: Heating block (Fisher Scientific Isotemp 125D), Incubator (New Brunswick Scientific), Benchtop mini centrifuge (Fisher Scientific accuSpin MicroR), 1.5 microcentrifuge tubes, 50ml falcon tubes, French Press, AKTA system (Amersham Biosciences), Magnetic stir bar, Stirrer, Gel electrophoresis apparatus, Gel imaging system with BioRad GelDoc system,

Spectrophotometer, nutator mixer (Labnet Rocker 25), Micropipettors, Pipettor tips, dialysis bags, clips, precast gels, 1ml cuvettes, amicon filters.

Reagents: Kanamycin, agar plates, IPTG, lysozyme, terrific broth Modified EZmix powder (Sigma), glycerol, Tris base, Tris maleate, sodium chloride, imidazole, calcium chloride, DTT, 2x Laemmli Sample Buffer (Bio-Rad Catalog #1610737), electrophoresis buffer, Avicel (PH101, Fluka, Buchs, Switzerland). Origami B (DE3) chemically competent cells were purchased from EMD Biosciences. Ni-NTA agarose was purchased from Qiagen. Complete-Mini EDTA-free protease inhibitor tablets were purchased from Roche Applied Science.

5.3 Methods

5.3.1 Molecular cloning of fusion proteins

The Cel48F-Cutinase plasmid was constructed from Cel48F plasmid, synthesized by GenScript Corporation. The restriction site for SalI was introduced by PCR. The resultant product was ligated with the DNA coding for the cutinase insert (amplified from previously constructed plasmid). The gene encoding Cel48F-linker-cutinase protein was then cloned into pET26b vector via NdeI and XhoI, resulting in Cel48F-Cut plasmid. pET26b(Cel48F-SNAP), was generated by replacing cutinase domain with SNAP domain between HindIII and XhoI. However, the resultant plasmid had a shorter linker than Cel48F-Cut plasmid.

Transformation of Cel48F plasmids

1. Set the heating block to a temperature of 42 °C.
2. Thaw 50ul of E.coli cells (Origami2 (DE3) strain). Add 2ul of plasmid (10-50ng) to 50ul of cells and incubate in ice bath for 30 minutes.
3. Heat at 42 °C for 45s, immediately incubate in ice for 2minutes.
4. Add 400ul of LB and incubate at 37 °C for 45-60 minutes.

5. Centrifuge the eppendorf tube for 2minutes.
6. Discard the media, resuspend in 50ul of media.
7. Plate the transformation reaction on LB-agar plate supplemented with kanamycin (50ug/ml) for 16-18 hours at 37 °C.

5.3.2 Expression and purification

Expression:

1. Pick a single colony from the agar plate, and suspend it in 50ml TB broth having kanamycin (50ug/ml) antibiotic. Allow it to grow for 12-16 hours at 37 °C with shaking at 225rpm. This is referred to as seed culture.
2. Inoculate 1L of autoclaved TB broth with 10mL of seed culture (1:100 dilution). Grow at 37°C with shaking at 225rpm till it reaches O.D=0.6. Transfer the flask to 18°C, and allow it to cool for an hour. Induce it with 20uM IPTG. Grow at 18°C with shaking at 225rpm for 16 hours.
3. Harvest cells by centrifuging at 4000rpm for 40minutes. Discard the supernatant and store the pellet at -20°C, or use it immediately for further purification.

Purification:

1. Preparation of buffers:

Buffer A: 50mM Tris, pH 8.0, 300mM sodium chloride

Buffer B: 50mM Tris, pH 8.0, 300mM sodium chloride, 1M imidazole

Dialysis buffer: 20 mM Tris, pH 8.0

Buffer QA: 20 mM Tris, pH 7.5.

Buffer QB: 20 mM Tris, pH 7.5, 1M NaCl

2. Preparation of affinity column: Take 2ml Ni-NTA agarose resin (Qiagen #30230) in affinity column and decant the supernatant. Continue to wash the resin 3 to 5 times with Buffer 1 (table 5.1) to completely remove the ethanol.

Buffer	Vol. (ml)	Imidazole (mM)	Buffer A (ml)	Buffer B (ml)
1	50	5	49.75	0.25
2	50	10	49.5	0.5
3	50	25	48.75	1.25
4	50	40	48	2
5	50	80	46	4
6	50	120	44	6
7	50	160	42	8
8	50	200	40	10
9	50	250	37.5	12.5
10	50	300	35	15
11	50	500	25	25
12	50	1000	0	50

Table 5.1. Preparation of buffers for affinity purification

3. Resuspend the frozen pellet in Buffer A. Add 3mg lysozyme, 1 tablet of EDTA-free protease inhibitor, 1mM of PMSF. Incubate the cell suspension at room temperature for 20 min.

4. Lyze the cells using French press. Repeat the cell lysis cycle for 4 times. Remove the insoluble cell debris by centrifugation at 8000rpm for 1 hour at 4 °C.

5. Load the lysate to the affinity column and incubate with the prepared Ni-NTA agarose resin at 4 °C for 1 hour on a nutator.

6. Wash the resin sequentially with 20 ml of *Buffer 1-12* (listed in table 5.1).

7. Check the fractions 1-12 with SDS-PAGE (200V, ~35min).

8. Pool the fractions containing target protein, and dialyse in 1 L of dialysis buffer at 4 °C.

9. Further purify the protein using Resource Q column (GE Healthcare #17-1177-01) on FPLC. Run a Linear gradient (0-100%B) in 12 CV; 1.5 ml/fraction at a flow rate of 2 ml/min.

10. Check the fractions with SDS-PAGE. (Figure 5.3)

11. Pool the fractions, which contains the desired protein.

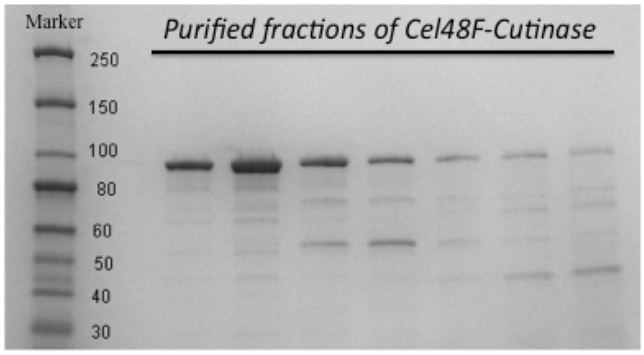

Figure 5.3 Gel analysis of purified fractions obtained after anion exchange of Cel48F-Cutinase.

5.3.3 Conjugation study of Cel48F with bi-functional polymer

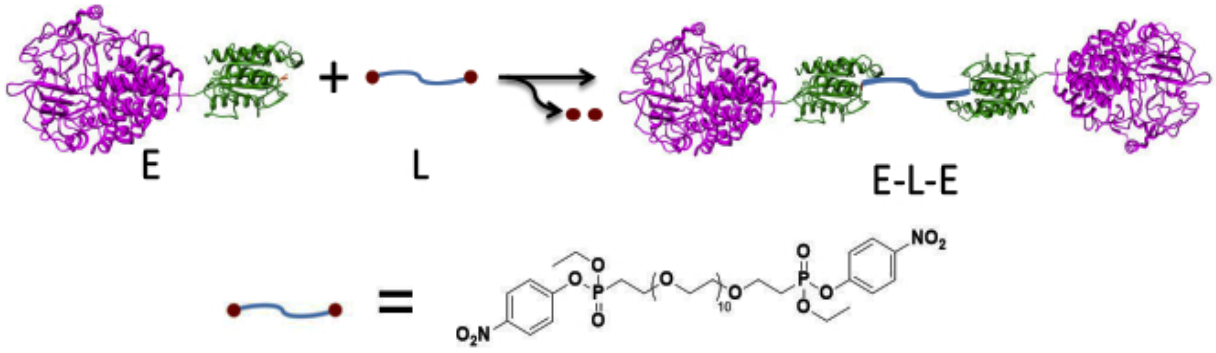

Figure 5.4 Scheme of conjugation reaction between modified Cel48F and bifunctional polymer linker

Optimizing the conjugation conditions

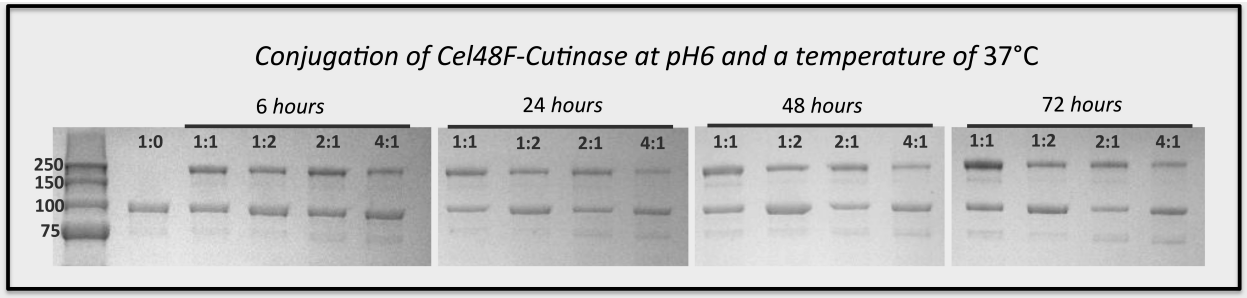

Figure 5.5 SDS-PAGE analysis of Cel48F-cutinase with bifunctional polymer. The samples were incubated at different ratios for 6, 24, 48 and 72 hours. The dimerization was observed at pH 6.0, at a temperature of 37°C after 6 hours.

1. Preparation of sample buffer: Add 50ul BME to 950ul of SDS buffer (as per the instructions: Laemmli Sample Buffer Bio-Rad Catalog #1610737)
2. Incubate 500ul protein (5mM Tris maleate, pH 6, 100mM NaCl) with DODEG polymer at 37°C at different E:L ratio: 1:0 1:1, 1:2, 2:1, 4:1, 1:10, 1:20.
3. Aliquot 50ul of samples after 6, 24, 48 and 72 hours.
4. Prepare 1:1 dilution of sample: sample buffer.
5. Heat the samples at 70°C for 5 minutes.

6. Load 25ul to the mini-protean gels. Run the gel at 200V for 35minutes.

   Dimerization was observed at 1:1, 1:2, 2:1, 4:1 after 6 hours, indicating that the enzyme conjugated with both the ends of the bi-functional polymer (Figure 5.5). When a higher concentration of polymer was used, no dimerization was observed (as in the case of 1:10, and 1:20) (data not shown).

Kinetics study for conjugation

1. Prepare 4uM of Cel48F cutinase in 20mM Tris, pH 8, 100mM NaCl.
2. Prepare 0.1M stock solution of DOPEG in DMSO. Dilute the stock solution to 200uM using the same buffer as above. (At 1:50 ratio, the dimer formation is suppressed).
3. The linker was added just before the UV analysis.
4. Monitor the release of p-nitrophenol of the reaction at 401nm using high throughput UV spectrophotometer for 15 minutes.
5. The linker was added just before the UV analysis.
6. Monitor the release of p-nitrophenol of the reaction at 401nm using high throughput UV spectrophotometer for 15 minutes.

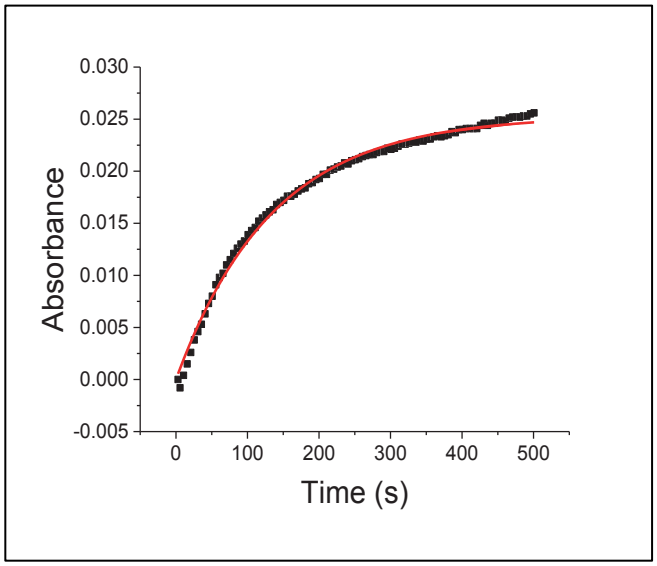

Figure 5.6 Determination of the rate constant for ligand functionalization of Cel48F-Cutinase EG10 bisphosphonate ligand by monitoring the release of p-nitrophenol at 401 nm. Data were fit to a pseudo-first order kinetic equation and divided by the concentration of the excess species to yield effective second order rate constants for the reactions.

The rate constant of the reaction between enzyme and the bisphosphonate linker was obtained by following the release of p-nitrophenol (λmax = 401nm) with time using UV-Vis absorption spectroscopy (Figure 5.6). The resulting kinetic trace was fit to a pseudo-first order equation and the effective second-order rate constant was obtained by dividing these quantities by the concentration of excess ligand. The observed rate constant was found to be 37.10 $M^{-1}s^{-1}$.

5.3.4 Cellulase activity assay of the fusion protein

Preparation of solutions:

Solution 1: Potassium ferricyanide solution (0.5g/L)

Solution 2: Carbonate-cyanide solution: (5.3g/L sodium carbonate and 0.65g/L potassium cyanide)

Solution 3: Ferric ammonium solution: (1.5g/L ferric ammonium sulfate, 2g/L SDS and 0.2N sulfuric acid)

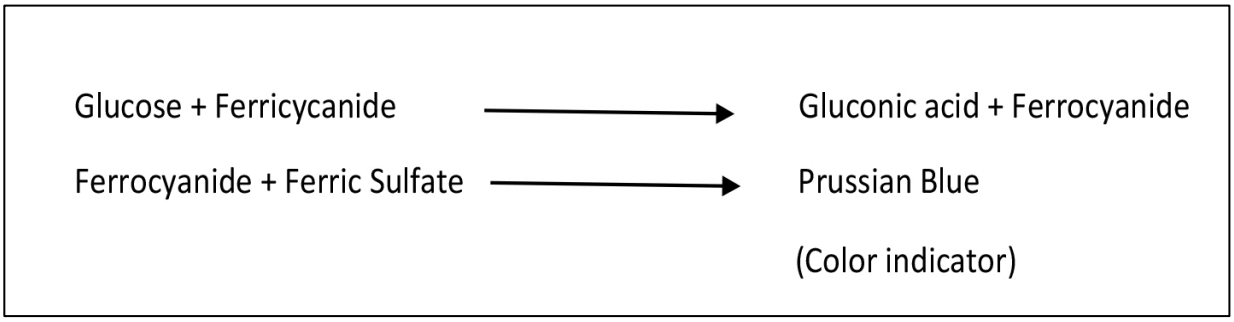

Figure 5.7 Mechanism of ferricyanide reducing sugar assay. The intensity of Prussian blue color is monitored at 690nm.

Protocol for performing ferricyanide reducing sugar assay: The mechanism of the assay [18] is explained in Figure 5.7.

1. To 300ul of sample, add 100ul of solution 1 and 100ul of solution 2.
2. Heat at 100°C for 15minutes.
3. Cool on ice for 3minutes.
4. Add 500ul of solution 3 to the mix.
5. Wait for 15 minutes. Examine the Prussian blue color formation.
6. Measure absorbance at 690nm (scan between 645-735nm). (Replace sample solution with buffer to use as your blank).

Cellulase activity assay

1. Perform buffer exchange of Cel48F-cutinase with 20 mM Tris maleate, pH 6.0, 100mM NaCl, 1 mM $CaCl_2$ using amicon fliter (Mw. Cut off 30kD).
2. Incubate the protein with DODEG polymer at 1:1 ratio.

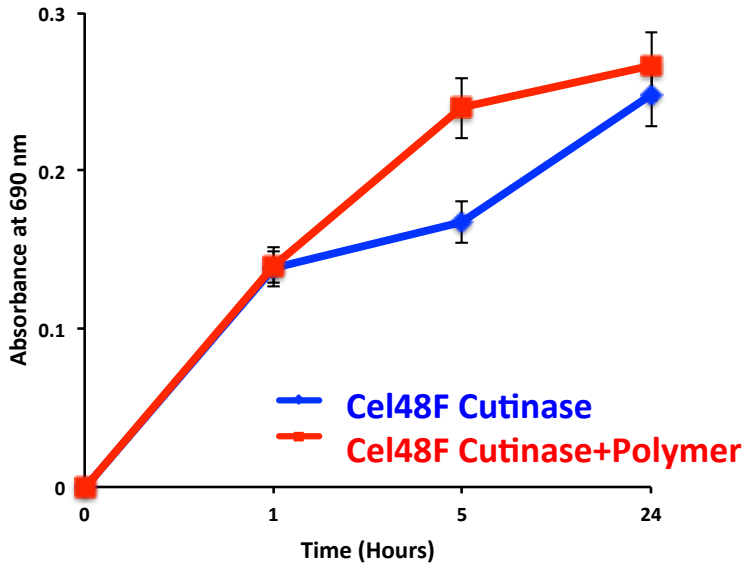

Figure 5.8 Avicel hydrolysis by Cel48F-Cutinase in free state (blue trace) or conjugated state (red trace).

3. Incubate 1uM of protein in free and conjugated state with 4ml of microcrystalline cellulose (Avicel PH101, Fluka, Buchs, Switzerland) at 20mg/ml in 20 mM Tris maleate, pH 6.0, 1 mM $CaCl_2$.
4. Aliquot 0.6ml at 0, 1, 5 and 24h, centrifuge and transfer the supernatant to a new 1.5ml eppendorf tube. Examine for soluble reducing sugars using ferricyanide assay.

Figure 5.8 compares the amount of soluble sugars released at different time intervals by the same amount of proteins, either in the free state or in the conjugated state with bifunctionalized polymer. The hydrolytic activity of Cel48F is retained upon conjugation and is comparable to free form.

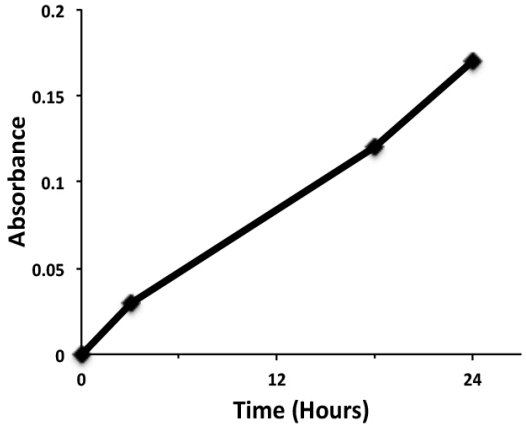

Figure 5.9 Avicel hydrolysis by Cel48F-SNAP in free state.

Additionally, we purified Cel48F-SNAP using the same purification protocol. The cellulase activity of the fusion protein was observed in the free form as depicted in Figure 5.9. While the polymers for Cel48F-SNAP are currently being synthesized, we tested its ability to conjugate with commercially available benzylguanine functionalized magnetic beads. We were successful in our attempt to immobilize the Cel48F-SNAP on magnetic capture beads.

5.4 Conclusions and Future directions

We were able to successfully create differently tagged cellulases that retain the cellulase activity and can further be conjugated with functionalized polymers. The conjugated enzyme (Cel48F-Cutinase) has a similar activity as its free form, however we strive to achieve a better activity profile. This can be observed by attaching cellulases from different families that work synergistically with Cel48F enzyme. Additionally, HPLC assay would provide quantitative results in measuring the hydrolytic activity of cellulases. It will also be interesting to develop brush polymer having multiple chain ends, which can be used to conjugate cellulase. Finally, this work serves as a foundation to prepare supramolecular assembly of enzymes conjugated to polymeric scaffolds using different bio-orthogonal chemistry.

5.5 References

1. Gauthier, M.A. and H.-A. Klok, *Polymer-protein conjugates: an enzymatic activity perspective.* Polymer Chemistry, 2010. **1**(9): p. 1352-1373.

2. Gauthier, M.A. and H.-A. Klok, *Peptide/protein-polymer conjugates: synthetic strategies and design concepts.* Chemical Communications, 2008(23): p. 2591-2611.

3. Biedermann, F., et al., *A supramolecular route for reversible protein-polymer conjugation.* Chemical Science, 2011. **2**(2): p. 279-286.
4. Haag, R. and F. Kratz, *Polymer therapeutics: concepts and applications.* Angew Chem Int Ed Engl, 2006. **45**(8): p. 1198-215.

5. Thordarson, P., B. Le Droumaguet, and K. Velonia, *Well-defined protein–polymer conjugates—synthesis and potential applications.* Applied Microbiology and Biotechnology, 2006. **73**(2): p. 243-254.

6. Sunbul, M. and J. Yin, *Site specific protein labeling by enzymatic posttranslational modification.* Org Biomol Chem, 2009. **7**(17): p. 3361-71.

7. van Vught, R., R.J. Pieters, and E. Breukink, *Site-specific functionalization of proteins and their applications to therapeutic antibodies.* Computational and Structural Biotechnology Journal, 2014. **9**: p. e201402001.

8. Hodneland, C.D., et al., *Selective immobilization of proteins to self-assembled monolayers presenting active site-directed capture ligands.* Proc Natl Acad Sci U S A, 2002. **99**(8): p. 5048-52.

9. Miller, W.L. and J.D. Baxter, *Synthesis of biologically active proteins by recombinant DNA technology.* Drug Development Research, 1981. **1**(4): p. 435-454.

10. Mannesse, M.L., et al., *Cutinase from Fusarium solani pisi hydrolyzing triglyceride analogues. Effect of acyl chain length and position in the substrate molecule on activity and enantioselectivity.* Biochemistry, 1995. **34**(19): p. 6400-7.

11. Keppler, A., et al., *A general method for the covalent labeling of fusion proteins with small molecules in vivo.* Nat Biotechnol, 2003. **21**(1): p. 86-9.

12. Martinez, C., et al., *Fusarium solani cutinase is a lipolytic enzyme with a catalytic serine accessible to solvent.* Nature, 1992. **356**(6370): p. 615-8.

13. Dijkstra, H.P., et al., *Selective and diagnostic labelling of serine hydrolases with reactive phosphonate inhibitors.* Organic & Biomolecular Chemistry, 2008. **6**(3): p. 523-531.

14. Juillerat, A., et al., *Directed Evolution of O6-Alkylguanine-DNA Alkyltransferase for Efficient Labeling of Fusion Proteins with Small Molecules In Vivo.* Chemistry & Biology. **10**(4): p. 313-317.

15. Fontes, C.M. and H.J. Gilbert, *Cellulosomes: highly efficient nanomachines designed to deconstruct plant cell wall complex carbohydrates.* Annu Rev Biochem, 2010. **79**: p. 655-81.

16. Bayer, E.A., et al., *The cellulosomes: multienzyme machines for degradation of plant cell wall polysaccharides.* Annu Rev Microbiol, 2004. **58**: p. 521-54.

17. Gonçalves, G.A.L., Y. Mori, and N. Kamiya, *Biomolecular assembly strategies to develop potential artificial cellulosomes.* Sustainable Chemical Processes, 2014. **2**(1): p. 1-5.

18. Park, J.T. and M.J. Johnson, *A submicrodetermination of glucose.* J Biol Chem, 1949. **181**(1): p. 149-51.

Chapter 6. Conclusions

6.1 Summary and future outlook

Much can be learned about proteins using biophysical and biochemical approaches. Each protein was investigated from a different perspective. Below, we highlight the conclusions of our studies on different protein systems, namely integrin-Src, CaM and Cellulase, and offer additional insights in further exploring these systems.

Extensive studies of both, integrin and Src kinase, have established a critical role of this interaction in thrombosis and hemostasis as well as in regulation of platelet adhesion. Src kinase plays an important role in integrin signaling by regulating cytoskeletal organization and cell remodeling. Previous in vivo studies revealed that SH3 domain of c-Src kinase directly associates with the C-terminus of β3 integrin cytoplasmic tail. Here, we explored this binding interface with a combination of different spectroscopic and computational methods. Chemical shift mapping, PRE, transferred NOE and CD data were used to obtain a docked model of the complex. This model suggests a different binding mode from the one proposed through previous studies wherein, the C-terminal end of β3 spans the region in between the RT and n-Src loops of SH3 domain. Furthermore, we show that tyrosine phosphorylation of β3 prevents this interaction, supporting the notion of a constitutive interaction between β3 integrin and Src SH3. We, further investigated the effect of tyrosine phosphorylation of β3, and identified its interaction with Src SH2. The platelet stimulation studies performed by another group corroborate our results, supporting the notion that Src can remain bound to activated β3. With identification of this novel binding mode, a variety of questions still remain unanswered. How integrin mediates Src activation, what is the role of β3BP in binding to Src SH2, does it displace the pY527 bearing C-terminal tail or are there any conformational changes associated with it? Proposed ITC studies

can identify the binding affinity and thermodynamic forces driving the interaction between SH2 domain and β3 CT in different phosphorylation states. Based on the Kd values, we can further provide insights into the mechanism of integrin mediated Src activation. It would also be interesting to prepare Src SH2 deletion mutants and further study the functional relevance of these interactions using cell-based assays.

In our second project, we focused our research efforts in understanding the effect of protein modification on protein's internal structure and its interaction with its binding partner. Calmodulin, a calcium modulated protein was modified using a disulfide linkage. A subtle change in the structure was enough to alter the enthalpy-entropy contributions, however, it was remarkable to observe that the free energy remain constant. To further qualify these changes, we studied the backbone dynamics of CaM. Despite the conformational change of the protein, the flexibility of backbone residues weren't significantly affected. Previous studies identified that dynamics of side chains (of wt-CaM) contribute significantly to the binding of smMLCK. It would be useful to study the dynamics of side chain residues and identify the factors contributing to the enthalpy-entropy compensation. Besides, one can also perform H-D exchange experiments in apo and bound forms to study the effect of solvation that contributes significantly to the entropy term.

Lastly, we investigated engineered proteins and developed its conjugates. Our engineered proteins and their conjugates maintain their cellulase activity in solution. We strive to achieve better activity of these enzyme-polymeric conjugates. Additionally, we aim to develop artificial cellulosome, consisting of a polymeric scaffold, which remains stable at extreme conditions used in industries. These artificial systems would be prepared by using brush polymers decorated with different functional groups to which differently tagged proteins can attach.

Taken together, our studies used multifarious approaches to improve and contribute to the existing knowledge of proteins involved in cell signaling pathways; addressing the physical impact of topological constrain on proteins; and developing a general route to site specifically link proteins to polymeric scaffolds.

APPENDIX A

ELSEVIER LICENSE
TERMS AND CONDITIONS

Sep 11, 2016

This Agreement between Priya Katyal ("You") and Elsevier ("Elsevier") consists of your license details and the terms and conditions provided by Elsevier and Copyright Clearance Center.

License Number	3946040998868
License date	Sep 11, 2016
Licensed Content Publisher	Elsevier
Licensed Content Publication	Biochimica et Biophysica Acta (BBA) - Proteins and Proteomics
Licensed Content Title	How to study proteins by circular dichroism
Licensed Content Author	Sharon M. Kelly,Thomas J. Jess,Nicholas C. Price
Licensed Content Date	10 August 2005
Licensed Content Volume Number	1751
Licensed Content Issue Number	2
Licensed Content Pages	21
Start Page	119
End Page	139
Type of Use	reuse in a thesis/dissertation
Intended publisher of new work	other
Portion	figures/tables/illustrations
Number of figures/tables/illustrations	1
Format	both print and electronic
Are you the author of this Elsevier article?	No
Will you be translating?	No
Order reference number	
Original figure numbers	Figure 3
Title of your thesis/dissertation	Biochemical Analysis of Protein-Protein and Protein-Polymer Interactions
Expected completion date	Sep 2016
Estimated size (number of pages)	105
Elsevier VAT number	GB 494 6272 12
Requestor Location	Priya Katyal 69 N.Eagleville Rd. STORRS MANSFIELD, CT 06269

THE AMERICAN ASSOCIATION FOR THE ADVANCEMENT OF SCIENCE LICENSE TERMS AND CONDITIONS

Sep 11, 2016

This Agreement between Priya Katyal ("You") and The American Association for the Advancement of Science ("The American Association for the Advancement of Science") consists of your license details and the terms and conditions provided by The American Association for the Advancement of Science and Copyright Clearance Center.

License Number	3946040581549
License date	Sep 11, 2016
Licensed Content Publisher	The American Association for the Advancement of Science
Licensed Content Publication	Science
Licensed Content Title	The Tail of Integrins, Talin, and Kindlins
Licensed Content Author	Markus Moser,Kyle R. Legate,Roy Zent,Reinhard Fässler
Licensed Content Date	May 15, 2009
Licensed Content Volume Number	324
Licensed Content Issue Number	5929
Volume number	324
Issue number	5929
Type of Use	Thesis / Dissertation
Requestor type	Scientist/individual at a research institution
Format	Print and electronic
Portion	Figure
Number of figures/tables	1
Order reference number	
Title of your thesis / dissertation	Biochemical Analysis of Protein-Protein and Protein-Polymer Interactions
Expected completion date	Sep 2016
Estimated size(pages)	105
Requestor Location	Priya Katyal 69 N.Eagleville Rd. STORRS MANSFIELD, CT 06269 United States Attn: Priya Katyal
Billing Type	Invoice
Billing Address	Priya Katyal 69 N.Eagleville Rd. STORRS MANSFIELD, CT 06269 United States Attn: Priya Katyal

NATURE PUBLISHING GROUP LICENSE
TERMS AND CONDITIONS

Sep 11, 2016

This Agreement between Priya Katyal ("You") and Nature Publishing Group ("Nature Publishing Group") consists of your license details and the terms and conditions provided by Nature Publishing Group and Copyright Clearance Center.

License Number	3946031385111
License date	Sep 11, 2016
Licensed Content Publisher	Nature Publishing Group
Licensed Content Publication	Nature Reviews Molecular Cell Biology
Licensed Content Title	The final steps of integrin activation: the end game
Licensed Content Author	Sanford J. Shattil, Chungho Kim and Mark H. Ginsberg
Licensed Content Date	Apr 1, 2010
Licensed Content Volume Number	11
Licensed Content Issue Number	4
Type of Use	reuse in a dissertation / thesis
Requestor type	academic/educational
Format	print and electronic
Portion	figures/tables/illustrations
Number of figures/tables/illustrations	1
High-res required	no
Figures	Bidirectional integrin signaling
Author of this NPG article	no
Your reference number	
Title of your thesis / dissertation	Biochemical Analysis of Protein-Protein and Protein-Polymer Interactions
Expected completion date	Sep 2016
Estimated size (number of pages)	105
Requestor Location	Priya Katyal 69 N.Eagleville Rd. STORRS MANSFIELD, CT 06269 United States Attn: Priya Katyal
Billing Type	Invoice
Billing Address	Priya Katyal 69 N.Eagleville Rd. STORRS MANSFIELD, CT 06269

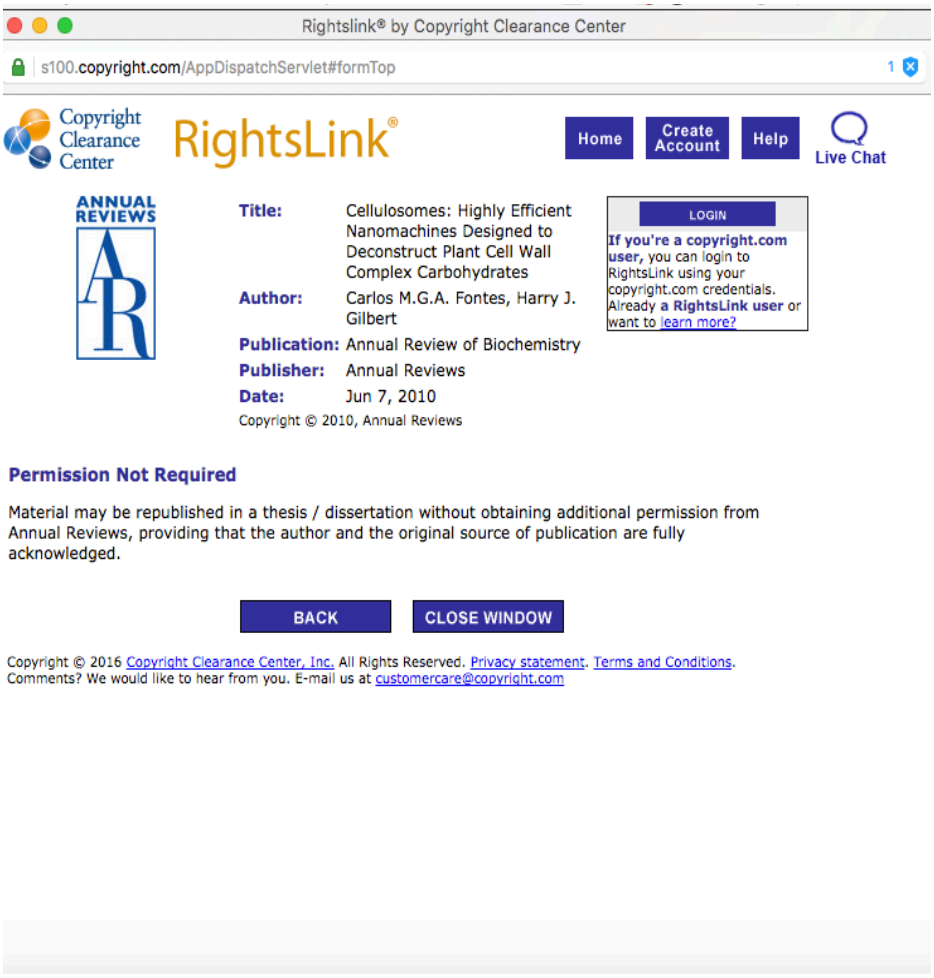
Rightslink® by Copyright Clearance Center
s100.copyright.com/AppDispatchServlet#formTop
Copyright Clearance Center
RightsLink®
Home
Create Account
Help
Live Chat
ANNUAL REVIEWS
Title: Cellulosomes: Highly Efficient Nanomachines Designed to Deconstruct Plant Cell Wall Complex Carbohydrates
Author: Carlos M.G.A. Fontes, Harry J. Gilbert
Publication: Annual Review of Biochemistry
Publisher: Annual Reviews
Date: Jun 7, 2010
Copyright © 2010, Annual Reviews
LOGIN
If you're a copyright.com user, you can login to RightsLink using your copyright.com credentials. Already a RightsLink user or want to learn more?
Permission Not Required
Material may be republished in a thesis / dissertation without obtaining additional permission from Annual Reviews, providing that the author and the original source of publication are fully acknowledged.
BACK
CLOSE WINDOW
Copyright © 2016 Copyright Clearance Center, Inc. All Rights Reserved. Privacy statement. Terms and Conditions.
Comments? We would like to hear from you. E-mail us at customercare@copyright.com

Hindawi Copyright and License Agreement

By submitting your work, you signify that you have read and agreed to the following terms.

In consideration for the publication of your article by Hindawi you hereby agree to pay the agreed fee and grant to Hindawi an irrevocable nonexclusive license to publish in print and electronic format, and further sublicense the article, for the full legal term of copyright and any renewals thereof in all languages throughout the world in all formats, and through any medium of communication.

You shall retain the perpetual royalty-free right to reproduce and publish in print and electronic format, and further sublicense the article in all languages throughout the world in all formats, and through any medium of communication provided that you make reference to the first publication by the Journal and Hindawi.

Upon publication, your article shall be openly licensed using the Creative Commons Attribution 4.0 License (http://creativecommons.org/licenses/by/4.0/). In addition, any data related to your article, including its reference list(s) and its additional files, shall be distributed under the terms of the Creative Commons Public Domain Dedication waiver (http://creativecommons.org/publicdomain/zero/1.0/).

You warrant that the article is your original work.

You warrant that you are the sole author(s) of the article and have full authority to enter into this Agreement and in granting rights to Hindawi Publishing Corporation that are not in breach of any other obligation.

You warrant that the article is submitted for first publication in the journal and that it is not being considered for publication elsewhere and has not already been published elsewhere, either in printed or electronic form.

You warrant that you have obtained all necessary permissions for the reproduction of any copyright works (including artistic works, e.g., illustrations, photographs, charts, maps, and other visual material) contained in the article and not owned by you and you have acknowledged all the sources.

You warrant that the article contains no violation of any existing copyright, other third party rights, or any libelous statements, and does not infringe any rights of others.

You warrant that the Contribution contains no violation of any existing copyright, other third party rights, or any libellous statements, and does not infringe any rights of others.

You warrant that you have taken due care to ensure the integrity of the article so that to your—and currently accepted scientific—knowledge all statements contained in it purporting to be facts are true and any formula or instruction contained in the article will not, if followed accurately, cause any injury, illness, or damage to the user.

You warrant that the article, in the form to be delivered to Hindawi, does not contain information that may violate the State Secrets Laws of the People's Republic of China ("PRC"), including (a) any information that has a vital bearing on Chinese state security and national interests; (b) any information defined as a "State Secret" under the PRC law, or (c) any classified information belonging to governmental authorities of the People's Republic of China, including government agencies, quasi-government agencies, public institutions, or state-owned enterprises (together the "State Secret Laws"). For the purposes of PRC law and this Agreement "State Secrets" shall include, but not be limited to: (i) unpublished information concerning major policy decisions on Chinese State affairs; (ii) confidential information concerning national defense and the activities of the armed forces; (iii) confidential information concerning national diplomatic policies and activities; (iv) confidential information concerning national economic and social development; (v) matters concerning classified science and technology; and (vi) unpublished Chinese State security matters and non-public information about the on-going investigation of criminal offenses.

You agree to indemnify Hindawi Publishing Corporation against any claims in respect of the above warranties.

You are urged to screen out any information that may constitute State Secrets under the law of the PRC or violate the State Secret Laws before submitting your article to Hindawi. Hindawi is not responsible for any consequences from inadvertent disclosure of such State Secrets or violation of the State Secret Laws in your work, and Hindawi makes no warranty, expressed, or implied, with respect to the contents of the publications. Hindawi does not assume any liability for any infringement of the State Secret Laws arising from its publication.